OPTICAL BIOSENSORS

By

Mohamed Ismail Elsherif

The dissertation submitted to

University of Birmingham

for the degree of

Doctor of Philosophy

School of Engineering and Physical sciences
Department of Mechanical Engineering
University of Birmingham
August 2019

Abstract

Continuous glucose monitoring facilitates the stringent control of blood glucose concentration in diabetic and intensive care patients. Low-cost, robust, and reusable continuous glucose monitoring systems that can provide quantitative measurements at point-of-care settings is an unmet medical need. Phenylboronic acids (PBAs) have emerged as synthetic receptors that can reversibly bind to *cis*-diols such as glucose molecules. The incorporation of phenylboronic acids in hydrogels offer exclusive attributes as the binding process with glucose induces Donnan potential that leads to osmotic pressure, resulting in volumetric changes in the hydrogel matrix. Optical glucose sensors based on PBA-functionalized hydrogels have emerged as strong candidates for commercialization; however, their complex and time-consuming fabrication process, and their bulky and expensive readouts methods made them undesirable for quantitative analyses. In this dissertation, optical hydrogel sensors have been developed and attached to contact lenses for continuous glucose detection in physiological conditions. A simple fabrication method was utilized, and smartphone technology was employed for recording the output signals. A 1D photonic structure was replicated on a PBA-functionalized hydrogel to function as a transducer and to improve the sensor performance. Upon binding glucose with boronate anions immobilized in the hydrogel matrix, a positive volumetric shift occurred modifying the periodic constant of the photonic structure, consequently its diffraction properties altered. A correlation has been established between the sensor's periodic constant and glucose concentration in the range of 0-50 mM. The hydrogel sensor was attached to a soft commercial contact lens (ACUVUE) and was interrogated for glucose detection in artificial

tears. The ambient light sensor of a smartphone captured the intensity of the laser diffracted signals and was correlated with glucose concentrations. The smart contact lens showed very short response time (3 s), and a saturation time of near 4 minutes in continuous monitoring conditions. However, a laser beam was necessary to interrogate the contact lens which is uncomfortable, and the frequent exposure might be harmful to the eye cornea. Alternatively, a novel transducer has been introduced to enable interrogating the smart contact lens by using a white light beam. Light diffusing microstructures (LDMs) have been introduced for the first time for the sensing applications. The LDMs can be considered as densely-packed microparticles of different shapes and dimensions which have the capacity to diffuse the polychromatic and monochromatic light in the forward and backward directions. The LDMs were imprinted on the glucose -responsive hydrogel to monitor the volumetric shift due to glucose complexation. The volumetric modification of the hydrogel upon glucose complexation induced a change in the dimensions and refractive index of the LDMs, resulting in a variation in the diffusion efficiency. The glucose sensor was attached to a commercial contact lens and a smartphone measured the optical output signals. The alternative transducer enabled interrogating the smart contact lens by a white light beam and retained on the simplicity of the fabrication and the readout methodology; however, the response time of the senor increased significantly. The proposed smart contact lenses can be considered as a non-invasive way for continuous glucose monitoring, and can detect many other biomarkers that are beneficial for medical diagnostic applications.

For implantable and remote monitoring of glucose concentration, fiber optic probes have been developed. Fiber optics have inherent advantages such as immunity to electromagnetic

interference, miniaturization, and small volumes of samples. These merits candidate them for biosensing applications; however, complexity of the manufacturing process, poor mechanical properties, unpracticality of the readout methodology have hindered their practical applications. We have developed fiber optic probes for glucose detection that overcome the limitations mentioned above. Capability of the LDMs to scatter/diffuse the incident light beam in the forward and backward directions was exploited. The glucose responsive hydrogel imprinted with the LDMs was attached to the tip of a multimode silica fiber. Swelling of the attached hydrogel led to a decrease in the refractive index of the LDMs, inducing a decrease in the light scattering angles. Whereas the numerical aperture of the optical fiber indicates the range of the angles of the incident rays those satisfy the total internal reflection condition. Accordingly, swelling the hydrogel attached to the fiber result in more incident rays fall within the accepted range of angles to be guided in the optical fiber. Hence, the optical power guided in the fiber increased with glucose concentration. The fabricated fiber probe was interrogated for glucose detection in transmission configuration and the smartphone was utilized to pick up the fiber's signals. Also, the probe was tested in reflection configuration which is a more practical mode for implantable biosensing applications. The probe overcame some limitations of the existing probes such as interferometric, SPR, and fluorescent probes in terms of ease of the fabrication and the interrogation processes. Additionally, the probe showed high sensitivity, rapid response, and selectivity for glucose over lactate. The lactate interference was found to be ~ 0.1% in the physiological condition. Furthermore, biocompatible hydrogel fibers were introduced to prevent or reduce the immune reaction in the implantation sites. The probes were tested for glucose detection and showed similar response to that of silica fiber probes; however, they

presented lower sensitivity which might be the result of a higher light loss in the hydrogel fiber. In order to emphasize the variety of applications of these novel fiber optic probes that we developed, two more probes were fabricated for alcohol detection and pH measurements. The alcohol probe showed real-time sensing of ethanol, propanol, and dimethyl sulfoxide with a response time in seconds and a saturation time around 60 s. Also, the pH probe showed high sensitivity and rapid response in the acidic region with a sensitivity near 20% pH^{-1}. For medical applications, the pH sensor was attached to a biocompatible fiber optic and was tested for pH sensing in reflection configuration. The probe can be recommended for gastric pH detection. The fabricated optical fiber sensors may also have applications in wearable and implantable point-of-care and intensive-care continuous monitoring systems.

Acknowledgement

I would like to express my genuine gratitude to my supervisors Dr Haider Butt and Dr Khamis Essa for their assistance and support during my PhD study. I am very much obliged to Dr Butt for his generous guidance, and constant feedback. I feel privileged to have been supervised by such a magnificent person. My thanks extend to our collaborators; Dr Ali K. Yetisen and Dr Umair Hassan for their valuable discussion and generous feedback. A special thanks to Dr Magdolena Bajgrowicz-Cieslak for her support and useful discussion.

Also, I'd like to thank my colleagues, Ijaz Rashid, Rajib Ahmed, Badr Alqattan. Tawfiq Alqurashi, Yousef Alqurashi, and Muhammed Waqas Khalid.

I would like to thank Prof. Reem Bhagat, the Egyptian cultural counsellor in London for her spiritual support and encouragement.

I am deeply grateful to Prof. Ehab Abdel Rahman who paved my way to pursue my research carrier and for supporting me in a time I was in great need for the support.

Most of all, I would like to pass my truthful thanks to my parents, my brother, Kamel, my wife, and my sisters, for their prayer and encouragement throughout my study.

Table of Contents

List of Figures

List of tables

List of publications

1. Mohamed Elsherif, Muhammed Umair Hassan, Ali K. Yetisen, and Haider Butt, "Wearable Contact Lens Biosensors for Continuous Glucose Monitoring using Smartphones'', **ACS Nano**, 2018, 12, 5452- 5462.

2. Mohamed Elsherif, Muhammed Umair Hassan, Ali K. Yetisen, and Haider Butt, "Glucose Sensing with Phenylboronic Acid Functionalized based Optical Diffuser", **ACS Nano,** 2018, 12, 2283−2291.

3. Mohamed Elsherif, Muhammed Umair Hassan, Ali K. Yetisen, and Haider Butt, "Hydrogel Optical Fibers for Continuous Glucose Monitoring", **Biosensors and Bioelectronics,** 2019, 137, 25-32.

4. Mohamed Elsherif, Muhammed Umair Hassan, Ali K. Yetisen, and Haider Butt, "Real-Time Fiber Optic Sensors based on Light Diffusing Microlens Arrays", **Lab on a Chip,** 2019, 19, 2060-2070.

Abbreviations

PBAs	Phenyboronic acids	PC	Photonic crystal

1D	One-dimensional	4-VBPA	4-vinylphenylboronic acid
2D	Two-dimensional	3-PBA	3-(acrylamido) phenylboronic acid
3D	Three-dimensional	PBS	Phosphate buffer saline
LDMs	Light diffusing microstructures	pK_a	Dissociation constant
SPR	Surface Plasmon resonance	KBr	Potassium bromide
ICU	Intensive care unit	5A-2F-PBA	5-amino-2-fluorophenylboronic acid
CGM	Continuous glucose monitoring	NA	Numerical aperture
CCAs	Crystalline colloidal arrays	FBG	Fiber Bragg Grating
PMMA	Polymethyl methacrylate	UV	Ultraviolet
HEMA	2-Hydroxyethyl methacrylate	LPG	Long period grating
FDA	Food and drug administration	*T*	Transmission
PA	Polyacrylamide	CO_2	Carbon dioxide
PET	Polyethylene terephthalate	CVD	Chemical vapor deposition
PVA	Poly vinyl alcohol	TOP	Tapered optical fiber
PDMS	Polydimethyl siloxane	OPL	Optical path length
BCR	Base curve radius	FBI	Fabry-Perot interferometer
CT	Center thickness	MZI	Mach-Zehnder interferometer
Na	Sodium	SMF	Single mode fiber
K	Potassium	MMF	Multimode fiber
Mg	Magnesium	MI	Michelson interferometer
Ca	Calcium	RI	Refractive index
Cl	Chlorine	SI	Sagnac interferometer
FRET	Forster resonance energy transfer	TM	Transverse magnetic
Ti	Titanium	LSPR	Localized surface plasmon resonance
Pb	Lead	PMBA	p-mercaptophenyl boronic acid
Pt	Platinum	AFFD	axisymmetric flow focusing microfluidics device
Ag	Silver	µm	Micrometer
Au	Gold	mM	Millimoles per Liter

MPC	2-methacryloyloxyethyl phosphorylcholine	nM	Nanometer
LED	Light emitting diode	min	Minute
PS	Photonic microstructure	s	Second
PCCA	Polymerized crystalline colloidal array	PHS	Photonic hydrogel sensor
P	Optical power	MBA	Mercaptophenyl boronic acid
BIS	*N*,*N*'-methylenebisacrylamide	PBG	Photonic band gap
AA	Acrylamide	IO	Inverse opal
DMSO	Dimethyl sulfoxide	P_{tmax}	Maximum optical transmitted power
DEAP	2,2-diethoxyacetophenone	KPa	Kilopascal
SERS	Surface enhance Raman scattering	P_t	Profile of the optical transmitted power
µW	Microwatt	P_r	Maximum optical reflected power
ml	milliliter	Mw	Molecular weight
L_t	Maximum transmitted illuminance	mol	Mole
PEGDA	Polyethylene glycol diacrylate	vol	Volume
dB	Decibel	EDH	Ethanol dehydrogenase
v/v	Volume to volume ratio	NAD^+	Nicotinamide adenine dinucleotide
LOD	Limit of detection	w/w	Weight to weight ratio
EGDMA	Ethylene glycol dimethacrylate	DI	deionized
2-HMP	2-hdroxy-2-methylpropiophenone	M	Glucose concentration

Nomenclature

λ	Free space Wavelength
θ_d	Diffraction angle
n_{eff}	Effective refractive index

α	Forward Debye diffraction angle
D	Diameter of Debye ring
n_{co}	Refractive index of the optical fiber core
n_{cl}	Refractive index of the optical fiber clad
V	Normalized frequency
Λ	Periodic constant
d_p	Penetration depth
θ_i	Incidence angle
δ	Optical phase difference
n	Refractive index
B	Birefringent coefficient
n_s	Effective refractive index of the slow mode
n_f	Effective refractive index of the fast mode
K_{sp}	Propagation constant of the surface Plasmon wave
K_o	Propagation constant of the incident light in free space
ε_s	Dielectric constant of the dielectric material
ε_m	Dielectric constant of the metallic layer
S	Sensitivity
L_d	Decay length of the electromagnetic waves
Δn	Refractive index shift
$\Delta\lambda$	Wavelength shift
θ_c	Critical angle
d_m	Thickness of the surrounding medium
λ_{res}	Resonance wavelength
l	Zero-first order interspace
m	Diffraction order
h	Distance between the sensor and the imaging screen
$\Delta\Lambda$	Change of the periodic constant
$\Delta\theta_d$	Change in the diffraction angle
d	Interspace among the particles
λ_m	Wavelength of the m^{th} cladding mode
L_g	Grating length
D_c	Coupling coefficient
V_{cl}	Normalized frequency of the fiber clad
L_c	Length of the cavity
δ_{SI}	Phase of interference in Sagnac interferometer
L	Length of the sensing fiber

Chapter 1: Introduction

1.1 Background

The human lifespans are increasing worldwide, which put more burden on the global healthcare systems. For example, by 2020 about 720 million people will be aged 65 or elder [1]. Also, four out of five people who are over the age of 75 will be taking at least one prescribed medicine [2]. Hence, the global healthcare systems under pressure for providing drugs and developing novel diagnostic techniques. Reliable medical diagnosis tests which are portable, available at low-cost, and offer rapid response are considered the first line of defense in healthcare systems. Currently, there are two universal assays that combine the advantages of compact size, light in weight, and provide qualitative results. Theses assays are known as dipstick and lateral-flow [3]. However, existing assays have limitations in quantification of analytes concentrations where samples preparation and further improved sensitivity are required.

The developing world has a shortage in trained healthcare personnel's, and limited basic healthcare infrastructure [4]. Hence, developing simple, low-cost, and reliable diagnostic tests are going to have a great impact, particularly on the local communities in developing regions. The impact will not only be limited on improving the healthcare but also on the environmental safety, animal health, and food quality [5-7]. In the poverty struck regions of the developing world, the medical diagnostics are outdated. However, physicians are obligated to make decisions based on the symptoms in absence of the diagnostic facilities. The symptoms method has limitations in detecting multiple infections, identifying the

disease window period, and distinguishing asymptomatic diseases [3]. Eventually, the deficiency in diagnostic tests results in an irreversible negative influence on developing economies. For example, the epidemic of Ebola has hit West Africa overwhelming the healthcare systems of Liberia, Sierra Leone, and Guinea [3]. Such outbreaks have catastrophic consequences on the emerging economies. Based on the symptoms it is difficult to distinguish Ebola from fever, malaria, or typhoid fever. Currently available laboratory techniques to diagnose these diseases are based on transcription polymerase chain reaction and quantitative PCR, which are nonportable and unaffordable in the developing countries [3]. On the other hand, portable, cost-effective tests suffer from poor sensitivity and selectivity, which might misdiagnose patients, putting the healthcare systems at risk. Epidemic of Ebola is an example of many difficulties that healthcare systems face and the Ebola highlights the great need for developing low-cost, portable, and rapid diagnostic devices. Besides, the medical diagnostic applications of the rapid tests, such assays are beneficial in environmental monitoring, and food quality testing. Rapid diagnostics tests would allow investigating the quality of products of farmers and entrepreneurs. Also, they can help in evaluating the potential risks due to enterhemorrhagic strain of E. coli, and Salmonella in undercooked meat and livestock products [7]. Furthermore, rapid diagnostic techniques are required to investigate the water supplies. In 2010, at Haiti after the earthquake, the epidemic of Cholera highlighted the inadequate environmental facilities [8]. The Cholera epidemic was not expected as Haiti was last out of 147 countries surveyed in 2002 Water Poverty Vortex [9]. Developing rapid and cost-effective diagnostic techniques are going to help in screening populations and large regions. The cost-effectiveness of the rapid diagnostic techniques is the priority; however, a reliable performance from these assays

is required. Also, desirable features such as functioning for small sample volume, portability, and cost-effectiveness have to be considered.

Smart hydrogels have emerged as a strong candiadte for developing rapid, cost-effective, and portable sensors which can be used in the field. The hydrogels are a class of polymers that absorb a large amount of water/aquious solutions meanwhile maintaining their structure and they can be considered as 3D networks of molecules with intermediate pores which are connected [10]. The water content in the hydrogel must be at least 10% of the total volume of a material to be a hydrogel. The hydrophilicity of the hydrgels is due to the presence of hydrophilic groups such as hydroxyl, amide, carboxyl, and sulfonic [11]. Smart hydrogels undergo a volumetric phase transition (swelling or deswelling) in response to certain physical and chemcal stimuli. The volumetric transtion may occure due to physical stimuli such as temperature, light intensity, pressure, and electromagentic fields, and also due to chemical stimuli such as ions concentrations, pH, protiens, glucose, and lactate. In most cases, hydrogels return to their intial volumetric state as soon as the trigger is removed. The hydrogel constituent monomer, charge density, and the degree of crosslining, determine the response of the hydrogels for external stimuli, in addition to the magnitude of the applied external stimulus.

To elaborate the sensing principle of the hydrogels, we consider the example of pH-responsive hydrogels. The pH responsive hydrogels must contain hanging acidic groups such as caroxylic, or sulfonic acids, or basic groups such as ammonium salts [11]. These groups respond to the change in pH by gaining or lossing protons. One of the well know pH sensitive hydrogel is poly(acrylic acid) (PAA). PAA depronates in basic pH medium, consequently

electrostatic repulsion force is generated among the pendant charged groups in the hydrogel network, which allow water molecules to penetrate the hydrogel causing swelling of the hydrogel. However, PPA pronates in acidic pH environment causing a reduction in the charge density in the hydrogel network leading to deswelling of the hydrogel volume.

1.2 Motivation

Diabetes is a significant global health challenge caused by either a deficiency or resistance to insulin. This epidemic is affecting more than 382 million people worldwide and this figure is on the rise. Diabetes has an annual cost burden of $245 billion for the United States healthcare system [12]. Diabetes as a chronic illness requires frequent monitoring of blood glucose concentration to manage insulin administration. Fluctuations of glucose concentration in blood may result in diabetic ketoacidosis that can lead to a seizure. Long-term complications of diabetes include neuropathy, cardiovascular diseases, kidney failure, and limb amputation. Hyperglycemia may be found in intensive-care patients even in those without a clinical history of diabetes such as patients of high-degree burns, trauma, hypoxia, sepsis, and shock as the stress of acute illness induces glucose production, insulin resistance, and relative insulin deficiency. A strict blood glucose management for the patients with acute illness or in the intensive care unit (ICU) decreases the risk of morbidity and mortality. A recent economic analysis of conventional and intensive glucose concentration management in ICUs has demonstrated a significant reduction in the overall medical care costs. The strict control of glucose concentration for acute illness saved around $1580 per adult patient resulting from shorter ICU periods, lower hospitalization rates, curtailment of the ventilator-

dependent days, and cutting down of the laboratory costs [13]. Therefore, tight control of glycemia might provide favorable results in terms of clinical outcome and cost-effectiveness.

The concentration of glucose is typically monitored by using fingerstick blood samples. Patients on multiple-dose insulin injection or insulin pump therapy should measure their blood glucose concentration 6-8 times a day. However, the test is performed more infrequently due to the pain and inconvenience associated with fingerstick, particularly among children with type 1 diabetes. Another strategy is to use subcutaneously inserted electrochemical sensors for continuous glucose monitoring (CGM) systems (e.g., Dexcom, Medtronic, and Freestyle Libre). These devices are designed to provide real-time, long-term measurements and it can also be used with insulin pumps to form an automated feedback loop to manage insulin delivery when hypo/hyperglycemia is developing. However, commercial CGM systems do not completely provide a solution for uncontrolled glycemic fluctuations due to low patient compliance [14]. Calibration of CGM systems is required at least 3-4 fingerstick blood tests per day. These devices are subject to signal drift due to electrochemical reaction instability resulting in time lags and sensor replacement every 3-7 days [15]. Therefore, the development of minimally-invasive continuous monitoring systems that can accurately measure the blood glucose concentration for long periods without necessity for frequent calibrations and replacement is an unmet need in diabetes care.

To overcome the instability issues with electrochemical sensors, alternative approaches involving phenylboronic acid (PBA) derivatives and optical sensors have emerged. Functionalizing hydrogels with PBA that exhibits affinity to cis-diol containing molecules can be exploited for developing glucose sensor capable of continuous monitoring. The

reversable binding of PBA with glucose alters the volume of the hydrogel matrix. This mechanism of volumetric changes in glucose-sensitive hydrogels has motivated the production of optical glucose sensors. For instance, optical hydrogel glucose sensors containing three- dimension crystalline colloidal arrays (CCAs) have been developed based on PBA derivatives [16]. Also, one-dimension holographic grating and two-dimension CCAs have been developed [17, 18]. However, the fabrication process is time-consuming, and complex. In addition, the sensor readout is complicated, required bulky instruments, signal processing, and expensive devices. These restrictions impeded the mass production and commercialization of the optical hydrogel sensors.

1.3 Research aims and objectives

The overall aim of this research is to develop minimally-invasive optical biosensors that are capable of continuous monitoring of glucose concentrations and other analytes. The developed sensors will overcome many limitations of the previously reported optical biosensors in terms of robust performance, easiness of fabrication and readout, portability, and compatibility with smartphones. In order to achieve this aim, novel optical transducers will be introduced to monitor the volumetric shifts of the stimuli-responsive hydrogels. These new transduction systems will expedite the fabrication process, and facilitate the readout methodology to be compatible with handy-held and portable readers such as smartphones. For minimally-invasive sensors, smart contact lenses for glucose concentration monitoring will be developed, and will be tested in artificial eye tears under the physiological conditions. For invasive or implantable biosensing, fiber optic probes will be produced for glucose, alcohol, and pH measurements. Performance of the sensors will be investigated in

transmission and reflection configurations. Swelling kinetics and reusability of the sensors will be checked. Potential interference of biomarkers such as lactate will be studied. Influence of the environmental parameters such as temperature, and pH will be studied. In addition, smartphones will be employed to record the output optical signals.

1.4 Thesis organization

This thesis is written according to the alternative format as each published paper is a separate chapter. General abstract and conclusion for the whole thesis is presented as well. The four published papers represent the chapters from 3 to 6. A visual representation of the thesis structure is shown in the flowchart below.

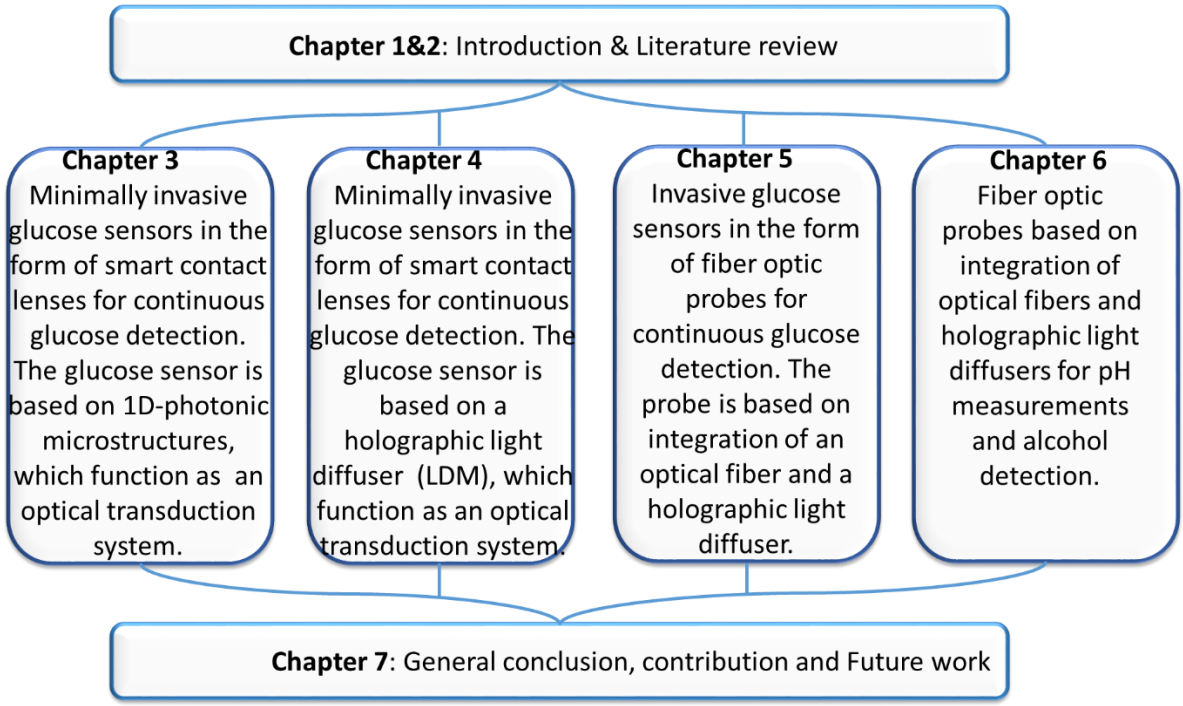

References

1. C. Hagist and L. Kotlikoff, "*Who's going broke? Comparing growth in Public Healthcare Expenditure in ten OECD countries*," Hacienda Publica Espanola/Revista de Economia Publica, 2009. **188** (1): p. 55-72.
2. G. Britain, *Medicines and Older People: Implementing Medicines-related Aspects of the NSF for Older People; National Service Framework*. Department of Health, 2001.
3. A. K. Yetisen, "Holographic Glucose Sensors," in *Holographic sensors*: Springer, 2015, pp. 101-134.
4. J. N. Nkengasong *et al.*, "*Critical role of developing national strategic plans as a guide to strengthen laboratory health systems in resource-poor settings*," American Journal of Clinical Pathology, 2009. **131** (6): p. 852-857.
5. G. M. Carr and J. P. Neary, *Water quality for ecosystem and human health*. UNEP/Earthprint, 2008.
6. T. Aluwong and M. Bello, "*Emerging diseases and implications for Millennium Development Goals in Africa by 2015-an overview*," Veterinaria italiana, 2010. **46** (2): p. 137-145.
7. WHO, "Global Strategy for Food Safety: safer food for better health," ed: Food Safety Programme Geneva, 2002.
8. D. Butler, "Cholera tightens grip on Haiti," ed: Nature Publishing Group, 2010.
9. P. C. Webster, "Lack of clean water exacerbates cholera outbreak in Haiti," ed: Can Med Assoc, 2011.
10. O. Wichterle and D. Lim, "*Hydrophilic gels for biological use*," Nature, 1960. **185** (4706): p. 117-118.
11. M. Bahram, N. Mohseni, and M. Moghtader, "An introduction to hydrogels and some recent applications," in *Emerging concepts in analysis and applications of hydrogels*: IntechOpen, 2016.
12. C. f. D. Control and Prevention, "*National diabetes fact sheet: national estimates and general information on diabetes and prediabetes in the United States, 2011*," Atlanta, GA: US Department of Health and Human Services, Centers for Disease Control and Prevention, 2011. **201** (1): p. 2568-2569.
13. J. S. Krinsley and R. L. Jones, "*Cost analysis of intensive glycemic control in critically ill adult patients*," Chest, 2006. **129** (3): p. 644-650.
14. C. Yang, C. Chang, and J. Lin, "*A comparison between venous and finger-prick blood sampling on values of blood glucose*," International Proceedings of Chemical, Biological and Environmental Engineering, 2012. **39**: p. 206-210.
15. V. R. Kondepati and H. M. Heise, "*Recent progress in analytical instrumentation for glycemic control in diabetic and critically ill patients*," Analytical and bioanalytical chemistry, 2007. **388** (3): p. 545.
16. M. Ben-Moshe, V. L. Alexeev, and S. A. Asher, "*Fast responsive crystalline colloidal array photonic crystal glucose sensors*," Analytical chemistry, 2006. **78** (14): p. 5149-5157.

17. A. Domschke, W. F. March, S. Kabilan, and C. Lowe, "*Initial clinical testing of a holographic non-invasive contact lens glucose sensor*," Diabetes technology & therapeutics, 2006. **8** (1): p. 89-93.
18. F. Xue, Z. Meng, F. Wang, Q. Wang, M. Xue, and Z. Xu, "*A 2-D photonic crystal hydrogel for selective sensing of glucose*," Journal of Materials Chemistry A, 2014. **2** (25): p. 9559-9565.

Chapter 2: Literature review

2.1 Contact lenses

2.1.1 Origin of Contact lenses

A contact lens is a thin curved layer of a soft or a rigid transparent material and is worn on the eye cornea. The contact lens material is quite clear, but it is often slightly tinted to make them easier for wearers to handle. However, contact lenses may seem modern addition to eyecare, they have a long development history starting from the sixteenth century [1]. In 1508, Leonardo da Vinci produced sketches proposing possible solutions for vision correction. He demonstrated that seeing through the bottom of a glass bowel filled with water could help to rectify the vision correction; however, his suggestion was impractical (Figure 2.1a) [2]. Later, in the seventeenth century, René Décrates introduced the concept of using a test-tube filled with water to achieve similar results to Leonardo da Vinci (Figure 2.1b). His suggestion of using a tube over an entire bowel of water was simpler, although still impractical solution. The first practical contact lenses were made of blown glass in 1887 and it was covering the whole eye surface [2]. Although, these lenses were beneficial for correcting vision, many issues were concerned. The lenses were made of glass, so they were heavy on the eye especially after wearing them for few hours. In addition, the thick glass material is not oxygen- permeable, which makes these lenses harmful for the eye cornea. In 1940s, hybrid contact lenses made of glass and polymer (Poly (methyl methacrylate) were introduced. The glass portion covered the cornea and the white of the eye (sclera) was covered by the polymethyl methacrylate (PMMA). These lenses were lighter and allowed

more oxygen permeability. Later, the lens design was transformed into the next stage; the lens covered only the cornea of the eye and the sclera was left free to breadth naturally. These lenses were small; however, PMMA is non-porous. Oxygen could reach the cornea only during blink as the lenses move, and hence the lenses could be worn for longer periods without causing irritation. A massive breakthrough in contact lenses manufacturing was made by Czech chemist Otto Wichterle by creating the first soft hydrogel contact lens. The lens were made of poly (2-hydroxethyl methacrylate) which is capable of absorbing up to 40% of water, transparent, and could be moulded into a comfortable lens shape [3]. In early 1970s the first commercial soft contact lenses were released after they received the Food and Drug Administration (FDA) approval. Since then, soft contact lenses were subjected to developments to increase their oxygen permeability and water absorption properties. In the late 90s and early 2000s, silicon hydrogel became the material of choice for most contact lens manufacturers [4]. Silicon hydrogel lenses allowed up to five times more oxygen permeability, which helped to keep the eye hydrated, healthy, and comfortable for longer times than before.

Commercially available contact lenses can be classified into three categories according to their constituent materials: i) soft contact lenses such as poly (2-hydroxy ethyl methacrylate) (HEMA), polyacrylamide (PA), polyethylene terephthalate (PET), poly (vinyl alcohol), and polydimethylsiloxane (PDMS), ii) rigid contact lenses such as poly (methyl methacrylate), iii) hybrid contact lenses, which combine soft and rigid materials; a center rigid gas permeable portion with an outer skirt made of soft lens material. Among these contact lenses,

soft lenses are the most commonly used in the integrated diagnosis technology because of their high oxygen permeability combined with user comfortability and usage prevalence [5].

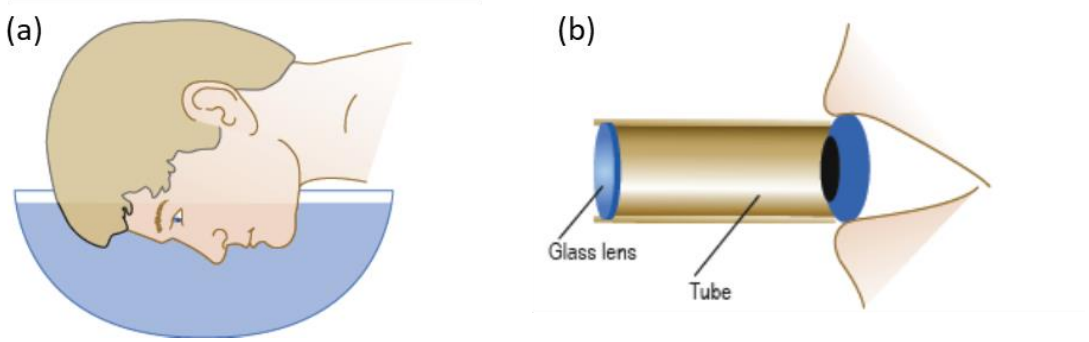

Figure 2.1. Schematics show the proposed ideas to modify the corneal power. (a) Idea of Leonardo da Vinci that shows a man looking through a bowel filled of water). (b) Idea of Rene Descartes that shows a man looking through a tube filled with fluid [6].

2.1.2 Contact lens design

In designing the contact lenses many parameters must be considered. The contact lenses have to be fabricated with base curve radius (BCR) which is in the range of 8-10 mm, to fit comfortably the eye cornea and to facilitate the tear exchange and oxygen permeability [7, 8]. Contact lenses are produced with a range of diameters of 14-15 mm to fit different eye sizes easily. The center thickness (CT) of the contact lens is a significant parameter as the oxygen permeability depends on it. Most of commercial contact lenses are produced with CT of about 0.1 mm [9]. Optical power of the contact lens is the responsible factor for the vision correction and it measures the degree to which the lens converges the light. The lens's optical power is given by the reciprocal of the focal length and its SI unit is inverse meter (m^{-1}), and is called diopter [10].

The worn contact lenses are subjected to stresses resulting from eye movements and repeated usage that might cause irreversible deformation or fracture, leading to deteriorating the

optical performance, and the comfort. Hence, the mechanical properties of the contact lens such as Young's modulus, and tensile strength have to be optimized [11].

The transparency of the contact lens material that allows the incident light to go through the lens to be focused in the eyes, is significant beside the relatively high refractive index. Chemical properties of the contact lens material such as water content, free-to-bound water ratio and biological inertness also affects the lens performance [12, 13].

2.1.3 Eye tear fluid

Intense investigations have been carried out for decades to find an alternative non-invasive human fluid (e.g. interstitial fluid, eye tears, salvia, and urine) to replace the blood samples in the clinical diagnosis. However, human fluids could not be an alternative for the blood samples except in very few cases such as in diagnosing the bladder cancer [14]. In the bladder cancer, urine is the ideal sample for diagnosing due to its direct contact with the morbid tissue [15].

Among the body fluids, eye basal tear fluid is a complex multilayer of fluid contains enzymes, proteins, lipids, and salts [1]. The basal tears encompass three layers which serve to protect, clean, and lubricate the eye. Also, the eye produces psychic tears resulting from laughing or crying and reflex tears from irritating conditions. Tear and blood are separated by a barrier, which makes a compositional difference between blood and tear fluid [16]. The blood supplies the brain pass through this barrier, hence certain metabolites leak from the blood to the tears. Therefore, a relationship is established between the concentrations of these metabolites in blood and tears, and the tear fluid can be used as a proxy to analyze

blood compositions [17-19]. Composition of some metabolites in eye tears and blood are shown in Table 2.1. It was found that concentration of glucose, lactate, Na^+, K^+, Mg^{2+}, Ca^{2+}, Cl^-, and urea are correlated with their counterparts in blood [19-21]. Also, the number of proteins detected in eye tears was in the range of 54 -1543 as their figure was strongly dependent on the sampling method [22].

Contact lenses which are in direct contact with eye tears can be functionalized or integrated with small sensors to continuously detect different metabolites to diagnose diseases based on the detected biomarkers, Table 2.1 summarizes some examples.

Table 2.1. Shows the different biomarkers which are present in both tear fluid and blood, their concentrations in each are given in millimolar, and the possible biomedical application of monitoring these biomarkers.

Analyte	Tear con.(mM)	Blood con. (mM)	Diagnostic disease	Reference
Glucose	0.01-0.05	3.3-6.5	Diabetes	[23]
Lactate	2.0-5.0	0.36-0.75	Cancer, sepsis, ischemia, and liver disease.	[24]
Urea	3.0-6.0	3.3-6.5	Renal function	[25]
Dopamine	0.37	$475x10^{-9}$	Glaucoma	[26]
Proteins	7 g/L	7 g/L	Dry eye syndrome	[27]
Pyruvate	0.05-0.35	0.1-0.2	Genetic disorders of mitochrondrial energy metabolism	[28]
Ascorbate	0.22-1.31	0.04-0.06	Diabetes	[29]
Na^+	120-165	130-145	Hypo/hypernatremia	[30]

2.1.4 Advantages of contact lenses as wearable medical diagnosis devices

Conventional diagnosis devices require blood or serum sampling, which is considered invasive, painful, inconvenient, and accompanied by the risk of infection. In addition, most of these devices are complicated, expensive, invasive, and immobile, hence they cannot be used at point-of-care-settings. Moreover, they are not prepared for continuous sensing over 24 h which is recommended for some diseases such as diabetes and glaucoma. In contrast, contact lenses combine many features that make them ideal medical devices for biosensing applications. In the United States, 45 million people were relying on contact lenses daily in 2016 and this figure has been increasing reflecting the popularity of contact lenses [31]. Also, contact lenses provide physical contact with eye tears and human tissues for long periods. In addition, the contact lenses are small in size, light in weight, cost-effective, portable, and are counted as minimally-invasive devices with the capacity on the integration with an assortment of sensors. The intimate relationship among the eye parts and contact lenses gave possibility to develop lenses as ideal continuous biosensors.

2.2 Contact lenses biosensors

The search on biomarkers in tear fluid which are correlated with various diseases is ongoing. Biomarker- responsive sensors can be integrated with contact lenses for developing diagnostic medical devices to be beneficial in continuous monitoring at point-of-care settings. For example, smart contact lenses for continuous glucose detection, and another for glaucoma monitoring are under development. Currently, researchers are investigating the fluid tear for healthy people and cancer patients to establish a relationship among the biomarkers and the different types of cancers. For instance, Evans et al. reported a

relationship between levels of lacryglobin in tears and the breast cancer [32, 33]. The group tested the tear samples collected from patients who suffer from different types of cancers. Lacryglobin was detected in tears of patients suffering with lung, colon, prostate, ovarian, and breast cancers. This study demonstrated that eye tears can provide a non-invasive investigation of cancer. Another study by Lebrecht et al, showed possibility of differentiation of patients suffering from breast cancer among the control subjects based on analysis their eye tears [34]. Several breast cancer biomarkers were detected in eye tears such as protein S 100A8 and triosephsphate isomerase as the concentration of these biomarkers were different in cancer patients compared to normal people. Also, L-lactate concentration in tear fluid was found to be correlated with different types of cancer [24].

In fact, limited number of studies focused on investigating possible biomarkers in eye tears which correlated with cancers. In addition, many types of cancers were found to share the same biomarkers making pinpointing a specific type of cancer based on tear analysis only a challenge. However, it is noteworthy to measure the susceptibility of cancer at early stages, so that the physicians can provide care early.

This section focuses on contact lenses integrated biosensors for continuous glucose detection based on various detection methods including electrochemical, fluorescent, and light diffraction.

2.2.1 Fluorescence-based contact lenses for glucose detection

Fluorescence denotes the light emission from a substance shortly after absorbing light of a higher energy. This phenomenon occurs when an incident light in the wavelength range from

200 nm to 800 nm is absorbed by fluorescent molecules raising certain electrons to a higher energy level [35]. Then, the excited molecule loses some of the absorbed energy by emitting light returning to the ground state. Some of the absorbed light is lost in form of heat or vibration, consequently the emitted light has lower energy than of that absorbed. The electronic transition from an energy level to a higher level resulting from light absorption is near instantaneous process (10^{-15}s) and the lifetime of the excited state is around 10^{-8} s. Accordingly, the whole process of fluorescence emission last about 10^{-8} s [36].

The fluorescent molecules are called fluorophores and the excited fluorophore can lose the absorbed light not only by re-emission, heat, or vibration but also by transferring the energy to another fluorophore nearby. In case, a portion of the exiting energy is transferred from a donor fluorophore to a ground state of an acceptor fluorophore, the process called Forster resonance energy transfer (FRET) [37]. The portion of the transferred exciting energy depends on the spectral overlapping between fluorophores and the interspace between the fluorophores [38]. Forster resonance energy transfer is considered a suppression process for the energy absorbed by the donner as the energy drains to an acceptor fluorophore nearby.

A fluorescence-based sensor can be constructed of a certain analyte-receptor/molecular recognition agent, a donor fluorophore, and an acceptor fluorophore, all in the vicinity of each other. Once the analyte binds with the receptor, the receptor is subjected to a chemical structural change shifting the fluorophores farther apart limiting transferring electrons to the acceptor fluorophore. Consequently, the FRET is decreased leading to an increase in the fluorescent emitted light which is correlated to the analyte concentration (Figure 2.2a). An additional mechanism can be used for fluorescent sensors; a receptor/molecular recognition

agent which competitively binds with the analyte and fluorophore can be utilized [39]. This case, the fluorophore binds with the receptor, the electrons transfer from the fluorophore to the receptor and the fluorophore re-emits light. However, existence of the analyte induces separation of the fluorophore from receptor and the energy levels of the fluorophore are full of electrons, hence no fluorescence occurs. Therefore, in this mechanism the higher the analyte concentration, the lower the fluorescence emission [40].

Fluorescent sensors have been utilized in various applications due to their versatility, sensitivity, and selectivity. Fluorescent glucose sensors were integrated to contact lenses for continuous glucose detection in the tear fluid. For instance, March et al, developed fluorescent glucose sensors based on a fluorophore and a glucose recognition agent trapped in hydrogel spheres that were inserted into the soft contact lens (PVA) (Figure 2.2b-c) [41]. When glucose molecules reacted with the glucose receptor, the fluorophores shifted away from the receptor, and as a result there was a decrease in Forster resonance energy transfer (FRET) and an increase in the fluorescence light with increasing glucose concentrations. However, a 15 min delay in the glucose concentration readouts were observed. Interestingly, the sensor was compatible with a hand-held fluorometer to collect the sensor's output signal. Also, pHEMA and PDMS -contact lenses have been integrated with fluorescent glucose sensors. The glucose-responsive molecules and an organic fluorescent dye were encapsulated in silica nanoparticles and embedded in the contact lenses. The silica retained the capsule shell integrity and prohibited the leakage. The contact lenses were able to detect glucose concentration in the range of 0.5–5 mM [42]. A daily disposal commercial contact lens was integrated with a fluorescent glucose sensor based on boronic acid-containing fluorophores.

The glucose concentration range of 50-500 µM was detected by the contact lens and the equilibrium time was around 10 min. The pH, chloride, and polarity changes were found to be interfering with readings [43, 44].

A variety of fluorescent sensors were developed and integrated with contact lenses to monitor many other biomarkers in tears. For example, Lakowicz and his group developed ion sensors (Cl^-, K^+, Na^+, Ca^{2+}, and Mg^{+2}) based on the fluorescence phenomenon, and integrated these sensors in silicon commercial lenses for long term sensing of dry eye syndrome (Figure 2.2d-e) [45]. These proof of concept studies paved the way for more fluorescent probes to be coupled with contact lenses and utilized for monitoring biomarkers present in tear fluid such as lactate, potassium, magnesium, sodium, and urea. Hence, diseases can be diagnosed through non-invasive assays.

Disadvantageously, fluorescent glucose sensors suffer from high intensity background fluorescence which commonly exists in biological media. The fluorescence-based molecular recognition agents are influenced by the ambient oxygen concentration and the temperature. The fluorophores have low chemical stability due to the photodegradation [46]. Furthermore, some fluorescence receptors require the presence of solvents to function [47].

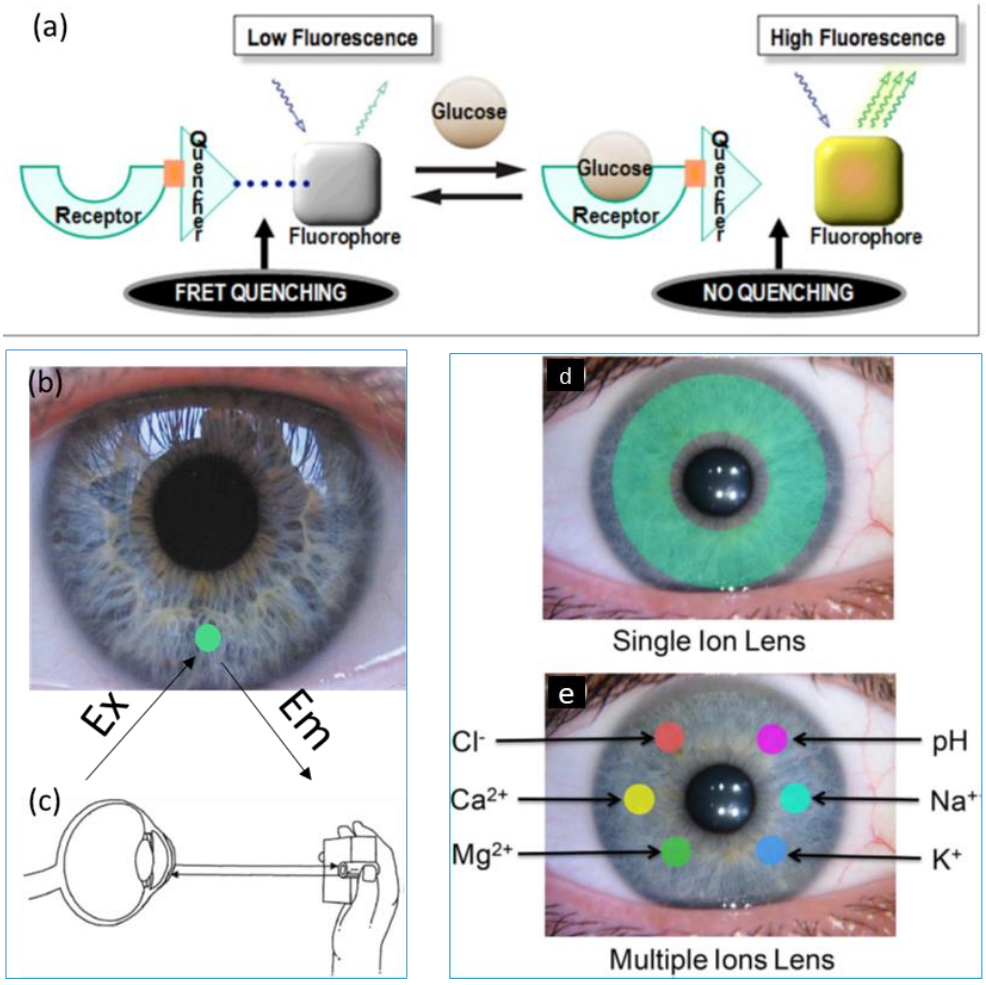

Figure 2.2. Fluorescence based biosensors. (a) Working principle of the fluorescent glucose sensor based on Forster energy transfer. (b) Fluorescent sensor attached to the surface of the contact lens. (c) Schematic of the readout device that can be utilized to interrogate the glucose sensor. (d) Contact lens covered with a skirt of a single ion fluorescent sensor. (e) Different fluorescent ion sensors spots on the surface of a contact lens [44, 45].

2.2.2 Electrochemical contact lenses sensor for glucose detection

Electrochemical sensors have been developed for medical diagnosis over the last few decades. Semiconductor fabrication technique beside many other fabrication techniques were employed for producing the electrochemical sensors [48]. Traditionally, electrochemical sensors are constructed from three electrodes; reference, working, and counter electrodes. Electrochemical sensors are produced for detecting various biomarkers such as glucose,

lactate, uric acid, cholesterol, dopamine, and drugs [49-52]. Commonly, enzymes are used in these sensors as the enzymes provide selectivity and rapid response. For example, the enzyme, glucose oxidase, is used in glucose detection where the enzymatic reaction converts glucose into gluoconolactone and hydrogen peroxide. Hydrogen ions, oxygen, and electrons come out of the dissociation process of the produced hydrogen peroxide. The generated electrons are utilized by the three-electrode system to measure the glucose concentration.

Soft contact lenses for glucose measurements in eye tear fluid have been realized by integrating electrochemical sensors with contact lenses [53]. For instance, a three electrode sensor was constructed of titanium, palladium, and platinum electrodes deposited on a polyethylene terephthalate substrate (PET) (Figure 2.3a-c). The spin coating method was used to deposit the photoresist layer (AZ4620) on the PET substrate and was baked at 65 ^{o}C for 20 min, then the mask is applied, and UV exposure was performed for pattering. Three layers of different metals; Ti of 10 nm, Pd of 10 nm, and Pt of 100 nm thickness were deposited by the thermal evaporation process in sequence onto the wafer. The wafer was immersed in acetone for 10 min for the lift-off purpose. Then, the wafer was cut into small pieces which took the contact lens shape under heating. Titania sol-gel layer trapping glucose oxidase was deposited on the contact lens surface. A potential interference of urea, ascorbic acid, and lactate was minimized by using Nafion. In order to test the sensor performance, electrical connections were established by three large pads of 2 mm^2 each and the current flow through the working electrode was recorded. The sensor exhibited a fast response time of 20 s and a low limit of detection lower than 0.01 mM. A sensitivity of 240 $\mu A\ cm^{-2}\ mM^{-1}$ was recorded in the glucose concentration range of 0.1-0.6 mM. Similarly, PDMS contact

lens were integrated with an electrochemical sensor for glucose detection in tears [54]. The sensor combines three electrodes made of Pt, silver, and silver chloride. Fabrication of the sensor has been carried in multi-stages. PDMS layer of 70 µm thickness was prepared on a silicon wafer by spin coating and cured for 30 min at 80 ^{o}C, followed by sputtering 200 nm thick of Pt layer. Thereafter, a silver layer of 300 nm was sputtered to constitute the reference electrode. The electrode system was peeled off the silicon wafer and covered with PDMS layer. The PDMS contact lens was created by molding process and was connected to flexible electrodes by PDMS as a binder. After that, a hydrogel layer was functionalized with glucose oxidase, and was spread on the sensing region. For *in vitro* glucose testing, the contact lens-integrated sensor measured glucose concentrations in the range from 0.03 to 5.0 mM. The in-situ testing was carried out by attaching the contact lens to an eyeball of rabbit and the results were correlated with blood glucose readings resulting from convention glucose devices. Glucose concentrations in both blood and tear were peaked following the oral intake of glucose. The tear glucose showed a delay of 15-20 min compared to the glucose levels in blood and both reach the maximum after 55 min of glucose intake.

Recently, Kim et al, developed a graphene field effect transistor combined with an antenna to function as a glucose sensor. The sensor was integrated with a soft contact lens and operated wirelessly [55]. The lens was tested for glucose quantification *in vitro* and *in vivo*. Glucose oxidase was chemically attached to the pyrene linker, then it was immobilized on the graphene channel. The signal receiver was fixed to be only 10 mm from the contact lens to be able to collect the antenna signals. More recently, a wireless electrochemical glucose sensor with display pixels was incorporated with a soft contact lens for monitoring glucose

concentration in eye tears (Figure 2.3d-e) [56]. At the first time, a display was introduced to the smart contact lens to eliminate the necessity for the bulky equipment used for signal detection. The performance of the lens was tested in a live rabbit eye for glucose concentration in the range of 0.1-0.9 mM. Upon increasing the glucose concentration above the normal levels, the display turned off.

The commercial company, Google, announced on 16 of January 2014 starting work on developing a smart contact lens that could measure glucose concentrations in eye tears continuously. By July 2014, Novartis'Alcon joined the project [57]. The proposed smart lens's prototype included a glucose sensor and a small wireless chip inserted between two layers of a soft lens material (PVA) to be located outside the pupil and iris to avoid eye vision obstruction (Figure 2.4) [58]. In January 2018, Google announced discontinuing the project as they faced various challenges in getting reliable readings from the prototype [59].

Although, the electrochemical glucose sensors incorporated in contact lenses provided many capabilities such as selectivity, high sensitivity, and rapid response, many challenges still have to be overcome to reach practical usage [60]. Electrochemical sensors are based on enzymes which are unstable by nature and suffer degradation in the short lifespan leading to limited function of the sensor for long periods. Furthermore, the operation conditions such as ambient oxygen, pH, temperature, and humidity influence the sensor's performance. Also, sterilizing the smart contact lens according to the health regulations probably leads to the denature of enzymes. Also, interaction of the hydrogen peroxide with tear's ingredients like ascorbic acid interferes with the sensor's response [61]. The microfabrication of the electrochemical sensor on polymer substrates is also a challenge due to the limitations of the

thermal and mechanical properties of the material [62]. The reading out process of electrochemical sensors requires an applied power to drive the chemical reaction which makes fabricating the contact lens integrated with the sensor more challenging. The electrochemical sensor may be made of opaque electronic materials; metal antennas, interconnects, and integrated circuit chips which may block the user's vision. Beside the aforementioned drawbacks, the necessity for costly and bulky instruments for recording the output signals limited applicability of smart contact lenses in the real-life applications [54, 63].

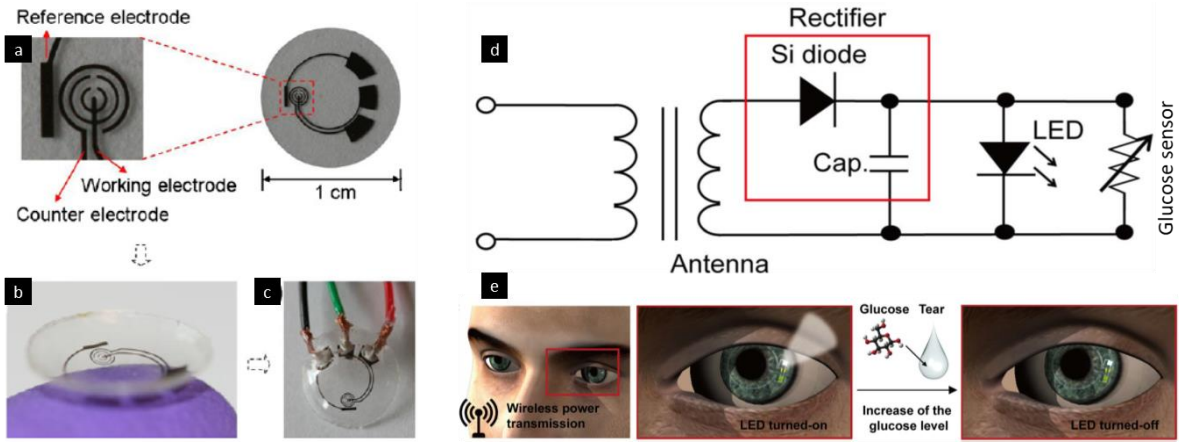

Figure 2.3. Electrochemical sensors integrated with contact lenses. (a) Images for the three electrodes that represent the electrochemical sensor. (b) A photo of the sensor attached onto the contact lens. (c) A photo of the smart lens hardwired for investigation. (d) Schematic diagram of the electric circuit integrated with the contact lens. (e) Schematic shows how the smart lens works as the antenna transmits the electric power into the electric circuit activating the LED and the glucose sensor. The LED turns off whenever the glucose concentration exceeds the threshold level [53, 56].

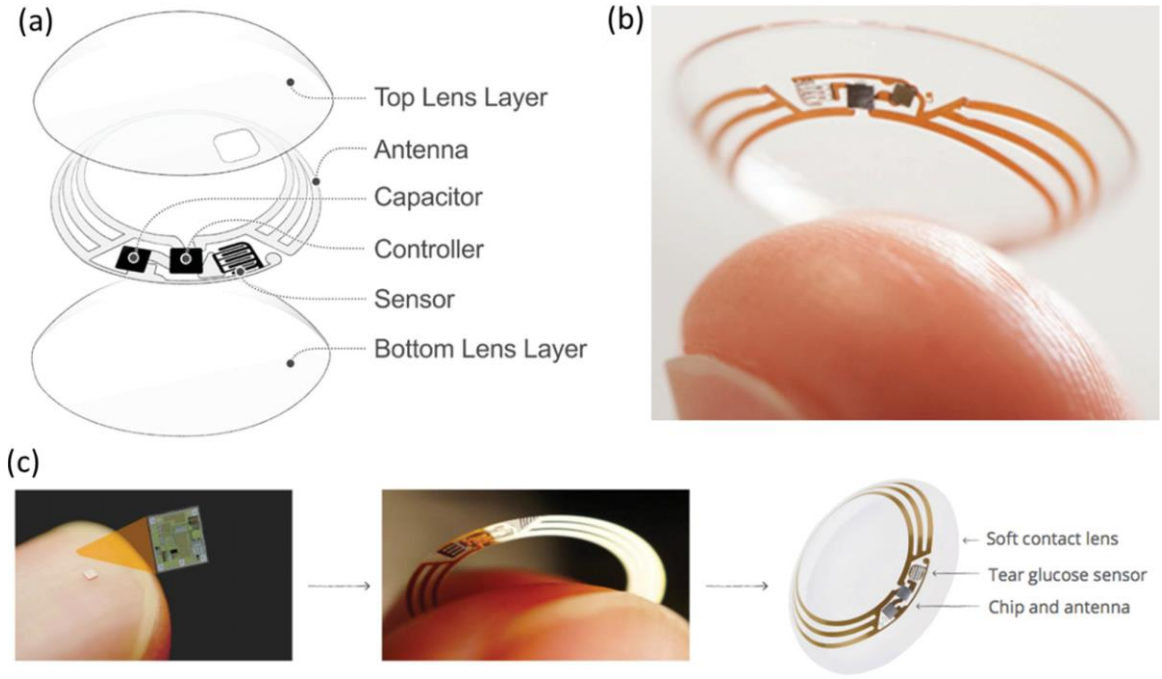

Figure 2.4. A prototype of the contact lens-integrated glucose sensor which was under construction by the giant companies, Google and Novartis. (a) Schematic of the prototype presenting the electrochemical sensor and the electric circuit. (b) Photo of the prototype. (c) The wireless chip sandwiched between the contact lens layers [1].

2.2.3 Photonic band gap-based contact lenses for glucose detection

Photonic crystals (PCs) are formed by periodically ordered materials of different refractive indices, and are classified into 1D, 2D, and 3D PCs, according to the number of periodicity directions [60]. When a photonic crystal is illuminated by a polychromatic beam, the diffracted light follows Bragg's law: $m\lambda_d = 2n_{eff}\Lambda \sin(\theta_d)$, where m is the diffraction order, λ_d represents the diffracted wavelength, n_{eff} is the effective refractive index of the PC, θ_d is the diffraction angle, and Λ is the periodic constant of the PC. Accordingly, the diffracted wavelength changes due to any modification in the periodic constant or the effective refractive index. Based on this principle, 1D- (holographic grating), 2D-, and 3D-PCs have been developed for sensing applications. If the periodicity, Λ , of the PC was

comparable to the visible light range (400-700 nm), the PC diffracts a visible color that can be seen by naked eyes according to the Bragg's law. Hence, PC-based sensors are accompanied with visual color change. Accordingly, PC sensors are a strong candidate to be used at point-of-care settings.

Unlike the electrochemical sensors, most photonic glucoses sensors are based on a phenyboronic acid (PBA) derivative as a glucose recognition element instead of enzymes. PBA derivatives form reversible covalent bonds with *cis*-diol molecules and α-hydroxyl acids such as glucose, and L-lactate, respectively [64]. Studies showed that 1D-hologram gratings (1D-PC) can be fabricated in many natural and synthetic hydrogel matrices which can be functionalized with appropriate receptor systems, for developing hydrogel sensors that can detect a variety of analytes [65]. A glucose-holographic sensor was fabricated of acrylamide functionalized with 4-vinylphenylboronic acid (4-VBPA). The sensor was prepared by the diffusion method and the laser interference technique. Complexation of glucose and the boronic acid moieties immobilized in the hydrogel network caused volumetric shifts of the hydrogel modifying the volumetric state, altering the periodic constant (Λ) and the diffracted wavelength/color [65]. The main concern for this sensor was that it could only work at a high pH [66]. Kabilan et al, created a glucose-holographic sensor based on an alternative phenylboronic acid derivative, 3-(acrylamido) phenylboronic acid (3-PBA) as a glucose recognition agent to develop a glucose sensor that operates at the physiological pH [65]. Its ability to bind with glucose under physiological conditions was attributed to the decrease in the pK_a (dissociation constant) of the 3-PBA, which results from the *meta* position of the acrylamido group on the phenyl ring. The sensor displayed visual,

and reversible response to glucose concentrations under physiological conditions. The prepared sensor appeared green in the reference buffer solution (PBS) and when glucose solution was introduced to the sensor the diffracted light shifted to red. The glucose molecules diffused into the hydrogel sensor to bind with the pendant boronic acid groups resulting in decreasing the pK_a, and allowing it to form the charged tetrahedral phenyl boronate anion [67]. These charged anions generate a Donnan potential, which induces osmotic pressure swelling the hydrogel [68]. The swelling appeared as a change in the diffracted wavelength due to change of the periodic constant of the sensor. Upon removing the glucose solution and washing the sensor in PBS buffer, the sensor returns to its original volume, and hence the diffracted spectrum returns to its original basal diffracted wavelength. Since the binding of the *cis*-diols with boronic acid is reversible, washing out the glucose decreases the concentration of the boronate anions leading to shrinkage the sensor due to the elastic force of the hydrogel network-expelling the water and counterions [69]. The hologram glucose sensor showed a sensitivity of near 18 nm mM^{-1} at glucose range of 0-11 mM. The sensor also showed higher sensitivity for glucose than for lactate. Later, the 1D-hologram sensor was attached to a PVA contact lens and the lens was autoclaved (Figure 2.5a) [70]. Toxicity and performance of the lens as a continuous glucose sensor were examined. The sensitivity of the glucose sensor incorporated in the lens showed a decrease. Meaning the processes of sterilization and incorporation have a negative influence on the sensor's performance. Although, the sensor responded to glucose and the response was reversible, the sensitivity decreased to 4.5 nm mM^{-1}, which is quite low compared to unsterilized conditions. Interrogating of the contact lens was carried out by a white light source connected to an optical fiber and a spectrometer connected to a computer to record the diffracted

wavelengths. The sensitivity of the contact lens must be improved, and a practical detection system must be developed for detecting the low glucose concentrations in eye tears. Another concern about this holographic sensor is the usage of phenyl boronic acid derivative that binds with other biomarkers such as lactate, galactose, fructose, and mannose. Another study on the same sensor considering the response and the equilibrium times, showed that the response time for a glucose concentration less than 1 mM was around 7 min; however, the response time decreased with glucose concentration. The equilibrium time for the sensor was near 50 min and 70 min for high and low glucose concentrations, respectively.

The 1D-hologram sensor was fabricated based on the diffusion method and the laser interference technique requiring 10 steps [65]. The appropriate quantities of the monomer, crosslinker, and photo-initiator were dissolved to prepare the pre-gel solution with the required molar ratios [66-69]. A few microliters of the monomer solution were layered on a chemically treated glass (silanized) substrate and was polymerized by UV for 30 min. The polymerized film was washed in deionized water and it was immersed in silver nitrate solution to allow silver nitrate to diffuse into the polymer. Followed by exposure of the polymer to the solutions of KBr, ascorbic acid, and methanol. Then, the film was rinsed in distilled water and immersed in the hologram exposure bath which contained PBS buffer of pH 7.4. The polymer was exposed to nanosecond laser pulses form a Nd:YAG laser (532 nm), followed by the immersion in the developer solution (ascorbic acid, 4-methylaminophenol sulphate, sodium carbonate, and sodium hydroxide). The fabricated hologram was washed and soaked in stop solution (5% (v/v) acetic acid). Then, the hologram sensor was rinsed and immersed in sodium thiosulphate to wash out the undeveloped silver

bromide. Finally, the hologram was rinsed in methanol and distilled water and stored dry. To conclude, the main concerns about the 1D-holographic grating (1D-PC) sensor is the long response time and the relatively complicated fabrication process.

While Prof. Lowe's group at Cambridge University was developing the 1D-hologram sensors, Prof. Asher's group at Pittsburg University was developing the 3D-PC glucose sensors. The 3D-PC sensor consisted of highly charged nanoparticles (polystyrene or silica) periodically arranged in three dimensions, in a polymer matrix. Asher's group developed 3D-PC glucose sensors based on polystyrene nanoparticles embedded in co-polymerized hydrogel (polyacrylamide-polyethylene glycol) [71]. Two phenyl boronic acid derivatives were attached separately to the hydrogel post the photopolymerization. The sensors were tested in synthetic tear fluids at physiological pH and ionic strength. Binding the glucose with the boronate anions occurred through the formation of a bis-bidentate cross-link, a 2:1 PBA-glucose complex, which shrunk the hydrogel volume resulting in a blue shift in the diffracted wavelengths. The appearance color of the sensor changed and was seen by naked eye to be shifting from red to blue over the physiological glucose concentration range. The selectivity of the sensor for glucose compared to galactose, mannose and fructose was also demonstrated. The sensitivity was close to 14 nm mM^{-1} and the limit of detection was as low as 1 μM in the synthetic tear fluid. Later, the same group promoted the response kinetics of the 3D-PC glucose sensor by copolymerizing *n*-hexylacrylate with the acrylamide polymer matrix and functionalized the sensor by 5-amino-2-fluorophenylboronic acid (5A-2F-PBA) [72]. The sensor showed a response time of 300 s in glucose concentration of 1 mM at pH 7.4 and room temperature (22 ^{o}C). However, the response time shortened with temperature

and glucose concentrations. When glucose concentration was 5 mM, the response time went down to 90 s at 37 $^{\circ}$C. The authors recommended attaching the sensor to a contact lens or inserting the sensor under the lower eyelid. Diabetic patients or sensor wearers could determine the levels of their glucose concentration by observing the color of the sensor using a compact device combines a white light source, a mirror, and a color chart (Figure 2.5b).

Recently, Braun group introduced a 3D-PC hydrogel that linearly and rapidly responded to glucose by implementing a volume resetting agent (poly vinyl alcohol (PVA)) [73]. The acrylamide pre-gel was polymerized with the highly charged polystyrene nanoparticles, followed by attaching the PBA derivative to the hydrogel and the PVA was diffused into the hydrogel as well, to bind with the boronate anions forming crosslinks shrinking the hydrogel. When the hydrogel was exposed to glucose, the PBA-PVA crosslinks were superseded with 1:1 PBA-glucose complexes, resulting in swelling of the hydrogel and subsequently a redshift of the diffracted light. The sensor covered the clinical relevant glucose range (2.2-38.9 mM) presenting a maximum sensitivity of 12 nm mM^{-1} in glucose concentration range of 0-10 mM when 5A-2FPBA was used [74, 75]. However, the best kinetic response was recorded for the 3D-PC glucose sensor functionalized by the 3-PBA as the time needed to reach 90% of equilibrium binding was 7 min and 12 min for glucose concentration range of 0-10 mM and 30-40 mM, respectively. Leakage of PVA from the sensor is expected, which significantly affect the sensor response/sensitivity and reusability. The highly charged, monodispersed polystyrene spheres are synthesized by emulsion polymerization process which takes three weeks, more details of the process can be found in references [56, 61].

More recently, rapid fabrication process of 2D-PC at the air/water interface has been reported [76]. The approach can produce a hexagonal arrangement of nanoparticles of area 280 cm^2 in 2 min. Later, studies showed that these arranged nanoparticles in a monolayer form can be incorporated into stimuli-responsive hydrogels. The forward diffracted monochromatic light passing through the 2D-PC hydrogel shows a Debye diffraction ring which is of a diameter dependent upon the particles interspace and it was exploited to monitor the hydrogel volumetric change. The Debye diffraction follows the formula: $\sin\alpha = 2\lambda/\sqrt{3}\,d$, where α is the forward diffraction angle of the Debye diffraction, d is the interspace among the particles, and λ is the incident wavelength. The forward diffraction angle is given by the relationship: $\alpha = \tan^{-1}\frac{D}{2h}$, where *D* denotes to the diameter of Debye ring and *h* represents the distance between the sensor and the screen. For instance, Xue et al, developed a 2D-PC glucose sensor and was investigated in artificial tears [76]. The sensor was selective for glucose over galactose and fructose at the physiological ionic strength (150 mM) and presented short response time (50 s); however, the sensor was functioning only at high pH. Another 2D-PC glucose sensor has been developed recently for glucose detection in tears which operate in the physiological pH [77]. The sensor showed high sensitivity and short response time 180 s.

The fast fabrication of the 2D-PC enhanced the preparation of the photonic sensors. Although, the diffraction response of the sensor was simple to detect, the approach is not practical especially when the sensor is attached to contact lenses. Because, the contact lens constrains the sensor's expansion/extraction in both x- and y- directions. Hence, the sensor is free only in z-direction. However, the expansion/extraction in z-direction has no effect on

the particles interspace. Consequently, the diameter of the Debye ring does not change even when the volumetric shift of the sensor occurs. In addition, measuring the Debye ring diameter in the transmission configuration is not practical in wearable devices. On top of that the response of the 2D-PC could not be distinguished by naked eye, which may limit its application at point- of-care settings.

Generally, photonic sensors offer inherent merits over their electrochemical counterparts such as the lack of electrical connections, immunity for electromagnetic interference, relatively easier fabrication process, possibility of remote sensing, and cost-effective [65]. Compared to fluorescent glucose sensors, the photonic sensors do not require dyes or fluorophores to operate eliminating the photobleaching issue [60].

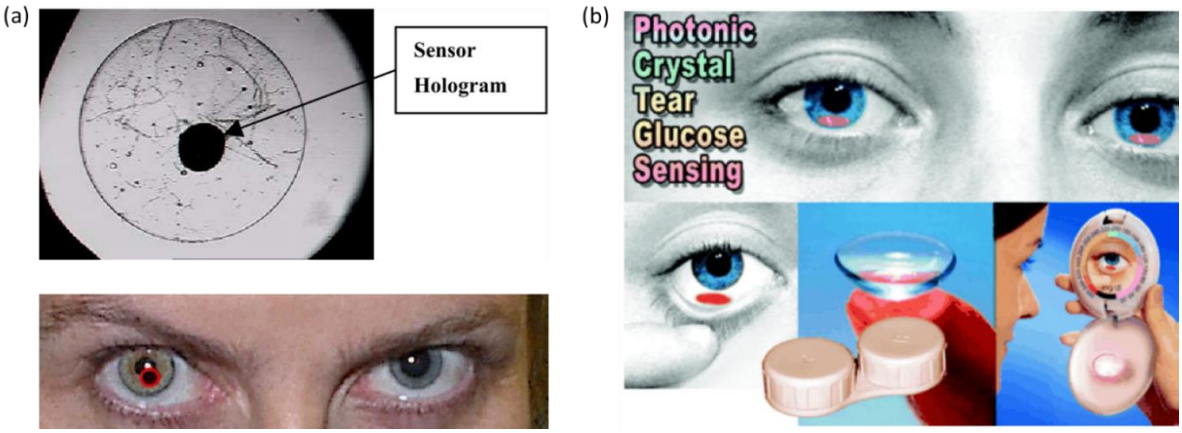

Figure 2.5. Photonic based glucose sensors. (a) Photos of a holographic glucose sensor attached to a PVA- contact lens and a volunteer wearing the lens. (b) Schematic shows the 3D-PC glucose sensor attached to a contact lens and fixed under the eyelid showing tools required for detection which are a mirror and a color chart [70, 71].

2.3 Optical fibers (OPs)

An optical fiber is a flexible, transparent cylindrical waveguide made of plastic or silica having a diameter slightly thicker than that of a human hair (Figure 2.6) [78]. Optical fibers

deliver/guide the light for long distances with low loss like a pipe delivers liquids. Single-index optical fibers consist of a core covered with a transparent cladding material of a lower refractive index. The total internal reflection phenomenon guides the light in the fiber core. Waveguide analysis shows that the transferred light energy is not fully trapped in the fiber core as a portion of energy travels in the cladding as evanescent waves. The incident light on the core-clad interface at high angles greater than the critical angle for this interface are completely reflected and guided, and those that meet the interface at smaller angles are refracted into the cladding to be lost. The critical angle is known as the minimum angle required to attain the total internal reflection, and in the optical fiber case it is determined by the refractive index difference between the core and cladding materials [78].

Fibers can be classified into two categories based on the number of guided modes; single mode and multi-mode fibers. Most commonly, single-mode fibers have a core diameter of 8-10 μm and are developed to be used in the short infrared region. While multi-mode fibers are manufactured with a core diameter in the range from 50 μm to hundreds of micrometers, and are used when high power is required to be transferred [78].

The numerical aperture (NA) of an optical fiber is the number that defines the range of angles over which the fiber can receive, guide, and release the light rays. The NA of a step-index fiber which is the type we cover in this study, is given by the difference in the refractive index between the core and cladding materials: $NA = \sqrt{n_{co}^2 - n_{cl}^2} = n_{air} \sin \theta_{air}$, (1)

where n_{co}, n_{cl}, and θ_{air} are the refractive indices of the core, cladding, and angle of incident of rays, respectively. The angle is measured relative to the longitudinal axis of the fiber core

[79]. Accordingly, the NA determines the accepted angles of the light entering or exiting the fiber. A normalized frequency (V) of an optical fiber provides information about number of optical modes that can propagate in the fiber and it depends on the NA and the core diameter, and it is given by: $V = (NA)\frac{2\pi a}{\lambda}$, (2)

where a is the radius of the fiber core, and λ is the free-space wavelength [79]. Optical fibers established their place in telecommunications and optoelectronics applications. Later, optical fibers showed a potential sensing technology due to their inherent advantages of cost-effective, small size, light weight, and immunity to electromagnetic interference. In this section, we will discuss the different types of optical fibers used in sensing applications.

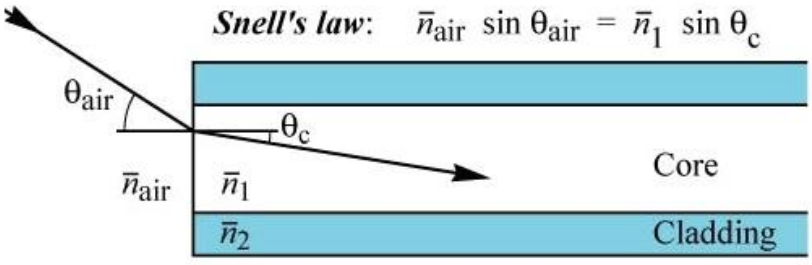

Figure 2.6. Schematic of the step-index optical fiber [80].

2.3.1 Fiber Bragg grating (FBG)

A fiber Bragg grating is a traditional fiber that combines a distributed Bragg reflector fabricated in a short segment of the fiber core, which reflects a specified wavelength range of the fiber guided modes and transmits all others (Figure 2.7). A Bragg reflector is a periodic variation in the refractive index of the fiber core in the guidance direction and works as a specific dielectric mirror [81]. Electromagnetic waves propagating through the FBG are transmitted except for the wavelengths that satisfy Bragg's law, which are reflected.

Initially, FBGs were developed for the telecommunications industry in the 1990's, then, later, FBGs started being used in sensing applications. The sensing principle is based on detecting the shift of the Bragg grating wavelength, which occurs due to the change of the grating period or the effective refractive index (n_{eff}). Advantageously, the FBG can be interrogated in reflection and transmission configurations where the latter is often more convenient. The reflection configuration does not require both ends of the fiber to be connected to the interrogation setup. Insensitivity of the FBG to the fluctuation of the illumination is another advantage as the output signals usually obtained by recording the wavelength shift induced by the measurand. FBG sensors were demonstrated for temperature, humidity, strain, and infrared radiation detection [81-85]. However, the most interesting application of the FBG that has been developed to date what is the fiber-optic smart structure. The FBG was imbedded into structures to monitor the strain distribution [86]. The real-time monitoring of smart structures helps to improve the safety of the structures allowing timely repair, and prevents unwanted damage [87]. For instance, FBG was developed for temperature detection based on the thermo-optic effect of the fiber core material induced by the temperature. The Bragg grating was fabricated in a single-mode silica fiber with a grating period of 1.55 μm [83]. For biosensing applications, step-index FBG was not applicable; however, tilted FBG was developed for this purpose. For instance, a tilted FBG was developed for selective glucose detection based on a glucose enzyme immobilized on the cladding of the FBG. The fiber showed a very poor sensitivity of 0.298 for nm/mM as the Bragg wavelength shifted only 1 nm over the change in glucose concentration in the physiological range [88].

Fabricating the Bragg gratings in optical fibers are commonly done by: i) laser interference technique where two coherent beams are used to tailor the desired grating period, ii) phase mask technique where a quartz glass with fixed corrugated surface is used for UV inscription of the gratings, and iii) point by point technique where a femtosecond laser is used for fabricating the gratings producing a groove per laser pulse. More details about fabrication methods can be found in the reference [82]. Based on the fabrication methods mentioned above, the fabrication process is relatively complex and requires advanced systems. Also, the interrogation system of the FBG costly and complex as high-resolution wavelength-shift detectors are commonly required. Furthermore, the FBG based sensors are sensitive to temperature and strain which is particularly a challenge when it is employed for detecting other measurands.

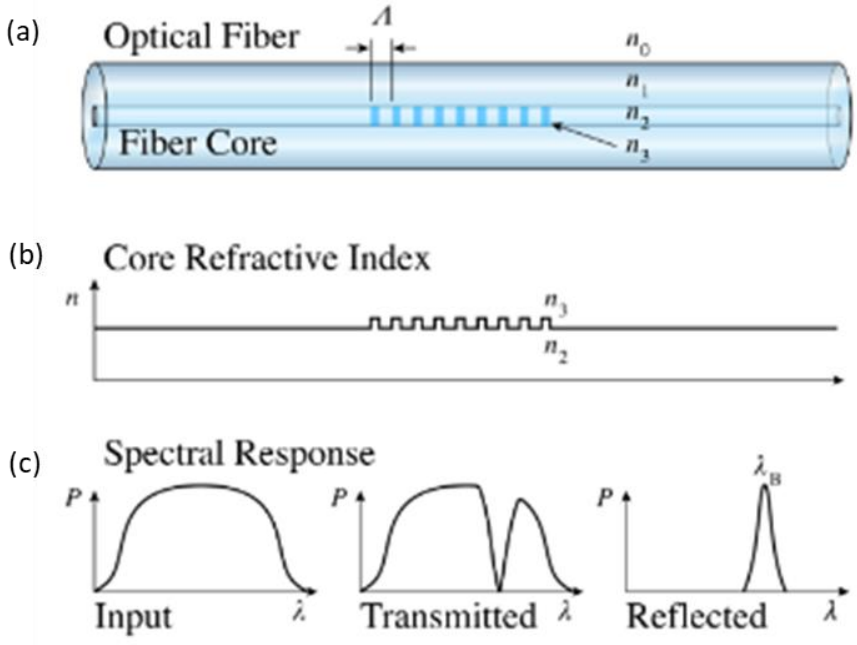

Figure 2.7. A fiber Bragg grating. (a) Schematic showing the fiber Bragg grating. (b) The refractive index profile of the fiber core. (c) The spectral response of the fiber Bragg grating [89].

2.3.2 Long Period grating (LPG) fiber probes

A LPG fiber is a traditional fiber involving a structure of a periodic modulated refractive index, similar to that of the fiber Bragg gratings (Figure 2.8a). However, the period is larger as it is on the millimeter scale which exceeds the wavelength of the electromagnetic waves guided in the fiber making the fabrication relatively simple [90]. The grating period is in the range of 100-1000 μm and having a length of few centimeters. LPG can be manufactured in the fiber using various processes. For example, irradiation with an ultraviolet (UV) source, laser source, mechanical pressure, and electric arc discharges [90]. In 1996, the first LPG was inscribed in an optical fiber for band rejection applications. In the same year, Bhatia et al, introduced the first LPG fiber for sensing application [91]. Since then, LPG fibers have been developed for optical communications and optical sensing systems. In optical communication systems, LPG fibers were employed as a gain equalizing filters, wavelength selective devices, and band pass and band rejection filters. In the field of sensing applications, LPG fibers were applied for structural bending, temperature, strain, refractive index, and biochemical sensors [92].

Long period gratings couple the core guided modes with those forward propagated in the cladding. The core-cladding coupling modes quickly attenuate resulting in a series of loss bands in the transmission spectra. The coupling is a wavelength dependent process as the LPG takes away the core wavelengths which phase matches with its periodic constant. Therefore, the phase-matched wavelengths are observed in the transmission spectrum as loss dips (Figure 2.8b). The coupling wavelengths are given by the phase-matching condition:

$$\lambda_m = \left(n_{eff,co} - n_{eff,cl}^m\right)\Lambda, \qquad (4)$$

where λ_m is the wavelength of the m^{th} cladding mode, Λ is the period of grating, $n_{eff,co}$ is the core effective refractive index, and $n_{eff,cl}^{m}$ is the effective refractive index of the m^{th} cladding mode [91]. Transmission of the resonance wavelength in the fiber is given by: $T = \cos^2(D_c L_g/2)$, where L_g is the grating length, D_c is the coupling coefficient. If the LPG section is exposed to an external stimulus, it leads to a modification of the cladding effective refractive index, core refractive index, or grating period, and as a result the loss/dip wavelengths shifts in accordance to the coupling equation (4). Biosensing applications are based on modifying the effective refractive index of the cladding by coating the LPG fiber with an analyte responsive layer. Changing the refractive index or the thickness of the responsive layer induces a change in the resonant wavelengths and this is the principle of sensing [93]. For instance, long period grating fibers of periodicity 550 μm were developed in a single mode fiber for selective glucose detection. The fiber core gratings were fabricated by the laser. The gratings region was silinazed to secure binding sites for immobilizing the glucose oxidase [94]. The change of the refractive index of the outer coating upon glucose-glucose oxidase binding led to a shift in the resonance wavelengths in the transmission spectra detecting the glucose concentration. The resonance wavelength shifted by only 2 nm over the change of glucose concentration in the physiological range (4 -8 mM) which reflects very poor sensitivity. The LPG fibers require multistage fabrication process, and are costly devices in fabrication and readout resulting in limited applications of LPG fibers. On top of that, LPG fibers suffer from poor mechanical properties, high sensitivity to temperature and strain, and low Q-factor due to the broad resonant wavelength band [88].

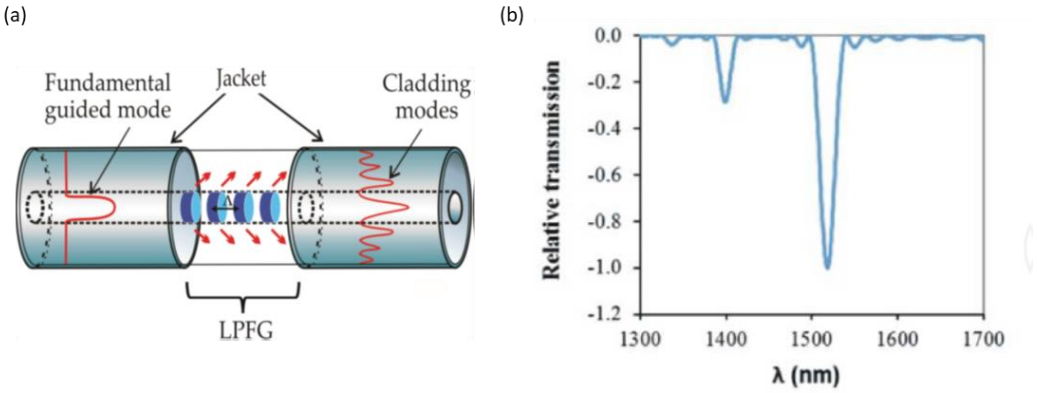

Figure 2.8. A long period grating fiber. (a) Schematic shows the working principle of the long period grating fiber. (b) An example of the transmission spectra of a long period grating fiber showing the loss dips in the fiber's transmitted spectra [95].

2.3.3 Tapered Optical Fiber (TOF)

A TOP is a traditional optical fiber stretched out over a small length to create a region of a very thin diameter (neck) (Figure 2.9). In traditional fibers, the light energy is guided in the fiber core but a minute portion of the energy penetrates to the fiber clad (evanescent waves) [96]. These evanescent waves decay exponentially into the cladding with a penetration depth given by:

$$d_p = \frac{\lambda}{2\pi\sqrt{n_{co}^2 \sin^2\theta_i - n_{cl}^2}}, \qquad (5)$$

where θ_i represents the incident angle of the waves at the core-cladding interface, n_{co} is the fiber core refractive index, n_{cl} is the clad refractive index [96]. Tapering a single mode fiber decreases the V-number of the core to be less than one due to decreasing the fiber core radius. However, the cladding V-number increases to be above 2.405. Hence, the light is no longer guided by the fiber core and spread to the cladding that starts to play the role of the new core. The refractive index difference between the cladding and the surrounding medium guides the modes in the tapered region and the new V-number is called V_{cl}, and is given by:

$$V_{cl}(z) = \frac{2\pi a(z)}{\lambda}\sqrt{n_{cl}^2 - n_{ex}^2} \quad , \qquad (6)$$

where $a(z)\,, and\ n_{ex}$ are the radius of the fiber waist and the RI of the external medium, respectively [97]. Thus, the tapering creates a region where the external surrounding medium plays a role in guiding the fiber modes. Also, the penetration depth of the evanescent waves in the taper segment depends on the RI of the medium surrounding the tapered region, and is given by: [98]

$$d_p = \frac{\lambda}{2\pi\sqrt{n_{cl}^2 \sin^2\theta_i - n_{ex}^2}} \quad , \qquad (7)$$

In sensing applications, stimuli-responsive layers are coated on the tapered segments to be the external surrounding media. The refractive index of the analyte-responsive layer changes due to its response to a certain analyte inducing a change in the light intensity. Therefore, measuring the transmitted light variation determines the refractive index of the responsive-coating layer and consequently the analyte concentration. For instance, a single mode silica fiber was tapered and functionalized at the tapering segment for bacterial growth detection [96]. The tapered fiber probe was fabricated under an applied tension and by using a carbon dioxide laser. The tapering process was observed by an optical microscope. A laser source of wavelength and power 1558.17 nm, 20 mW, respectively, was illuminating the fiber and the transmitted optical signal was collected at the other end of the tapered fiber by a photodetector. For glucose sensing, Qiu et al, developed tapered fibers made of poly methyl methacrylate (PMMA) having a core of diameter 980 μm and fluorinated polymeric clad of thickness 20 μm [99]. The tapered segment of the fiber was 1.5 cm long, and was coated with a single layer of graphene. Introducing the aqueous glucose solution into the tapered

region caused a change in the RI of the fiber's surrounding medium affecting the evanescent field leading to a change in the optical signals. The fiber showed very poor sensitivity that limits its application at physiological glucose concentration range. The interrogation setup combined light emitting diode as a light source which generates a wavelength of 628 nm, a constant current source as a power supply for the light source, convex lenses to focus the light into the fiber, a light polarizer, a spectrometer, and a computer.

The limitations of TOP are concentrated in the relative complex fabrication process, the low sensitivity, the influence of the light source's intensity, the poor mechanical properties, and the complexity of the interrogation setup.

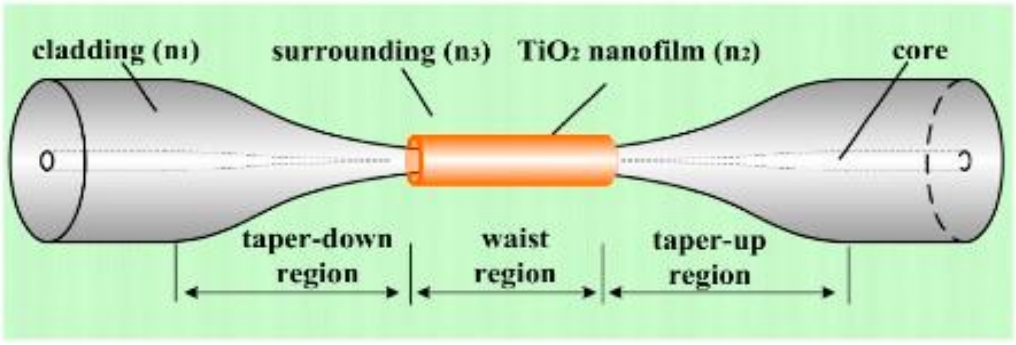

Figure 2.9. Schematic of a tapered single-mode fiber. The tapered segment is covered by the stimuli-responsive layer [100].

2.3.4 Interferometric fiber optic probes

Fiber optic interferometers are based on the interference between two light beams propagating through different optical path lengths (OPLs) in the same optical fiber or in two different fibers. The fiber probe consists of a beam splitter, and beam combining tools in any configuration [101]. In sensing applications, one of the optical path lengths is configured to be influenced by the external perturbations. The interferometric fiber probe detects

quantitatively the perturbation by monitoring the change in the wavelength, phase, intensity, frequency, or band width [102]. Currently, the trend of the interferometric optical fibers is to miniaturize them to be convenient for microscale applications, hence bulk optical tools such as objective lenses, beam splitters, and beam combiners have been replaced by small-sized tools to develop simple and compact probes [103]. Interferometric fiber optic sensors are classified into four categories based on the interferometric technique synergistic with the optical fiber; Fabry-Perot, Mach-Zehnder, Michelson, and Sagnac interferometers [103].

2.3.4.1 Fabry-Perot interferometer (FBI) fiber probes

In general, Fabry-Perot interferometer fiber probes encompass an optical fiber, two parallel reflecting surfaces isolated by a certain distance, a light source, a spectrophotometer, and a computer for signal processing [104]. The reflecting surfaces can be constructed inside or outside the fiber, and based on that the FBI probes are classified to two groups; intrinsic and extrinsic (Figure 2.10) [105-107]. The transmission and reflection spectra of FBIs depend upon the optical phase difference (OPD) between the two interfering light beams. The spectra of FBIs display maximum and minimum peaks which refer to that both beams at that particular wavelength are in phased and out of phase, respectively. The optical phase difference of the FBI is given by: $\delta = (2\pi/\lambda)2nL_c$, where λ refers to the wavelength of the free-space incident light, *n* represents the refractive index of the cavity material, and L_c refers to the length of the cavity [103]. Any perturbation affected the cavity region of the fiber probe causes a change in the difference of the optical path length resulting in modifications in the transmission and reflection spectra. If an applied longitudinal strain on the fiber probe altered the cavity length /the refractive index, the optical phase shifts. By detection the

change in the transmission or reflection spectra of the FBI, the applied strain is detected [108].

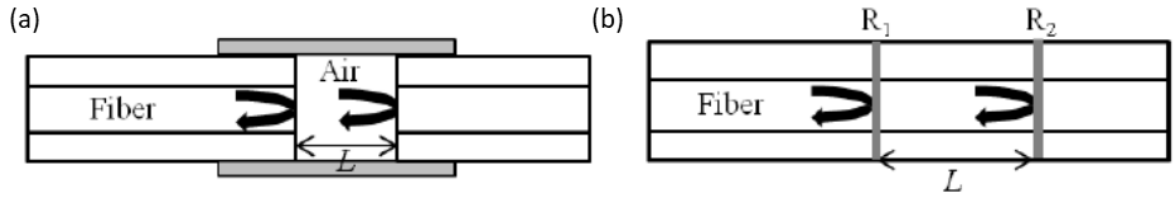

Figure 2.10. Categories of the FBI fibers. (a) An extrinsic FBI constructed by fabricating an external air cavity. (b) An intrinsic FBI made by creating two reflecting surfaces along the fiber [103].

For biosensing applications, the FBI fiber probes based on stimuli-responsive polymers have been developed. The nanocavity was made of an analyte-responsive polymer and attached to the fiber's tip to form an extrinsic FBI fiber. The interfaces; fiber core-polymer interface and the polymer-environment interface, represent the reflecting mirrors and the Fresnel reflected beams from these interfaces produce the interference fringes that appear in the reflection spectrum. Upon changing the refractive index or the thickness of the responsive-polymer cavity, the OPD changes and consequently the optical phase shifts. For instance, Nafion film was deposited on the fiber tip constituting extrinsic Fabry-Perot cavity for humidity sensing application (Figure 2.11a). Upon absorption of the water vapor by the Nafion film, the refractive index and the thickness changed inducing an optical phase shift and consequently, a change in the interference fringes of the recorded reflected spectrum [109]. Similarly, a thin film of cellulose acetate butyrate was deposited on a fiber tip constructing a Fabry-Perot cavity for sensing application [110].

In a trial to eliminate the necessity for the high quality responsive-films in the Fabry-Perot fiber sensing, Tierney et al, developed Fabry-Perot fiber probe by binding a half-spherical

hydrogel to the end of the optical fiber (Figure 2.11b). The radius of hydrogel sphere was in the range of 50-60 μm and the probe was able to detect the change in the radius of the pH-responsive hydrogel with a precision of 2 nm [111]. Thus, this probe eradicated the need to high-quality films. However, two constrains were originated; i) the refractive index difference between the bound hydrogel and the environment must be significant to enable high reflectivity at this interface and this condition put constrains on the selected monomer and cross-linker concentrations, ii) depositing the polymer on the fiber's tip in the form of a half sphere was a challenge because the gel droplet doesn't retain the spherical shape during the polymerization [111]. FBI fiber probes for glucose sensing were developed based on the same idea. The probe presented a high sensitivity, low limit of detection, and short response time ~ 20 min at pH 7.4 and temperature 37 $^{\circ}$C. Currently, Glucoset Ltd. company is working on commercializing this probe. In a trail to eradicate the necessity to the coherent light sources, which increased the cost of the FBI fiber probe setup, Goicoechea et al, deposited multilayer hydrogel on the fiber's end -building up a Fabry-Perot nanocavity by the electrostatic self-assembly technique. Low-coherent light source, halogen lamp (950 nm) was coupled to the fiber probe for pH sensing applications [112].

Limitations of the FBI probes result from the necessity for high-quality films and coherent light sources. Also, the readout setup requires bulky instrumentation such as computers to process the output signals.

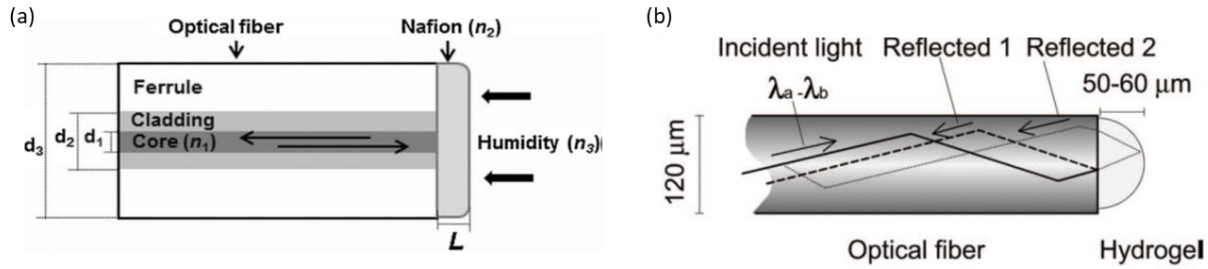

Figure 2.11. Fabry-Perot interferometer fiber probes, (a) Schematic shows the FBI fiber probe for humidity sensing, the probe consisted of a high-quality film deposited on the fiber tip representing the external cavity, (b) Schematic of the FBI fiber probe whose a microcavity in a half-sphere shape [109, 111].

2.3.4.2 Mach-Zehnder interferometer (MZI) fiber probes

Mach-Zehnder interferometer fiber probes have been used in sensing applications for long time. Early probes were combining two independent arms function as reference and sensing arms (Figure 2.12). The fiber probe is constructed of an optical fiber which guides the light to the splitter to enter the reference and sensing arms, then light is recombined to be guided through another optical fiber to reach the photodetector [103]. The recombined light presents interference fringes that depend on the optical path difference between the arms. For remote sensing applications, the sensing arm is exposed to the tested analyte and the reference arm is kept isolated. The analyte influences the sensing arm inducing a changes in the optical path difference of the MZI [103]. Rapidly, the configuration of the MZI which based on the two separate arms was replaced with in-line interferometer by introducing the long period grating fiber (Figure 2.13a). The LPG played the role of the light splitter and the light combiner. The beam guided in the single mode fiber (SMF) is split into two modes; core mode and cladding mode by an LPG and both modes are re-combined by another LPG producing interference fringes [113-118]. MZI fiber was utilized for refractive index sensing as the sensitivity of the cladding modes to the refractive index of the surrounding medium was observed [115]. The

MZI based on a pair of LPGs has limited operation wavelength as the LPG function in small ranges of wavelengths because of the phase matching phenomenon of the fiber gratings. Additionally, the LPG pair in the MZI has to be identical to achieve maximum performance [119]. Therefore, alternative methods have been used to split the core guided modes through the fiber into core and cladding modes. For instance, two fibers can be spliced with a minute lateral offset (Figure 2.13b). The offset makes part of the core mode split into cladding modes and core modes and re-combine them at the other side. This type of MZI is less costly and rapid in fabrication compared to the LPG-MZI -without limitation on the working wavelength [103]. Also, tapering the optical fiber at two points can construct an effective in-line MZI (Figure 2.13f). The core mode is split at the first point to core mode and cladding mode which both re-combine at the second tapering point producing interference fringes. However, this type of MZIF is compact, it suffers from weak mechanical regions (tapering regions) [103].

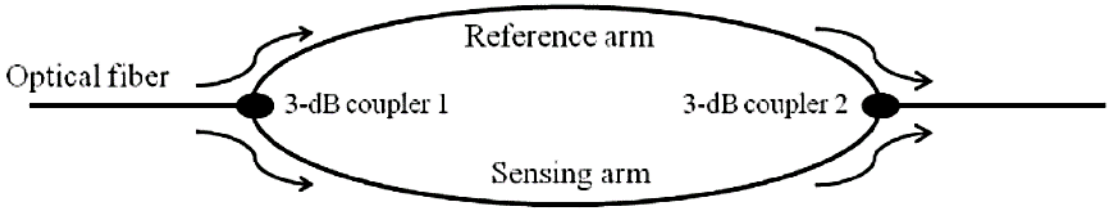

Figure 2.12. A diagram shows the Mach-Zehnder fiber interferometer [103].

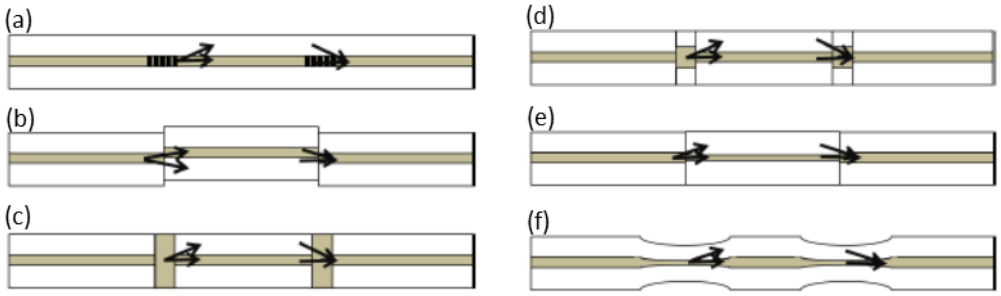

Figure 2.13. Various configurations of in-line MZIs based on; (a) A pair of LPGs, (b) mismatching of fiber cores, (c) Collapsing of air-hole of a photonic crystal fiber, (d) Multimode fiber segment, (e) Single mode fiber between two multimode fiber segments, (f) Two tapered regions [103].

2.3.4.1 Michelson interferometer (MI) fiber probes

Fiber optic probes based on Michelson interferometers and those based on MZI are quite similar and their working principle are almost same [103]. Similarly, the guided light in the fiber core is split to propagate in two arms; reference arm and sensing arm. The light is reflected at the end of each arm by mirrors to re-combine in the fiber, so the main difference compared to MZI is the reflectors which provide the probe the advantage of working in the reflection configuration (Figure 2.14a). MI fiber probes are compact, handy, practical in use and installation because they work in the reflection mode. Multiplexing possibility with parallel connector of several sensors is another advantage of the MI fiber probes. However, adjusting the fiber length difference between the sensing arm and the reference arm with the coherent light source is essential. An in-line configuration of the MI was developed based on a single LPG fabricated in a cladded fiber (Figure 2.14b). The LPG divides the guided mode into two paths forming the two arms of Michelson interferometer. The light in each path is reflected by a mirror manufactured on the fiber's end, hence the reflected light recombines in the core by the same LPG –giving rise to interference fringes in each resonance band [120-

122]. An in-line configuration of Michelson interferometer probe based on a single LPG was developed for quantitative measurements of glucose concentrations in aqueous solutions. The interference fringes and its intensity shifted with glucose concentration which induced a RI change [120]. The fringe position shifted 55 nm upon increasing the refractive index of the aqueous glucose solution from 1.33 to 1.44. Processing the output signal, and necessity for a bulky instrument and coherent light sources can be considered the main drawbacks of these probes.

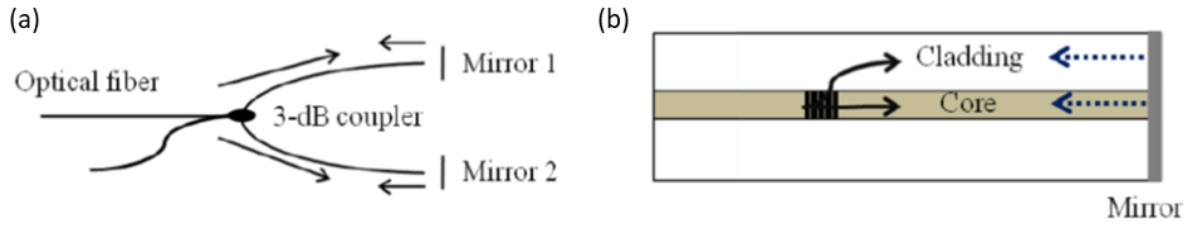

Figure 2.14. Michelson interferometer configurations. (a) The initial configuration of the MI. (b) In-line configuration of MI based on a LPG [103].

2.3.4.3 Sagnac interferometer (SI) fiber probes

The SI fiber probe is composed of three terminal couplers, light detector, computer for signal processing, two polarization controller, and an optical fiber loop along with two light beams of different polarization states which propagate in counter directions (Figure 2.15). The launched light beam is split by the coupler into two counter-propagating beams which recombine again at the same coupler. A birefringent fiber is utilized in the sensing section of the loop to maximize the polarization dependence of the SI. The phase of the interference is obtained from: $\delta_{SI} = (2\pi/\lambda)\, BL$, $B = \left| n_f - n_s \right|$, where B refers to the birefringent coefficient of the sensing fiber, L denotes to the length of the sensing fiber, n_s and n_f represent the effective refractive index of the slow and fast modes, respectively [123]. Sagnac

interferometer fiber probes have been employed recently in sensing applications such as temperature, strain, and pressure; however, they have not been employed yet in the biosensing applications to the best of our knowledge [123-125]. The complexity of the polarimetric sensors prohibited their popularity [123].

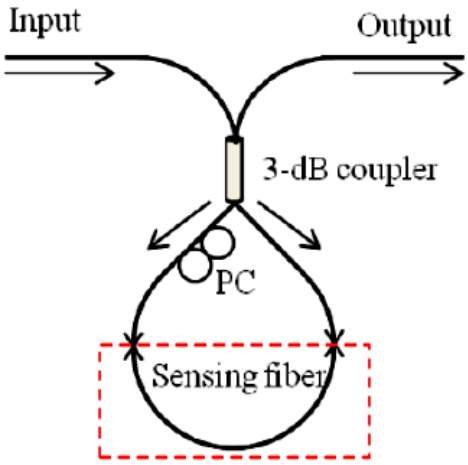

Figure 2.15. diagram of Sagnac interferometer [103].

2.3.5 Surface Plasmon resonance-based fiber probes (SPRF)

Fiber optic probes that depend on the surface Plasmon resonance phenomenon (SPR) are classified into two categories; planer surface Plasmons and localized surface plasmons.

2.3.5.1 Planar Surface Plasmon resonance (SPR)

Surface Plasmons was discovered in 1902 by Wood who reported anomalies in the spectrum of the light reflected from a metal diffraction grating [126]. Later, Fano proved that this anomalies are due to excitation of electromagnetic surface wave on the diffraction grating surface [127]. Otto demonstrated that bringing a prism close to a metal-dielectric interface can excite surface plasmons. In the same year, Kretchman and Raether built an optical setup

to demonstrate excitation of surface plasmons. This optical setup is considered the basis of the most current research and commercial surface Plasmon resonance instrumentations. The setup involved a quartz 60^{o} prism of a base coated with a silver thin film of thickness 50 nm (Figure 2.16). The excited surface Plasmons was maximum at the silver-air interface and followed an exponential decay trend in silver and air media.

Transverse magnetic (TM) polarized waves are required to excite surface plasmons because the surface plasmons are TM waves in nature. The propagation constant of surface plasmons according to Maxwell's equations solution for the metal-dielectric interface is given by: $K_{sp} = K_o (\varepsilon_s \varepsilon_m / \varepsilon_s + \varepsilon_m)^{1/2}$, where K_{sp} denotes to the propagation constant of the surface plasmons, K_o is the free space propagation constant of the incident light, and ε_s and ε_m are the dielectric constants of dielectric and metallic layers, respectively [128]. It is noticed that the propagation constant of the surface plasmon is higher than that of the incident light. Therefore, direct light lonely is not enough to excite surface plasmons. Thus, an additional energy or momentum to the light is essential to excite surface plasmons. Coupling the incident light with a prim, grating, waveguide, or a fiber optic can achieve this target [129].

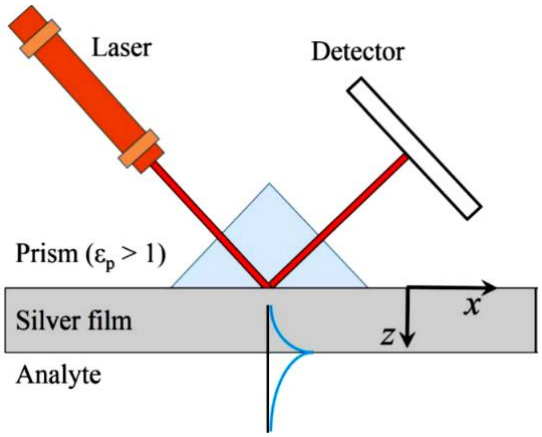

Figure 2.16. The Kretschmann setup for exciting surface Plasmon resonance. The blue curve represents the profile of the excited fields [130].

2.3.6 Localized surface Plasmon resonance (LSPR)

Light interaction with nanoparticles induces collective oscillations of the metal free electrons in the conduction band and is defined as localized surface plasmon resonance (Figure 2.17). Unlike the planar surface plasmon resonance (SPR) where the surface plasmon waves are confined at the metal-dielectric interface, the LSPR are localized in the surface of the metal nanoparticles [129]. Interaction of the electric field of the incident light with the free electrons of the metal nanoparticles, separates the electrons from the positive ions (nuclei). The Coulomb attraction force between the ions and the free electrons leads to recombination. Therefore, the collective oscillations of the free electrons induces excitation of localized surface plasmons (Figure 2.17) [131, 132]. Excitation of LSPR is marked by an enhancement in the absorption of the incident light at the surface of the metal nanoparticles. The LSPR phenomenon depends on the size, type, shape of the nanoparticles, the wavelength of the incident light, and the refractive index of the surrounding dielectric medium [133]. In LSPR, the absorbed wavelength of the incident light changes based on the refractive index of the surrounding medium of the nanoparticles. Thus, changing the refractive index of the particles medium is transformed into a shift in the absorption spectrum and this is the working principle of LSPR sensors [134]. The relationship of the absorbed wavelength and the refractive index medium of the nanoparticles is given by: $\Delta\lambda = S(\Delta n)[1- \exp(-2d_m/L_d)]$, where $\Delta\lambda$ is the wavelength shift in the absorption spectra corresponding to the change in the refractive index of the nanoparticles medium (Δn), S is the refractive index sensitivity, d_m refers to the thickness of the surrounding medium of the nanoparticles, and L_d denotes to the decay length of the associated electromagnetic field [135].

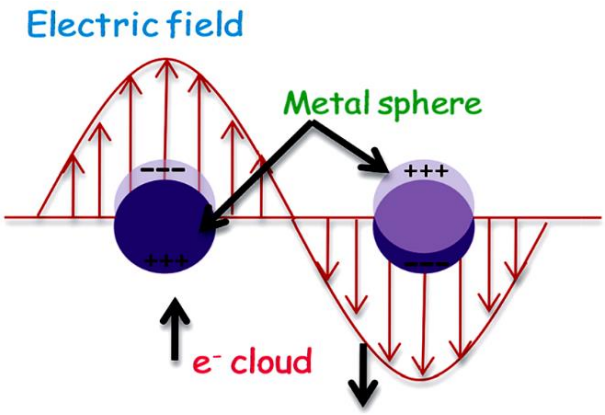

Figure 2.17. Schematic shows light interaction with a metal nanoparticle [136].

2.3.6.1 Fiber optic coupling

Surface Plasmons are excited in optical fibers through the total internal reflection. In case, a polychromatic light beam is launched in the fiber, the guided modes propagate in the fiber core and the evanescent waves propagate in the fiber cladding. The guided modes are subjected to the total internal reflection at the core-cladding interface and they exponentially decay into the fiber cladding. In the fiber optic, the core guided waves are the incident light rays on the core-clad interface with angles in the range of θ_c to 90^o, where θ_c is the critical angle of the fiber core-cladding interface. For inducing surface plasmons in the optic fiber, a small section of the fiber is removed subsequently a thin plasmonic film (silver or gold) of thickness ~ 50 nm was deposited. Matching the wave vector of evanescent waves propagating at the fiber core-metal interface with that of surface plasmon waves propagating at the metal-dielectric sensing layer interface induces a sharp SPR dip in the transmission light spectra. The dip SPR in the transmission spectra is wider than those produced by gratings and prisms coupling techniques. Because the guided waves in the fiber have a range of total internal reflection angles and at each angle a dip SPR is induced resulting in broadening the SPR

band, which influences the sensing parameters of the fiber probe such as limit of detection and sensitivity. Among the coupling components, excitation of surface plasmon waves by optical fibers presents a compact and efficient method that has superior advantages compared to prims or gratings.

2.3.6.2 Plasmonic fiber optic probes for sensing

In order to fabricate the plasmonic fiber probe, the fiber cladding is peeled off from a small region followed by coating with a thin layer of plasmonic material. The analyte to be tested is introduced into the sensing region. Upon launching the polychromatic light into the fiber, evanescent waves are originated at the fiber core-metal interface inducing surface plasmons at the metal-analyte interface. Consequently, a sharp dip in the transmission spectra of the fiber is recorded confirming the resonance absorption at specified wavelengths called the resonance wavelengths. Modulation in the refractive index of the analyte medium result in a shift in the resonance wavelength, and this is the sensing mechanism of the fiber probes based on SPR. The selection of the plasmonic material for exciting surface plasmons has a significant role in flexibility of fabrication and performance of the fiber probe [129]. Silver and gold are preferable as plasmonic metals due to their superior optical properties in the visible and near infrared ranges. Silver presents unparallel plasmonic characteristics in the visible region, which resulting from its low dielectric loss; however, it suffers from poor chemical stability [137, 138]. Gold is the most common metal used in SPR applications because of its high chemical stability. Although, SPR probes have been used for a broad range of sensing applications, the limited penetration depth of the evanescent waves into the analyte medium is a challenge posing restrictions on sensing large molecules such as proteins

[139]. For instance, a straight fiber optic probe for non-selective glucose detection was reported [140]. A small segment of the fiber was coated with a gold layer and the fiber's tip was coated with gold as well. The reflection spectra from the probe shifted to longer wavelengths by increasing the glucose concentration in the tested solution. The glucose concentration was correlated to the resonance wavelength by the relationship: λ_{res}= 634.3+0.13M +0.001M^2, where λ_{res} denotes the resonance wavelength and *M* refers to the glucose concentration in mg mL^{-1}. Iga et at, developed unconventional optical fiber probe which comprise two different core diameter fibers (50 µm and 3 µm) to increase the leakage of the fiber guided light into the cladding region to improve the probe sensitivity [141]. Sliver film was uniformly sputtered on the cladding surface for SPR excitation. The probe demonstrated a response for the refractive index change from 1.333 to1.398 due to excitation of the SPR and the resonant wavelength red-shifted from 527 nm to 735 nm. Similar fiber probe was introduced for pH sensing by coating a pH-responsive hydrogel on the fiber clad covered with silver film [142]. Reaction of different pH solutions with the responsive hydrogel induced volumetric and refractive index shift, which led to shifting the SPR wavelength. Singha et al, introduced fiber probe for glucose sensing in aqueous fluid [143]. The probe was fabricated by coating a small section of the optical fiber core by a silver layer, then a silicon film followed by the hydrogel film that trapped glucose oxidase. The silicon film was deposited on the silver to enhance the sensitivity. A 20 nm blue shift in the resonance wavelength was detected with glucose concentration in the range of 0-260 mg/dL. The fabrication process of the probe is summarized to highlight the requirements and the level of complexity. A multimode fiber of a core thickness 600 µm, and numerical apertures of 0.4. A tungsten cutter was used to sharp the fiber ends for improving the light coupling

and a sharp blade was utilized to peel off the cladding of the fiber segment. The unclad region was cleaned by nitric acid, rinsed with deionized water 4-5 times, and acetone followed by ion bombardment in vacuum chamber. Silver film of 40 nm thickness was deposited on the cleaned unclad section followed with a silicon layer of thickness 7 nm. Both layers (silver and silicon) were prepared by the thermal evaporation technique at room temperature under pressure of 5×10^{-6}. Glucose oxidase was trapped in the gel and the probe was dipped in the gel covering the silicon film constituent the probe sensing region. The readout procedures were carried out as follow: i) unpolarized light source was coupled with the fiber at one end with the help of a microscope objective lens, ii) the transmitted light from the fiber was collected from the other end by a spectrometer which was connected to a personal computer. The output spectra were processed, and the resonance wavelength was detected at various glucose concentrations.

As the penetration of the evanescent waves and subsequently the interaction with the dielectric analyte medium are the basis of the SPR fiber sensors, it is significant to adequately expose the evanescent waves to the analyte medium. Therefore, numerous geometries have been proposed to attain this objective including D-tube, tapered, and U-bent [144-148]. For example, a U-shape fiber probe was developed for glucose detection [147]. Gold nanoparticles were attached on the fiber core followed by immobilizing the glucose oxidase over. Oxidizing glucose oxidase due to glucose presence, changed the refractive index of the glucose oxidase film -inducing a change in the absorbance of the gold nanoparticles. It was found that the fiber probe bending has a significant influence on the probe sensitivity and the bending radius 0.982 mm achieved the maximum sensitivity. The required blood sample was only 150 µl which is less than the amount demanded for commercial sensors, 1500 µl. Also,

selective glucose probes were developed based on a phenyl boronic acid derivative by a self-assembled monolayer of p-mercaptophenyl boronic acid (PMBA) on a gold-coated optical fiber [149]. Interaction of c*is*-diol molecules such as glucose with the PMBA monolayer deposited on the gold layer induced a change in the monolayer's refractive index. The probe response for glucose was insignificant because of the low molecular mass of glucose, consequently no shift in SPR wavelength was recorded. Therefore, gold nanoparticles modified with 2-aminoethanethiol (AET) and PMBA were introduced to enhance the probe sensing performance. The resonance wavelength of the probe was red-shifted with glucose concentration demonstrating a significant response to glucose concentration in the range of 0.01-30 mM. The probe was highly sensitive for glucose concentration presenting a limit of detection of 80 nM. However, the probe performance was limited by long response and saturation times 12 min, and 53 min, respectively.

Generally, the SPR probes require multistage and sophisticated fabrication process as observed in the aforementioned example. Additionally, the readout setup is bulky and costly as a computer is demanded for processing the probe signal, and a spectrometer is necessary for collecting the probe signal. Furthermore, SPR probes based on phenyl boronic acid derivative provided long response time and saturation time, which make them unpractical for continuous glucose monitoring [149].

2.3.7 Fluorescence-based fiber optic probes

The recent progress in polymer technology and applications have led to enhance the optical performance of the hydrogel optical fibers to be commercialized [150, 151]. For instance, Shortreed et al, introduced a fluorescent probe for calcium monitoring in the physiological

applications [152]. The distal end of a silica multimode fiber of diameter 125 µm was functionalized with the calcium-responsive hydrogel. The calcium-fluorescent indicator was crosslinked with the acrylamide through the vinyl group in the free radical polymerization process. The fluorescent light recorded at the opposite end of the probe increased with calcium concentration. Recently, fluorescent hydrogel fibers were developed for implantable *in vivo* sensing. For example, a hydrogel fiber was made of a biocompatible material (polyethylene glycol-polyacrylamide) for glucose detection (Figure 2.18) [153]. The fiber was functionalized with glucose-responsive fluorescent microbeads, and was inserted underneath skin. Images of the fluorescent fiber were taken by a camera and processed on a computer software to measure the fluorescence intensity at various glucose concentrations. It was found that the fluorescent intensity at wavelength 488 nm increased with glucose concentration in the range from 0 to 500 $mg.dL^{-1}$ [153]. The glucose-responsive fluorescent microbeads were prepared by axisymmetric flow focusing microfluidics device (AFFD). The microfluidic device produces monodisperse droplet of the glucose-responsive pregel. The droplets were polymerized and washed to remove the unreacted ingredients, further details about the fabrication procedures of the microbead can be found in reference [154]. The fluorescent microbeads were mixed with the optical fiber pregel (acrylamide and polyethylene glycol diacrylate) and injected into an optical fiber mold stored for 30 min in temperature 37 ^{o}C to polymerize [153].

The application of fluorescent fiber probes are limited due to photobleaching of the fluorophore, the uneconomic cost of the probe, and fluctuation of the illuminating light source which leads to under/overestimation of the analyte concentration [155]. Furthermore,

these probes are not applicable to individuals with skin pigmentation as the performance is effected by the thickness of the skin epidermal [156]. In top of that, expensive instruments such as computers, fluorometers or spectrophotometers are required for output signals detection.

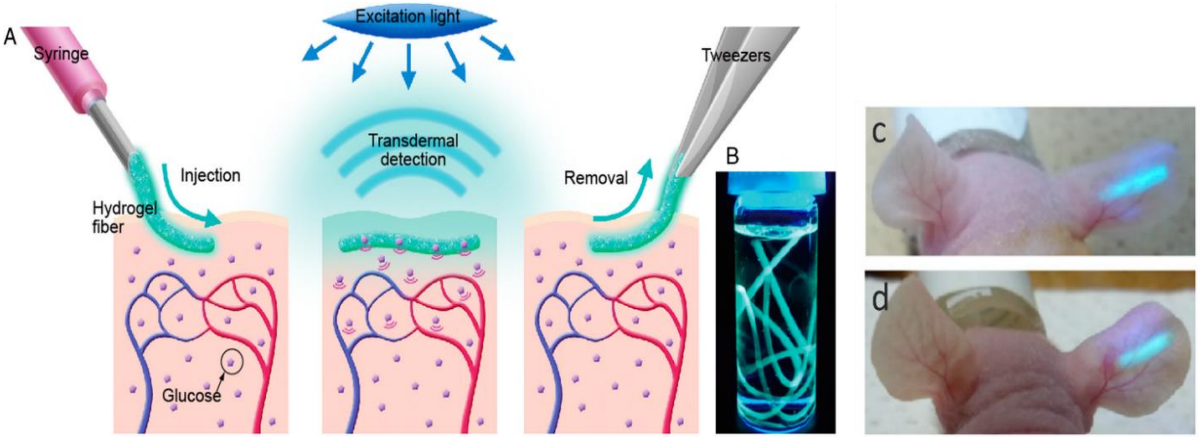

Figure 2.18. A schematic of the fluorescent hydrogel fiber designed for glucose detection in the subcutaneous tissues. (a) A schematic illustration of the fiber injection, working principle, and fiber removal. (b)The fluorescent hydrogel fiber in a glass vial soaked in a 50 % glucose solution. (c-d) Photos of the fiber immediately after insertion in a mouse ear and after 30 days, respectively [153].

2.3.8 Light diffuser-based fiber optic probes (LDF)

In this dissertation we have developed novel fiber optic probes. The developed probes are based on optical fibers integrated with light diffusing microstructures (LDMs). The LDMs can be considered as a dense-packed microparticles on a substrate, where the particles and the substrate were made of the same material (Figure 2.19a-b). The dense-packed particles have various geometry and dimensions, so they scatter the incident light beam (in the forward and backward directions) at different angles to project a diffused light spot of a large diameter on the screen in transmission or reflection configurations (Figure 2.19d-e). The LDMs were made of analyte responsive-hydrogels and attached to the tip of the optical fiber. The LDM

hydrogel underwent a positive volumetric shift upon a certain analyte/molecule interaction, which induced a decrease in the refractive index of the LDMs that led to decreasing the scattering efficiency of the LDMs (Figure 2.19c-e). Accordingly, more back scattered light rays satisfy the guidance condition in the fiber. The fiber probe setup consists of a monochromatic or broad band light source to illuminate a 3-teriminal coupler which is coupled with the fiber-integrated LDMs, and the third terminal of the coupler is connected to a photodetector to measure the reflected power guided in the fiber. In case, the functionalized fiber's tip is immersed in a free-analyte buffer, the LDMs scatter light backwards in the fiber with a certain range of angles, only rays scattered with small angles are guide in the fiber to reach the photodetector. While when the fiber tip is submersed in a high concentration of analyte solution, the LDMs hydrogel swells scattering the light rays backward into the fiber with smaller scattering angles (more light rays are scattered in the guidance range), subsequently more light rays are guided in the fiber resulting in an increase in the reflected power. For example, if the fiber has a NA of 0.22, the maximum incidence angle of the fiber guided light rays coming from air medium is about 12.7^{o} , and for those reflected from the fiber's tip (with a hydrogel attached of refractive index 1.4) is ~ 9^{o} (calculation is based on equation 1). Thus, light rays reflected in the fiber with angles higher than 9^{o} do not satisfy the total internal reflection condition, and they are lost into the cladding.

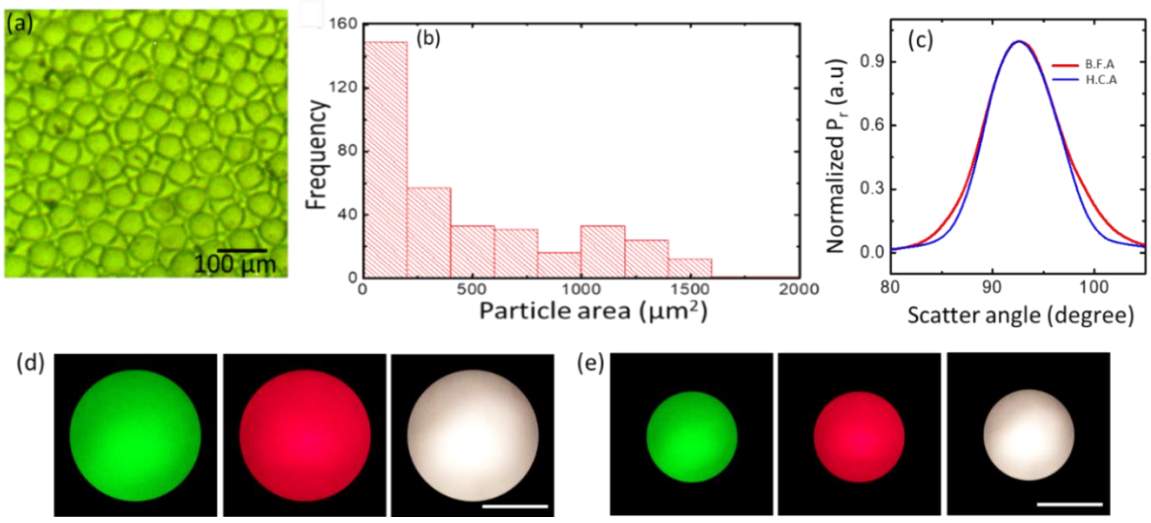

Figure 2.19. Light diffusing microstructures. (a) An optical microscopic image of the LDMs engraved on a hydrogel surface. (b) The distribution of the LDMs which can be considered as a dense-packed microparticles. (c) Optical profile of the light diffused spot in the reflection configuration when the LDMs was immersed in buffer free analyte (B.F.A) and high concentration analyte (H.C.A). (d-e) Photos of light diffused spots on screens collected when different light beams illuminated the LDMs hydrogel in buffer-free analyte and high concentration analyte, respectively. The LDMs hydrogel was illuminated at incident angle of 45^{o} and the reflected diffused light was recorded on screen at the same angle. Scale bar of 5 cm.

References

1. N. M. Farandos, A. K. Yetisen, M. J. Monteiro, C. R. Lowe, and S. H. Yun, "*Contact lens sensors in ocular diagnostics*," Advanced healthcare materials, 2015. **4** (6): p. 792-810.
2. E. Goodlaw, "*A personal perspective on the history of contact lenses*," International Contact Lens Clinic, 2000. **4** (27): p. 139-145.
3. W. Otto and L. Drahoslav, "Process for producing shaped articles from three-dimensional hydrophilic high polymers," ed: Google Patents, 1961.
4. C. S. A. Musgrave and F. Fang, "*Contact lens materials: A materials science perspective*," Materials, 2019. **12** (2): p. 261.
5. W. F. March, A. Mueller, and P. Herbrechtsmeier, "*Clinical trial of a noninvasive contact lens glucose sensor*," Diabetes technology & therapeutics, 2004. **6** (6): p. 782-789.
6. N. Efron, *Contact Lens Practice E-Book*. Elsevier Health Sciences, 2016.
7. E. S. Bennett and B. A. Weissman, *Clinical contact lens practice*. Lippincott Williams & Wilkins, 2005.
8. G.-Z. Chen, I.-S. Chan, and D. C. Lam, "*Capacitive contact lens sensor for continuous non-invasive intraocular pressure monitoring*," Sensors and Actuators A: Physical, 2013. **203**: p. 112-118.
9. B. A. Fink, G. L. Mitchell, and R. M. Hill, "*Rigid gas-permeable contact lens base curve radius and transmissibility effects on corneal oxygen uptake*," Optometry and vision science, 2006. **83** (10): p. 740-744.
10. W. A. Douthwaite, *Contact lens optics and lens design*. Elsevier Health Sciences, 2006.
11. I. Tranoudis and N. Efron, "*Tensile properties of soft contact lens materials*," Contact Lens and Anterior Eye, 2004. **27** (4): p. 177-191.
12. I. Tranoudis and N. Efron, "*Water properties of soft contact lens materials*," Contact Lens and Anterior Eye, 2004. **27** (4): p. 193-208.
13. I. Tranoudis and N. Efron, "*In-eye performance of soft contact lenses made from different materials*," Contact Lens and Anterior Eye, 2004. **27** (3): p. 133-148.
14. C. Lin *et al.*, "*Toward the Development of a Glucose Dehydrogenase-Based Saliva Glucose Sensor Without the Need for Sample Preparation*," Journal of diabetes science and technology, 2018. **12** (1): p. 83-89.
15. S. H. Lim *et al.*, "*Rapid diagnosis of tuberculosis from analysis of urine volatile organic compounds*," ACS sensors, 2016. **1** (7): p. 852-856.
16. J. Van Delft, F. Meijer, J. Van Best, and N. Van Haeringen, "*Permeability of blood-tear barrier to fluorescein and albumin after application of platelet-activating factor to the eye of the guinea pig*," Mediators of inflammation, 1997. **6** (5-6): p. 381-383.
17. A. Panaser and B. J. Tighe, "*Function of lipids–their fate in contact lens wear: an interpretive review*," Contact Lens and Anterior Eye, 2012. **35** (3): p. 100-111.
18. J. H. Thaysen and N. A. Thorn, "*Excretion of urea, sodium, potassium and chloride in human tears*," American Journal of Physiology-Legacy Content, 1954. **178** (1): p. 160-164.
19. J. T. Baca, D. N. Finegold, and S. A. Asher, "*Tear glucose analysis for the noninvasive detection and monitoring of diabetes mellitus*," The ocular surface, 2007. **5** (4): p. 280-293.
20. R. N. Khuri, "Device for determination of tear constituents," ed: Google Patents, 1994.

21. A. Domschke, W. F. March, S. Kabilan, and C. Lowe, "*Initial clinical testing of a holographic non-invasive contact lens glucose sensor*," Diabetes technology & therapeutics, 2006. **8** (1): p. 89-93.
22. L. Zhou and R. W. Beuerman, "*Tear analysis in ocular surface diseases*," Progress in retinal and eye research, 2012. **31** (6): p. 527-550.
23. C. R. Taormina, J. T. Baca, S. A. Asher, J. J. Grabowski, and D. N. Finegold, "*Analysis of tear glucose concentration with electrospray ionization mass spectrometry*," Journal of the American Society for Mass Spectrometry, 2007. **18** (2): p. 332-336.
24. N. Thomas, I. Lähdesmäki, and B. A. Parviz, "*A contact lens with an integrated lactate sensor*," Sensors and Actuators B: Chemical, 2012. **162** (1): p. 128-134.
25. Á. Farkas, R. Vámos, T. Bajor, N. Müllner, Á. Lázár, and A. Hrabá, "*Utilization of lacrimal urea assay in the monitoring of hemodialysis: conditions, limitations and lacrimal arginase characterization*," Experimental eye research, 2003. **76** (2): p. 183-192.
26. V. Andoralov, S. Shleev, T. Arnebrant, and T. Ruzgas, "*Flexible micro (bio) sensors for quantitative analysis of bioanalytes in a nanovolume of human lachrymal liquid*," Analytical and bioanalytical chemistry, 2013. **405** (11): p. 3871-3879.
27. Y. Ohashi, M. Dogru, and K. Tsubota, "*Laboratory findings in tear fluid analysis*," Clinica chimica acta, 2006. **369** (1): p. 17-28.
28. W.-M. Zhang and M. R. Natowicz, "*Cerebrospinal fluid lactate and pyruvate concentrations and their ratio*," Clinical biochemistry, 2013. **46** (7-8): p. 694-697.
29. L. Stankova *et al.*, "*Plasma ascorbate concentrations and blood cell dehydroascorbate transport in patients with diabetes mellitus*," Metabolism, 1984. **33** (4): p. 347-353.
30. H. K. Walker, W. D. Hall, and J. W. Hurst, *Peripheral Blood Smear--Clinical Methods: The History, Physical, and Laboratory Examinations*. Butterworths, 1990.
31. J. R. Cope, S. A. Collier, H. Nethercut, J. M. Jones, K. Yates, and J. S. Yoder, "*Risk Behaviors for Contact Lens–Related Eye Infections Among Adults and Adolescents—United States, 2016*," MMWR. Morbidity and mortality weekly report, 2017. **66** (32): p. 841.
32. A. LEBRECHT, D. BOEHM, M. SCHMIDT, H. KOELBL, R. L. SCHWIRZ, and F. H. GRUS, "*Diagnosis of breast cancer by tear proteomic pattern*," Cancer Genomics-Proteomics, 2009. **6** (3): p. 177-182.
33. V. Evans, C. Vockler, M. Friedlander, B. Walsh, and M. D. Willcox, "*Lacryglobin in human tears, a potential marker for cancer*," Clinical & experimental ophthalmology, 2001. **29** (3): p. 161-163.
34. A. LEBRECHT, D. BOEHM, M. SCHMIDT, H. KOELBL, and F. H. GRUS, "*Surface-enhanced laser desorption/ionisation time-of-flight mass spectrometry to detect breast cancer markers in tears and serum*," Cancer Genomics-Proteomics, 2009. **6** (2): p. 75-83.
35. D. C. Klonoff, "Overview of fluorescence glucose sensing: a technology with a bright future," ed: SAGE Publications, 2012.
36. R. Williams and J. Bridges, "*Fluorescence of solutions: A review*," Journal of clinical pathology, 1964. **17** (4): p. 371.
37. P. Kaláb and J. Soderholm, "*The design of Förster (fluorescence) resonance energy transfer (FRET)-based molecular sensors for Ran GTPase*," Methods, 2010. **51** (2): p. 220-232.
38. A. R. Clapp, I. L. Medintz, and H. Mattoussi, "*Förster resonance energy transfer investigations using quantum-dot fluorophores*," ChemPhysChem, 2006. **7** (1): p. 47-57.

39. G. Springsteen and B. Wang, "*Alizarin Red S. as a general optical reporter for studying the binding of boronic acids with carbohydrates*," Chemical Communications, 2001 (17): p. 1608-1609.
40. H. Cao, D. I. Diaz, N. DiCesare, J. R. Lakowicz, and M. D. Heagy, "*Monoboronic acid sensor that displays anomalous fluorescence sensitivity to glucose*," Organic letters, 2002. **4** (9): p. 1503-1505.
41. W. March, D. Lazzaro, and S. Rastogi, "*Fluorescent measurement in the non-invasive contact lens glucose sensor*," Diabetes technology & therapeutics, 2006. **8** (3): p. 312-317.
42. J. Zhang and W. G. Hodge, "Contact lens integrated with a biosensor for the detection of glucose and other components in tears," ed: Google Patents, 2013.
43. R. Badugu, J. R. Lakowicz, and C. D. Geddes, "*Noninvasive continuous monitoring of physiological glucose using a monosaccharide-sensing contact lens*," Analytical chemistry, 2004. **76** (3): p. 610-618.
44. R. Badugu, J. R. Lakowicz, and C. D. Geddes, "*A glucose-sensing contact lens: from bench top to patient*," Current Opinion in Biotechnology, 2005. **16** (1): p. 100-107.
45. R. Badugu, B. H. Jeng, E. A. Reece, and J. R. Lakowicz, "*Contact lens to measure individual ion concentrations in tears and applications to dry eye disease*," Analytical biochemistry, 2018. **542**: p. 84-94.
46. W. Yang, J. Yan, G. Springsteen, S. Deeter, and B. Wang, "*A novel type of fluorescent boronic acid that shows large fluorescence intensity changes upon binding with a carbohydrate in aqueous solution at physiological pH*," Bioorganic & medicinal chemistry letters, 2003. **13** (6): p. 1019-1022.
47. T. D. James, K. S. Sandanayake, and S. Shinkai, "*A glucose-selective molecular fluorescence sensor*," Angewandte Chemie International Edition in English, 1994. **33** (21): p. 2207-2209.
48. H. Lee, Y. J. Hong, S. Baik, T. Hyeon, and D. H. Kim, "*Enzyme-based glucose sensor: from invasive to wearable device*," Advanced healthcare materials, 2018. **7** (8): p. 1701150.
49. W. Dungchai, O. Chailapakul, and C. S. Henry, "*Electrochemical detection for paper-based microfluidics*," Analytical chemistry, 2009. **81** (14): p. 5821-5826.
50. Z. Nie, F. Deiss, X. Liu, O. Akbulut, and G. M. Whitesides, "*Integration of paper-based microfluidic devices with commercial electrochemical readers*," Lab on a Chip, 2010. **10** (22): p. 3163-3169.
51. P. Rattanarat, W. Dungchai, W. Siangproh, O. Chailapakul, and C. S. Henry, "*Sodium dodecyl sulfate-modified electrochemical paper-based analytical device for determination of dopamine levels in biological samples*," Analytica chimica acta, 2012. **744**: p. 1-7.
52. L. Y. Shiroma, M. Santhiago, A. L. Gobbi, and L. T. Kubota, "*Separation and electrochemical detection of paracetamol and 4-aminophenol in a paper-based microfluidic device*," Analytica chimica acta, 2012. **725**: p. 44-50.
53. H. Yao, A. J. Shum, M. Cowan, I. Lähdesmäki, and B. A. Parviz, "*A contact lens with embedded sensor for monitoring tear glucose level*," Biosensors and Bioelectronics, 2011. **26** (7): p. 3290-3296.
54. M. X. Chu *et al.*, "*Soft contact lens biosensor for in situ monitoring of tear glucose as non-invasive blood sugar assessment*," Talanta, 2011. **83** (3): p. 960-965.
55. J. Kim *et al.*, "*Wearable smart sensor systems integrated on soft contact lenses for wireless ocular diagnostics*," Nature communications, 2017. **8**: p. 14997.
56. J. Park *et al.*, "*Soft, smart contact lenses with integrations of wireless circuits, glucose sensors, and displays*," Science advances, 2018. **4** (1): p. eaap9841.

57. M. Senior, "Novartis signs up for Google smart lens," ed: Nature Publishing Group, 2014.
58. B. Otis and N. Pletcher, "Contact lens that facilitates antenna communication via sensor impedance modulation," ed: Google Patents, 2014.
59. J. Kim, A. S. Campbell, B. E.-F. de Ávila, and J. Wang, "*Wearable biosensors for healthcare monitoring*," Nature biotechnology, 2019: p. 1.
60. R. Tseng, C.-C. Chen, S.-M. Hsu, and H.-S. Chuang, "*Contact-lens biosensors*," sensors, 2018. **18** (8): p. 2651.
61. S. Park, H. Boo, and T. D. Chung, "*Electrochemical non-enzymatic glucose sensors*," Analytica chimica acta, 2006. **556** (1): p. 46-57.
62. E. Saeedi, S. Kim, and B. A. Parviz, "*Self-assembled crystalline semiconductor optoelectronics on glass and plastic*," Journal of Micromechanics and Microengineering, 2008. **18** (7): p. 075019.
63. M. Leonardi, P. Leuenberger, D. Bertrand, A. Bertsch, and P. Renaud, "*First steps toward noninvasive intraocular pressure monitoring with a sensing contact lens*," Investigative ophthalmology & visual science, 2004. **45** (9): p. 3113-3117.
64. J. P. Lorand and J. O. EDWARDS, "*Polyol complexes and structure of the benzeneboronate ion*," The Journal of Organic Chemistry, 1959. **24** (6): p. 769-774.
65. S. Kabilan *et al.*, "*Holographic glucose sensors*," Biosensors and Bioelectronics, 2005. **20** (8): p. 1602-1610.
66. S. Kabilan *et al.*, "*Glucose-sensitive holographic sensors*," Journal of Molecular Recognition, 2004. **17** (3): p. 162-166.
67. C. J. Ward, P. Patel, and T. D. James, "*Molecular color sensors for monosaccharides*," Organic letters, 2002. **4** (4): p. 477-479.
68. S. A. Asher *et al.*, "*Photonic crystal carbohydrate sensors: low ionic strength sugar sensing*," Journal of the American Chemical Society, 2003. **125** (11): p. 3322-3329.
69. A. Ravve, *Principles of polymer chemistry*. Springer Science & Business Media, 2013.
70. A. Domschke *et al.*, "Holographic sensors in contact lenses for minimally-invasive glucose measurements," in *SENSORS, 2004 IEEE*: IEEE, p. 1320-1323.
71. V. L. Alexeev, S. Das, D. N. Finegold, and S. A. Asher, "*Photonic crystal glucose-sensing material for noninvasive monitoring of glucose in tear fluid*," Clinical Chemistry, 2004. **50** (12): p. 2353-2360.
72. M. Ben-Moshe, V. L. Alexeev, and S. A. Asher, "*Fast responsive crystalline colloidal array photonic crystal glucose sensors*," Analytical chemistry, 2006. **78** (14): p. 5149-5157.
73. C. Zhang, G. G. Cano, and P. V. Braun, "*Linear and fast hydrogel glucose sensor materials enabled by volume resetting agents*," Advanced Materials, 2014. **26** (32): p. 5678-5683.
74. S. J. Updike, M. C. Shults, B. J. Gilligan, and R. K. Rhodes, "*A subcutaneous glucose sensor with improved longevity, dynamic range, and stability of calibration*," Diabetes care, 2000. **23** (2): p. 208-214.
75. T. Koschinsky and L. Heinemann, "*Sensors for glucose monitoring: technical and clinical aspects*," Diabetes/metabolism research and reviews, 2001. **17** (2): p. 113-123.
76. F. Xue, Z. Meng, F. Wang, Q. Wang, M. Xue, and Z. Xu, "*A 2-D photonic crystal hydrogel for selective sensing of glucose*," Journal of Materials Chemistry A, 2014. **2** (25): p. 9559-9565.
77. C. Chen, Z.-Q. Dong, J.-H. Shen, H.-W. Chen, Y.-H. Zhu, and Z.-G. Zhu, "*2D Photonic Crystal Hydrogel Sensor for Tear Glucose Monitoring*," ACS Omega, 2018. **3** (3): p. 3211-3217.
78. J. M. Senior and M. Y. Jamro, *Optical fiber communications: principles and practice*. Pearson Education, 2009.

79. I.-L. Bundalo, O. Bang, and K. Nielsen, "*Fibre Bragg Grating and Long Period Grating Sensors in Polymer Optical Fibres*," 2017.
80. S. Yin and P. Ruffin, "*Fiber optic sensors*," Wiley Encyclopedia of Biomedical Engineering, 2006.
81. R. Kashyap, *Fiber bragg gratings*. Academic press, 2009.
82. J. Canning, "*Fibre gratings and devices for sensors and lasers*," Laser & Photonics Reviews, 2008. **2** (4): p. 275-289.
83. Y.-J. Rao, "*In-fibre Bragg grating sensors*," Measurement Science and Technology, 1997. **8** (4): p. 355.
84. A. D. Kersey *et al.*, "*Fiber grating sensors*," Journal of Lightwave Technology, 1997. **15** (8): p. 1442-1463.
85. J.-M. Renoirt, C. Caucheteur, M. Olivier, P. Mégret, and M. Debliquy, "Infrared Radiation Detection Using Fiber Bragg Grating," in *Infrared Radiation*: IntechOpen, 2012.
86. E. Udd, "*Fiber optic smart structure technology*," Fiber optic smart structures(A 95-34976 09-39), New York, NY, John Wiley & Sons, Inc.(Wiley Series in Pure and Applied Optics), 1995, 1995: p. 5-21.
87. B. Lee, Y. Jeong, S. Yin, P. Ruffin, and F. Yu, *Interrogation techniques for fiber grating sensors and the theory of fiber gratings*. Boca Raton, FL, USA: CRC Press, 2008.
88. B. Luo, Z. Yan, Z. Sun, J. Li, and L. Zhang, "*Novel glucose sensor based on enzyme-immobilized 81° tilted fiber grating*," Optics express, 2014. **22** (25): p. 30571-30578.
89. L. Grattan and B. Meggitt, *Optical fiber sensor technology: Advanced applications-Bragg gratings and distributed sensors*. Springer Science & Business Media, 2013.
90. S. W. James and R. P. Tatam, "*Optical fibre long-period grating sensors: characteristics and application*," Measurement Science and Technology, 2003. **14** (5): p. R49.
91. C. Silva, J. M. Coelho, P. Caldas, and P. Jorge, "Fibre sensing system based on long-period gratings for monitoring aqueous environments," in *Fiber Optic Sensors*: IntechOpen, 2012.
92. V. Bhatia and A. M. Vengsarkar, "*Optical fiber long-period grating sensors*," Optics letters, 1996. **21** (9): p. 692-694.
93. J. M. Corres, I. R. Matias, I. del Villar, and F. J. Arregui, "*Design of pH sensors in long-period fiber gratings using polymeric nanocoatings*," IEEE sensors journal, 2007. **7** (3): p. 455-463.
94. A. Deep *et al.*, "*Immobilization of enzyme on long period grating fibers for sensitive glucose detection*," Biosensors and Bioelectronics, 2012. **33** (1): p. 190-195.
95. J. M. Coelho, C. Silva, M. Nespereira, M. Abreu, and J. Rebordão, "*Writing of long period fiber gratings using CO2 laser radiation*," Advances in Optical Fiber Technology: Fundamental Optical Phenomena and Applications, 2015: p. 287-314.
96. M. I. Zibaii, A. Kazemi, H. Latifi, M. K. Azar, S. M. Hosseini, and M. H. Ghezelaiagh, "*Measuring bacterial growth by refractive index tapered fiber optic biosensor*," Journal of Photochemistry and Photobiology B: Biology, 2010. **101** (3): p. 313-320.
97. A. W. Snyder and J. Love, *Optical waveguide theory*. Springer Science & Business Media, 2012.
98. W. Stewart, "*Design limitation on tapers and couplers in single-mode flbers*," Technical Digest of IOOC-ECOC, 1, 1985: p. 559-562.
99. H. Qiu *et al.*, "*A novel graphene-based tapered optical fiber sensor for glucose detection*," Applied Surface Science, 2015. **329**: p. 390-395.
100. S. Zhu *et al.*, "*High sensitivity refractometer based on TiO2-coated adiabatic tapered optical fiber via ALD technology*," sensors, 2016. **16** (8): p. 1295.

101. B.-H. Lee, J.-B. Eom, K.-S. Park, S.-J. Park, and M.-J. Ju, "*Specialty fiber coupler: fabrications and applications*," Journal of the Optical Society of Korea, 2010. **14** (4): p. 326-332.
102. K. T. Grattan and B. T. Meggitt, *Optical fiber sensor technology*. Springer, 1995.
103. B. H. Lee *et al.*, "*Interferometric fiber optic sensors*," sensors, 2012. **12** (3): p. 2467-2486.
104. J. Sirkis, D. Brennan, M. Putman, T. Berkoff, A. Kersey, and E. Friebele, "*In-line fiber etalon for strain measurement*," Optics letters, 1993. **18** (22): p. 1973-1975.
105. W.-H. Tsai and C.-J. Lin, "*A novel structure for the intrinsic Fabry-Perot fiber-optic temperature sensor*," Journal of Lightwave Technology, 2001. **19** (5): p. 682-686.
106. J. J. Lee, S. H. Kim, D. C. Lee, and I. B. Kwon, "Transmission-type extrinsic fabry-perot interferometric optical fiber sensor," ed: Google Patents, 2004.
107. S.-H. Kim, J.-J. Lee, D.-C. Lee, and I.-B. Kwon, "*A study on the development of transmission-type extrinsic Fabry-Perot interferometric optical fiber sensor*," Journal of Lightwave Technology, 1999. **17** (10): p. 1869-1874.
108. K. Koo, M. LeBlanc, T. Tsai, and S. Vohra, "*Fiber-chirped grating Fabry-Perot sensor with multiple-wavelength-addressable free-spectral ranges*," IEEE photonics technology letters, 1998. **10** (7): p. 1006-1008.
109. J. S. Santos, I. M. Raimundo Jr, C. M. Cordeiro, C. R. Biazoli, C. A. Gouveia, and P. A. Jorge, "*Characterisation of a Nafion film by optical fibre Fabry–Perot interferometry for humidity sensing*," Sensors and Actuators B: Chemical, 2014. **196**: p. 99-105.
110. W. Xu, W.-B. Huang, X.-G. Huang, and C.-y. Yu, "*A simple fiber-optic humidity sensor based on extrinsic Fabry–Perot cavity constructed by cellulose acetate butyrate film*," Optical Fiber Technology, 2013. **19** (6): p. 583-586.
111. S. Tierney, D. R. Hjelme, and B. T. Stokke, "*Determination of swelling of responsive gels with nanometer resolution. Fiber-optic based platform for hydrogels as signal transducers*," Analytical chemistry, 2008. **80** (13): p. 5086-5093.
112. J. Goicoechea, C. Zamarreño, I. Matias, and F. Arregui, "*Utilization of white light interferometry in pH sensing applications by mean of the fabrication of nanostructured cavities*," Sensors and Actuators B: Chemical, 2009. **138** (2): p. 613-618.
113. J. H. Lim, H. S. Jang, K. S. Lee, J. C. Kim, and B. H. Lee, "*Mach–Zehnder interferometer formed in a photonic crystal fiber based on a pair of long-period fiber gratings*," Optics letters, 2004. **29** (4): p. 346-348.
114. Y.-J. Kim, U.-C. Paek, and B. H. Lee, "*Measurement of refractive-index variation with temperature by use of long-period fiber gratings*," Optics letters, 2002. **27** (15): p. 1297-1299.
115. T. Allsop, R. Reeves, D. J. Webb, I. Bennion, and R. Neal, "*A high sensitivity refractometer based upon a long period grating Mach–Zehnder interferometer*," Review of scientific instruments, 2002. **73** (4): p. 1702-1705.
116. Y.-H. Kim, M.-J. Kim, M.-S. Park, J.-H. Jang, B.-H. Lee, and K.-T. Kim, "*Hydrogen sensor based on a palladium-coated long-period fiber grating pair*," Journal of the Optical Society of Korea, 2008. **12** (4): p. 221-225.
117. M. Kim, Y. Kim, G. Mudhana, and B. Lee, "*Simultaneous measurement of temperature and strain based on double cladding fiber interferometer assisted by fiber grating pair*," IEEE photonics technology letters, 2008. **20** (15): p. 1290-1292.
118. J.-F. Ding, A. P. Zhang, L.-Y. Shao, J.-H. Yan, and S. He, "*Fiber-taper seeded long-period grating pair as a highly sensitive refractive-index sensor*," IEEE photonics technology letters, 2005. **17** (6): p. 1247-1249.

119. B. H. Lee and U.-C. Paek, "*Multislit interpretation of cascaded fiber gratings*," Journal of Lightwave Technology, 2002. **20** (9): p. 1750.
120. D. W. Kim, Y. Zhang, K. L. Cooper, and A. Wang, "*In-fiber reflection mode interferometer based on a long-period grating for external refractive-index measurement*," Applied optics, 2005. **44** (26): p. 5368-5373.
121. A. Van Brakel and P. L. Swart, "*Temperature-compensated optical fiber Michelson refractometer*," Optical Engineering, 2005. **44** (2): p. 020504.
122. L. Yuan, J. Yang, and Z. Liu, "*A compact fiber-optic flow velocity sensor based on a twin-core fiber Michelson interferometer*," IEEE sensors journal, 2008. **8** (7): p. 1114-1117.
123. H. Fu *et al.*, "*Pressure sensor realized with polarization-maintaining photonic crystal fiber-based Sagnac interferometer*," Applied optics, 2008. **47** (15): p. 2835-2839.
124. D. S. Moon *et al.*, "*The temperature sensitivity of Sagnac loop interferometer based on polarization maintaining side-hole fiber*," Optics express, 2007. **15** (13): p. 7962-7967.
125. G. Kim *et al.*, "*Strain and temperature sensitivities of an elliptical hollow-core photonic bandgap fiber based on Sagnac interferometer*," Optics express, 2009. **17** (4): p. 2481-2486.
126. R. W. Wood, "*XLII. On a remarkable case of uneven distribution of light in a diffraction grating spectrum*," The London, Edinburgh, and Dublin Philosophical Magazine and Journal of Science, 1902. **4** (21): p. 396-402.
127. U. Fano, "*The theory of anomalous diffraction gratings and of quasi-stationary waves on metallic surfaces (Sommerfeld's waves)*," JOSA, 1941. **31** (3): p. 213-222.
128. H. Raether, "Surface plasmons on smooth surfaces," in *Surface plasmons on smooth and rough surfaces and on gratings*: Springer, 1988, pp. 4-39.
129. B. D. Gupta and R. Kant, "*Recent advances in surface plasmon resonance based fiber optic chemical and biosensors utilizing bulk and nanostructures*," Optics & Laser Technology, 2018. **101**: p. 144-161.
130. A. Vinogradov, A. Dorofeenko, A. Pukhov, and A. Lisyansky, "*Exciting surface plasmon polaritons in the Kretschmann configuration by a light beam*," Physical review B, 2018. **97** (23): p. 235407.
131. V. Myroshnychenko *et al.*, "*Modelling the optical response of gold nanoparticles*," Chemical Society Reviews, 2008. **37** (9): p. 1792-1805.
132. S. Unser, I. Bruzas, J. He, and L. Sagle, "*Localized surface plasmon resonance biosensing: current challenges and approaches*," sensors, 2015. **15** (7): p. 15684-15716.
133. W. H. Yang, G. C. Schatz, and R. P. Van Duyne, "*Discrete dipole approximation for calculating extinction and Raman intensities for small particles with arbitrary shapes*," The Journal of chemical physics, 1995. **103** (3): p. 869-875.
134. J. Cao, T. Sun, and K. T. Grattan, "*Gold nanorod-based localized surface plasmon resonance biosensors: A review*," Sensors and Actuators B: Chemical, 2014. **195**: p. 332-351.
135. L. S. Jung, C. T. Campbell, T. M. Chinowsky, M. N. Mar, and S. S. Yee, "*Quantitative interpretation of the response of surface plasmon resonance sensors to adsorbed films*," Langmuir, 1998. **14** (19): p. 5636-5648.
136. J. Jana, M. Ganguly, and T. Pal, "*Enlightening surface plasmon resonance effect of metal nanoparticles for practical spectroscopic application*," RSC Advances, 2016. **6** (89): p. 86174-86211.
137. P. B. Johnson and R.-W. Christy, "*Optical constants of the noble metals*," Physical review B, 1972. **6** (12): p. 4370.

138. P. R. West, S. Ishii, G. V. Naik, N. K. Emani, V. M. Shalaev, and A. Boltasseva, "*Searching for better plasmonic materials*," Laser & Photonics Reviews, 2010. **4** (6): p. 795-808.
139. A. Leung, P. M. Shankar, and R. Mutharasan, "*A review of fiber-optic biosensors*," Sensors and Actuators B: Chemical, 2007. **125** (2): p. 688-703.
140. J. Wu, Y. Yan, S. Li, X. Ding, S. Ding, and Y. Huang, "*Monitoring of patient glucose infusion using a surface plasmon resonance-based fiber optic sensor*," Measurement Science and Technology, 2015. **26** (10): p. 105701.
141. M. Iga, A. Seki, and K. Watanabe, "*Hetero-core structured fiber optic surface plasmon resonance sensor with silver film*," Sensors and Actuators B: Chemical, 2004. **101** (3): p. 368-372.
142. Y. Zhao, M. Lei, S.-X. Liu, and Q. Zhao, "*Smart hydrogel-based optical fiber SPR sensor for pH measurements*," Sensors and Actuators B: Chemical, 2018. **261**: p. 226-232.
143. S. Singh and B. D. Gupta, "*Fabrication and characterization of a surface plasmon resonance based fiber optic sensor using gel entrapment technique for the detection of low glucose concentration*," Sensors and Actuators B: Chemical, 2013. **177**: p. 589-595.
144. Y. Ying, G.-y. Si, F.-j. Luan, K. Xu, Y.-w. Qi, and H.-n. Li, "*Recent research progress of optical fiber sensors based on D-shaped structure*," Optics & Laser Technology, 2017. **90**: p. 149-157.
145. K. Gasior, T. Martynkien, M. Napiorkowski, K. Zolnacz, P. Mergo, and W. Urbanczyk, "*A surface plasmon resonance sensor based on a single mode D-shape polymer optical fiber*," Journal of Optics, 2016. **19** (2): p. 025001.
146. S. Weng, L. Pei, J. Wang, T. Ning, and J. Li, "*High sensitivity D-shaped hole fiber temperature sensor based on surface plasmon resonance with liquid filling*," Photonics Research, 2017. **5** (2): p. 103-107.
147. S. K. Srivastava, V. Arora, S. Sapra, and B. D. Gupta, "*Localized surface plasmon resonance-based fiber optic U-shaped biosensor for the detection of blood glucose*," Plasmonics, 2012. **7** (2): p. 261-268.
148. M. Irigoyen, J. A. Sánchez-Martin, E. Bernabeu, and A. Zamora, "*Tapered optical fiber sensor for chemical pollutants detection in seawater*," Measurement Science and Technology, 2017. **28** (4): p. 045802.
149. H. Yuan *et al.*, "*Fiber-optic surface plasmon resonance glucose sensor enhanced with phenylboronic acid modified Au nanoparticles*," Biosensors and Bioelectronics, 2018. **117**: p. 637-643.
150. L. Bilro, N. Alberto, J. L. Pinto, and R. Nogueira, "*Optical sensors based on plastic fibers*," sensors, 2012. **12** (9): p. 12184-12207.
151. Y. Koike and K. Koike, "*Progress in low-loss and high-bandwidth plastic optical fibers*," Journal of Polymer Science Part B: Polymer Physics, 2011. **49** (1): p. 2-17.
152. M. Shortreed, R. Kopelman, M. Kuhn, and B. Hoyland, "*Fluorescent fiber-optic calcium sensor for physiological measurements*," Analytical chemistry, 1996. **68** (8): p. 1414-1418.
153. Y. J. Heo, H. Shibata, T. Okitsu, T. Kawanishi, and S. Takeuchi, "*Long-term in vivo glucose monitoring using fluorescent hydrogel fibers*," Proceedings of the National Academy of Sciences, 2011. **108** (33): p. 13399-13403.
154. H. Shibata, Y. J. Heo, T. Okitsu, Y. Matsunaga, T. Kawanishi, and S. Takeuchi, "*Injectable hydrogel microbeads for fluorescence-based in vivo continuous glucose monitoring*," Proceedings of the National Academy of Sciences, 2010. **107** (42): p. 17894-17898.

155. A. K. Yetisen *et al.*, "*Glucose-Sensitive Hydrogel Optical Fibers Functionalized with Phenylboronic Acid*," Advanced Materials, 2017. **29** (15): p. 1606380-1606391.
156. E. A. Moschou, B. V. Sharma, S. K. Deo, and S. Daunert, "*Fluorescence glucose detection: advances toward the ideal in vivo biosensor*," Journal of fluorescence, 2004. **14** (5): p. 535-547.

Chapter 3: Wearable Contact Lens Biosensors for Continuous Glucose Monitoring using Smartphones

This chapter of the alternative format thesis is published in journal of ACS Nano. The publishing details and authors contributions are outlined below.

Mohamed Elsherif**, Mohammed Umair Hassan, Ali K. Yetisen, and Haider Butt*, Wearable Contact Lens Biosensors for Continuous Glucose Monitoring using Smartphones, ACS Nano, 2018, 12, 5452-5462.

Authors Contributions

M.E. and H.B. conceived the project idea. **M.E**. designed the project, carried out experiments, analyzed results and wrote the article. H.B. supervised experiments and led the project. M.U.H and A.K.Y. revised the manuscript and provided intellectual contributions throughout the project.

Keywords: contact lenses, photonic nanostructures, glucose sensors, phenylboronic acid, smartphone diagnostics, wearable sensors

3.1 Abstract

Low-cost, robust, and reusable continuous glucose monitoring systems that can provide quantitative measurements at point-of-care settings is an unmet medical need. Optical glucose sensors require complex and time-consuming fabrication processes, and their readouts are impractical for quantitative analyses. Here, a wearable contact lens was created for the continuous quantification of glucose at the physiological conditions, simplifying the fabrication process and facilitating the sensor's readouts. A photonic microstructure having a periodicity of 1.6 μm was printed on a glucose-responsive hydrogel film functionalized with phenylboronic acid. Upon binding glucose with the phenylboronic acid immobilized in the hydrogel matrix, the microstructure volume swelled -modulating the periodic constant. The resulting change in Bragg diffraction modified the space between zero and first order spots. A correlation was established between the periodic constant and glucose concentration within 0-50 mM. The sensitivity of the sensor was 12 nm mM^{-1} and the saturation response time was 25, and 20 min for low and high glucose concentrations, respectively. The sensor was integrated with commercial contact lenses and tested for continuous glucose monitoring using smartphone readouts. The reflected power of the first order diffraction was measured *via* the ambient light sensor of a smartphone and correlated to the glucose concentrations. A short response time of 3 s and a saturation time of 4 min was achieved in the continuous monitoring mode. The proposed glucose sensitive contact lens may have applications in point-of-care continuous monitoring devices and diagnostics in home settings.

3.2 Introduction

The concentration of glucose is typically monitored by using fingerstick blood samples [1]. Patients on multiple-dose insulin injection or insulin pump therapy should measure their blood glucose concentration 6-8 times a day. However, the test is performed more infrequently due to the pain and inconvenience associated with fingersticks, particularly among children with type 1 diabetes [2, 3]. Another strategy is to use subcutaneously inserted electrochemical sensors for continuous glucose monitoring (CGM) systems (e.g., Dexcom, Medtronic) [4, 5]. These devices aim to provide real-time, and long-term measurements that can also be used with insulin pumps to form an automated feedback loop to manage insulin delivery when hypo/hyperglycemia is developing [6-8]. The primary application of these CGM devices is in type 1 diabetic patients. CGM systems also help prediabetic and type 2 diabetic patients to self-regulate their exercise and achieve effective intervention programs and to optimize insulin regimen [9-11]. However, commercial CGM systems do not completely provide an ideal solution for uncontrolled glycemic fluctuations due to low patient compliance, and the daily basis calibration as 3-4 fingerstick blood tests is demanded [12]. These devices are subjected to signal drift due to electrochemical reaction instability resulting in time lags and sensor replacement every 3-7 days [13]. Therefore, the development of minimally-invasive continuous monitoring systems that can accurately measure the blood glucose concentration for long periods without frequent calibration and replacement is an unmet need in diabetes care.

To overcome the instability issues with electrochemical sensors, alternative approaches involving phenylboronic acid (PBA) derivatives and optical sensors have emerged.

Functionalizing a hydrogel with PBA that exhibits affinity to *cis*-diol molecules can be exploited for continuous monitoring of glucose. PBA binds reversibly with glucose molecules altering the volume of the hydrogel matrix [14-16]. This mechanism of volumetric changes in glucose-sensitive hydrogels has motivated the investigation of glucose sensors. For example, hydrogels containing 3D crystalline colloidal arrays (CCAs) have been synthesized and functionalized with PBA [17-19]. Periodic arrangement of the dielectric particles in the three dimensions inside the hydrogel matrix form 3D photonic crystals (PC) which acts as a wavelength filter and diffracts specific wavelengths according to Bragg's law. Thereby, any volumetric change result from a variation in glucose concentration can be sensed as the Bragg peak shifts. Recent studies focused on improving the selectivity, sensitivity, and response time of the inverse opal 3D PC hydrogels functionalized with PBA for glucose sensing [15, 20-23]. Nevertheless, the preparation of a 3D PCs has stringent constraints; their fabrication is complex (monodispersed, highly-charged microparticles), time consuming (*e.g.* ion depletion, dialysis), and requires considerable optimization to realize the required lattice order [24]. Recently, a hydrogel-based 2D CCA monolayer sensor has also been demonstrated [25, 26]. The volumetric changes of the hydrogel upon binding with glucose in 2D CCA sensors induce a change in the particle interspace that leads to shift of the diameter of the Debye diffraction ring. Although, fabrication of the 2D-PCs sensor is relatively less time consuming as compared to 3D PCs, it still requires a well-ordered monolayer of particles, optimization to not disrupt the array, and post-polymerization functionalization with PBA. Based on glucose-induced hydrogel volume modulation, reflection hologram based sensors have been also realized [27, 28]. These sensors are sensitive to glucose but require a sophisticated fabrication technique based on continuous or

pulsed laser interference recording. The complications in fabricating photonic crystal sensors hinder their way to mass production at low cost. Additionally, it remains a challenge to obtain visual quantitative readouts.

Here, photonic microstructure (PS)-based sensors were developed *via* the replica mould method of the microstructure on the surface of glucose-responsive hydrogel networks. As a free-standing sensor, the volumetric changes of the hydrogel in response to the variation of glucose concentration modulated the periodic constant of the microstructure, changing the diffraction angle and the zero-first order interspacing for the diffracted monochromatic light in transmission mode. The sensor was also attached to a commercial contact lens (ACUVUE) and a smartphone application was utilized to record the reflected power of the first order diffracted spot. The groove depth of the constrained sensor on the contact lens surface increased with glucose complexation leading to a change in the diffraction efficiency. This sensor offers advantages in terms of fast and facile preparation, swift response time, and simple readouts within physiological conditions.

3.3 Results and Discussion

The photonic microstructures (PS) were replicated on a hydrogel matrix during the UV curing process (Figure 3.1). Surface characterization has confirmed successful replication of the 1D master PS on the hydrogel film as probed by optical microscope images (Figure 3.2a-b). Optical microscopy images revealed that the replicated structure on the hydrogel matrix was intact and well ordered. The diffraction of the broadband light in transmission mode by the PS hydrogel sensor produced visible colors (rainbow), a schematic of the diffraction pattern is displayed on a screen (Figure 3.2c). Figure 3.2c shows a schematic of the setup

used for diffraction experiments in transmission mode. The setup was fixed on an optical bench and consisted of a 3D translation stage for controlling the position of the sample, a broadband light source for illuminating the sample, and a screen for displaying the projected transmitted diffraction pattern.

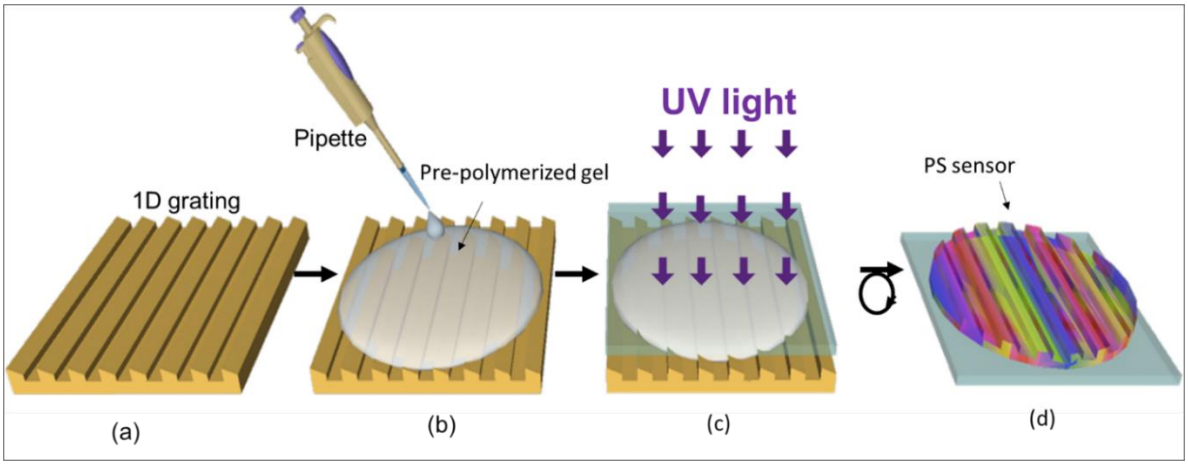

Figure 3.1. Schematic of the fabrication process of the hydrogel glucose sensor, (a) PS master, (b) The PS was coated with a monomer solution by drop casting method, (c) UV polymerization of the monomer solution, and (d) The replica of the PS was peeled off from the master PS.

The diffraction of monochromatic blue (405 nm), green (532 nm), and red (650 nm) laser light by the PS sensor in transmission mode was studied in 40% relative humidity and fully-hydrated conditions (equilibration in PBS buffer solution) to record the swelling effect in terms of change in diffraction properties. When the sensor was illuminated at normal incidence, the diffracted light on the screen perpendicularly placed to the laser beam was observed in the form of 1D interference fringe array. Photographs of the diffraction patterns for the three laser wavelengths were captured from a fixed distance to the imaging screen, and zero-first order interspace (l), diffraction angles (θ_d), and diffraction efficiency were measured using ImageJ program (Figure 3.3). The linear array of diffracted light resulting

from the PS sensor obeyed the transmission grating formula; $m\lambda_d = \Lambda\,(sin\theta_i - sin\theta_d)$, where m is an integer represent the diffraction order, λ_d is the diffraction wavelength, Λ is the periodic constant or groove constant, and θ_i and θ_d are the incidence and diffraction angles, respectively. In the experimental configuration, the transmission diffraction angle, θ_d, can be obtained from the relationship, $\theta_d = \tan^{-1} l\, h^{-1}$, where h is the distance between the PS sensor and the imaging screen. The volumetric changes in the PS sensor affected the periodic constant, which subsequently altered the zero-first order interspace. Conversely, change in periodic constant ($\Delta\,\Lambda$), and in diffraction angles ($\Delta\theta_d$) could be determined by measuring the interspace between zero and first order fringes – and this principle allowed the measurements of the glucose concentration for the free-standing glucose sensor.

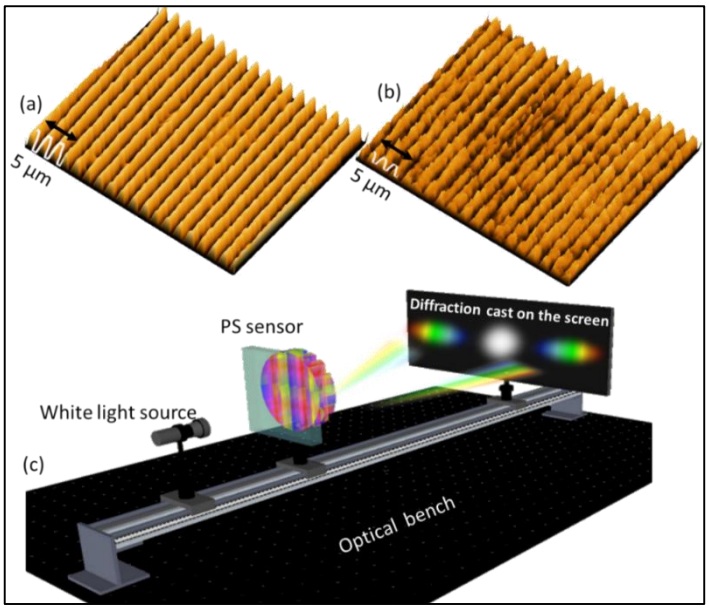

Figure 3.2. Optical microscope images of the master PS (a), and the glucose responsive hydrogel sensor (b), (c) The schematic of the setup used to project transmitted diffraction patterns.

In 40% relative humidity condition, θ_d and l for blue, green, and red laser beams were larger as compared to their counterpart values in the fully hydrated case. The PS sensor swelled upon immersion in PBS solution, increasing the periodic constant that decreased the diffraction angle and consequently the zero-first order interspace shrunk. That is, for the red, green and blue beams, l shrunk from its pristine values of around 18, 16, and 14 cm to 15, 13, and 11 cm, respectively and the diffraction angles decreased from 23°, 18°, and 14°, to 18°, 14°, and 11°, respectively. The diffraction angle was wavelength-dependent, where the smallest angle was for the blue light and the largest angle was for the red light, as expected according to the grating formula. In 40% relative humidity condition, the calculated values of θ_d and l using the grating formula were found to be consistent with the measured values using the identical experiment parameters; Λ = 1.6 μm, θ_i = 0°, and λ = 405, 532, and 650 nm. The calculated diffraction angles were 22.2°, 19.0° and 14.6° for red, green, and blue lasers, respectively. These slight differences in the calculated values are attributed to the slight expansion of the PS hydrogel due to the humidity. The absolute diffraction efficiency of the first order for PS sensor was wavelength dependent and it subtly decreased in fully-hydrated condition. The highest diffraction efficiency was recorded for blue light which decreased with increasing the illumination wavelength. In 40% relative humidity condition, as Λ and θ_i were constants, the absolute efficiencies were recorded to be 0.030%, 0.020%, and 0.009% for blue, green and red laser beams, respectively. Thus, these results match with the grating formula that states the absolute diffraction efficiency is depended upon the wavelength, incident angle, and the periodic constant [29]. The absolute diffraction efficiency of the PS sensor was inversely proportional to the periodic constant – the first

order efficiency in fully-hydrated condition for blue, green, and red lasers were ~ 0.027%, 0.015%, and 0.006% that were less than their counterparts in 40% relative humidity condition.

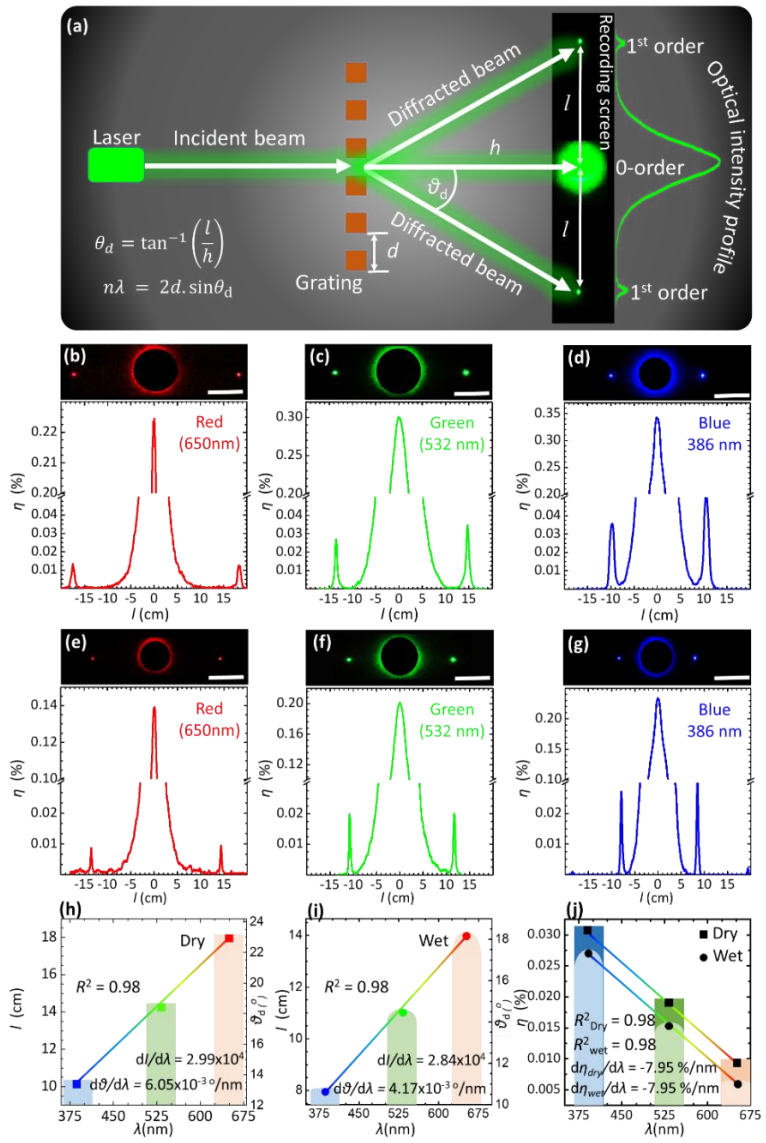

Figure 3.3. The diffraction pattern of the PS hydrogel sensor when it is illuminated by a monochromatic light in 40% relative humidity and fully hydrated conditions. (a) A schematic set up for recording the diffraction in transmission mode, (b, c, and d) the diffraction pattern of the PS sensor when it is illuminated by red (650 nm), green (532 nm), and blue (405 nm) lasers in 40% relative humidity conditions, respectively. (e,f, and g) shows the diffraction pattern of the sensor in fully hydrated conditions when it is shined by red, green, and blue lasers, respectively, scale bar 8 cm (h, i) Zero-first order interspace *versus* laser wavelengths

in 40% relative humidity and fully hydrated conditions, (j) Diffraction efficiency in 40% humidity and fully hydrated conditions for various laser wavelengths.

Transmission characteristics of the PS sensor were investigated at different polarization angles (0-90°) to study the swelling effect on the transmission properties and the sensor response to polarized light in 40% relative humidity and fully hydrated conditions. Figure 3.4a shows the schematic of the experimental setup for transmittance measurements. Transmittance of the sensor in fully hydrated condition was higher than that in the 40% relative humidity condition; this was because of swelling in the hydrogel due to imbibing more water which led to decrease the refractive index, and to an increase in the periodic constant that induced a decrease in the diffraction efficiency of the sensor (Figure 3.4b-c). The trend of transmission curves for all polarization angles remained similar in 40% relative humidity and fully hydrated conditions – transmittance increased gradually from shorter to longer wavelengths and decreased systematically with polarization angles. This could be also explained from the results in figure 3.3 which showed that the diffraction efficiency was higher for short wavelengths (blue laser beam) than longer wavelength laser beams (green and red). The decrease of the transmission spectra over all the wavelength range with polarization angle confirmed that the PS sensor was insensitive to polarized light and exhibited no polarization effects itself.

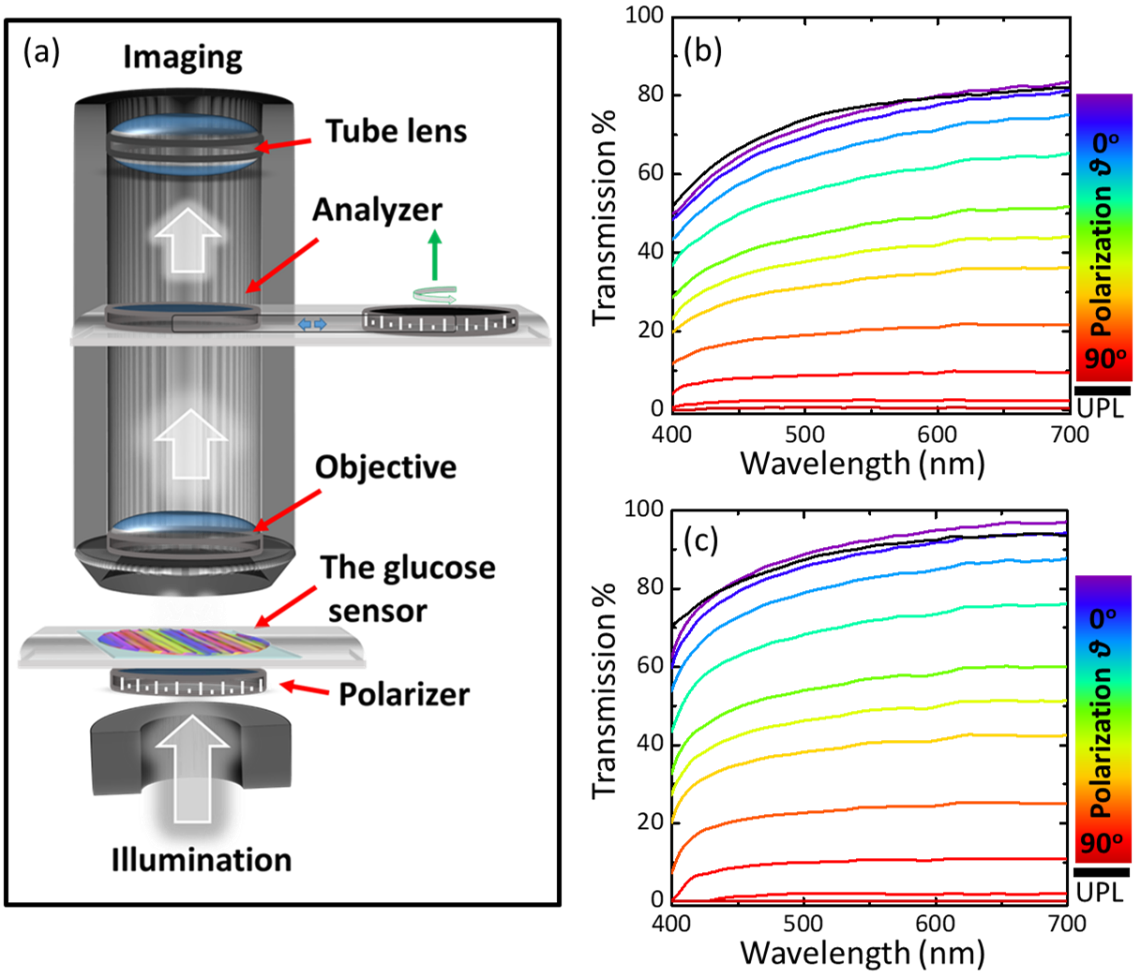

Figure 3.4. Transmittance properties of PS sensor. (a) Schematic of the setup used for measuring the transmission of the sensor under various polarization angles. (b and c) Transmission spectra of unpolarized (UPL) and polarized light versus wavelengths at various polarization angles while the sensor was in 40% relative humidity and fully hydrated, respectively.

Angle-resolved diffraction measurements in reflection mode for the PS sensor in 40% relative humidity and fully hydrated conditions were recorded to analyze the hydrogel swelling effect (Figure 3.5a-b). First order diffraction of the PS sensor in reflection mode was recorded using a spectrophotometer, while the sensor was fixed horizontally on an aluminum mirror and illuminated by a fiber optic halogen light source. In 40% relative

humidity condition, the detector was rotated 18° (20°-38°), to pick up the first order diffraction rainbow in the spectral range 450-850 nm. However, for the fully hydrated condition, the same spectral range was picked up by traversing the detector by only 13° (20-33°), which is 5° less than that of the 40% relative humidity condition. This was because of expanding the periodic constant upon hydrogel swelling of the PS sensor that led to a decrease in the angular dispersion of PS and to shrink the spatially separated rainbow.

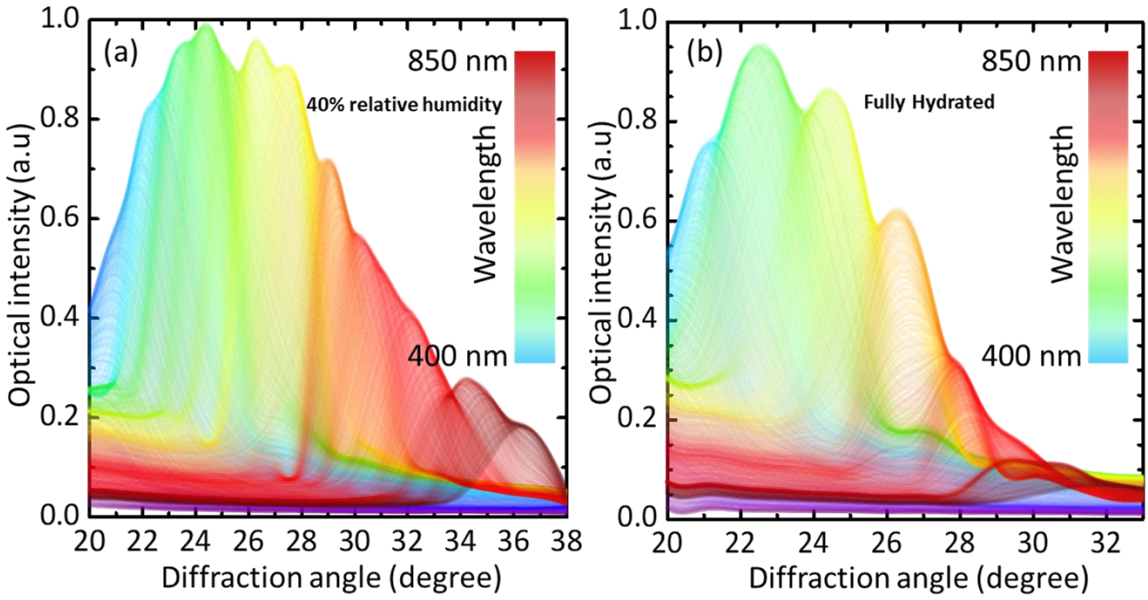

Figure 3.5. Angle-resolved measurements of the diffracted light in the reflection mode for photonic structure sensor on a plane mirror in 40% relative humidity (a), and fully-hydrated conditions (b).

The glucose sensing test was first carried out by investigating the cross-section variation of the PS sensor in various glucose concentrations at 24 °C. The cross-section dynamics of the hydrogel matrix was measured under an optical microscope and correlated with glucose concentrations (Figure 3.6). Boronic acid has a $pK_a \sim 8.8$ and at low pH values ($pH < pK_a$), PBA exists in an uncharged trigonal planar configuration. When PBA interacts with *cis*-diol molecules, a cyclic ester is formed whose pK_a is less than the boronic acid and it dissociates

into the hydrogen ion and the stable boronate anion (Figure 3.6b). While at higher pH values in an aqueous solution ($pH > pK_a$), the trigonal form of PBA dissociate donating proton forming boronate anion of tetrahedral configuration that binds to *cis*-diol molecules (Figure 3.6b) [30]. PBA reversibly binds with diols in glucose forming either 1:1 complex or a 2:1 crosslinking complex. Glucose-induced PS sensor swelling resulted from the formation of anionic boronate-glucose 1:1 complexation in the hydrogel matrix that increased the boronate anions, inducing the Donnan potential, which generates osmatic pressure that leads to swelling the hydrogel [31]. The hydrogel swelling upon glucose binding occurs not only across the cross-section, but also in-plane to the surface, increasing the periodic constant. First, the sensor was equilibrated in PBS solution (pH 7.4, ionic strength, 150 mM) for 2 h, then thickness measurements of the hydrogel cross-section were carried out after 60 min for each concentration. Glucose concentrations (0-50 mM) in PBS solution with 10 mM increments were presented to the PS and analyzed under an optical microscope (Figure 3.6c). The sensor swelled due to glucose binding and the cross-section linearly increased with increasing concentrations. When the glucose concentration was increased from 0 to10 mM, the sensor's cross-section thickness increased from an original value of 100 μm to 110 μm, and reached 130 μm for 50 mM glucose concentration (Figure 3.6d).

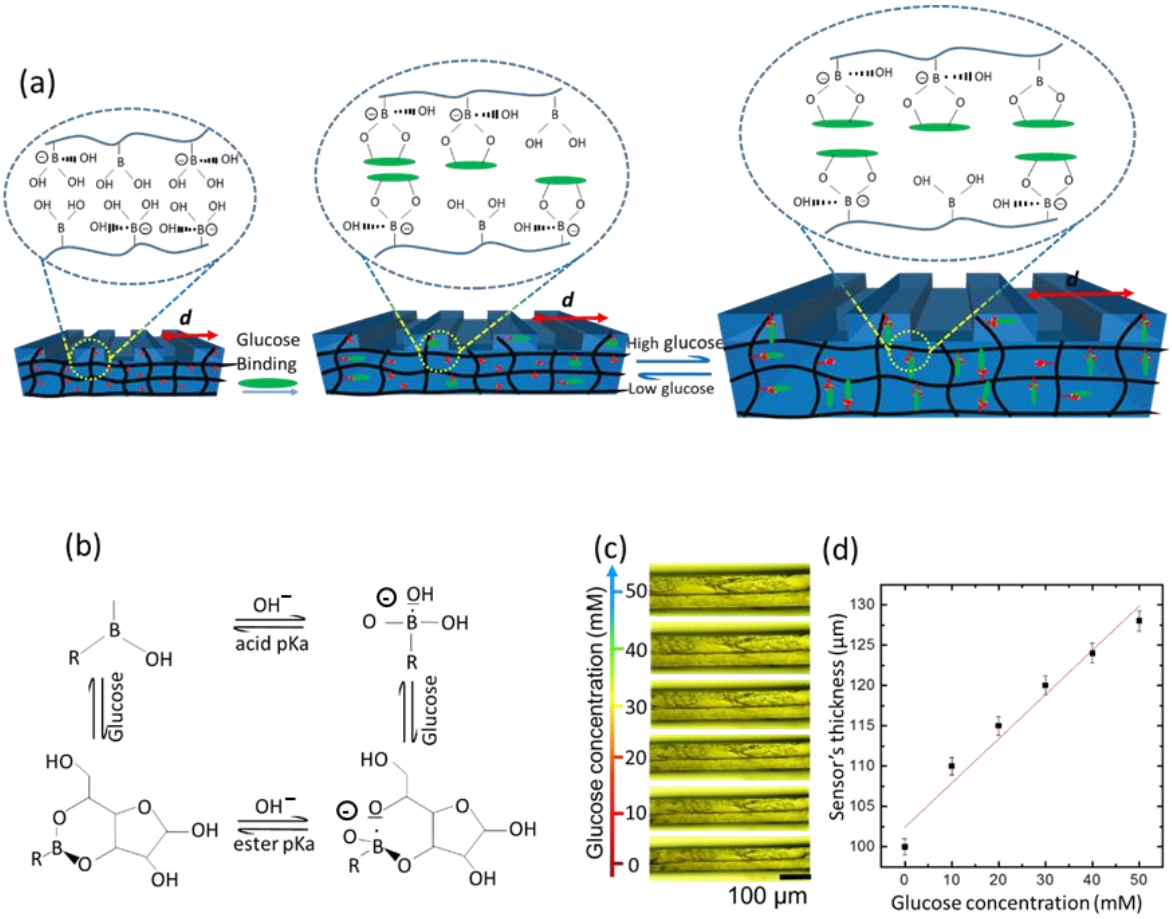

Figure 3.6. Sensing principle of the PS sensor (a) Effect of the glucose-boronate complexation on the PS sensor, (b) Complexation equilibrium between the boronic acid and glucose, (c) Microscopic images of the PS sensor's cross-section in various glucose concentrations, (d) Change in the sensor's cross-section as a function of glucose concentration. The scale bars show standard error (n=3).

Diffraction experiments in transmission mode for the PS sensor under physiological conditions were carried out to quantify glucose concentrations (Figure 3.7& 3.8). The setup used for the sensor readout consisted of an image screen, and a red laser pointer as a beam source (Figure 3.2c). The glucose binding induced swelling in the periodic constant, leading to shrinkage of zero-first order interspace and decrease in the diffraction angle (θ_d). For low glucose concentrations, the interspace linearly decreased from 20.2 cm to 18.2 cm, in response to an increase in glucose concentrations from 0 to 10 mM -reflecting an increase of

Λ from 1840 nm to 1968 nm with overall 128 nm increase (Figure 3.7a-b). For high glucose concentrations from 10 to 50 mM, the sensor produced linear response and the periodic constant increased by 180 nm to reach 2150 nm, shrinking the zero-first order interspace by 2.1 cm to become 16.1 cm (Figure 3.8a-b). When the glucose concentration increased to 100 mM, the periodic spacing increased to 2270 nm recording a 120 nm shift. The slope of the linear relation for the periodic constant versus the glucose concentration was 12 nm/mM in the low glucose concentration range (0-10 mM), which was more than double the slope of the linear relation (4.5 nm/mM) for the high glucose concentration range (10-50 mM) (Figures 3.7c & 3.8c). This indicated that the sensor's sensitivity decreased above 10 mM and this might be due to the decrease in the elasticity of the hydrogel matrix resulting from the glucose complexation, which increased the cross-link density [32]. The sensor's sensitivity decreased subtly with increasing glucose concentrations and had a nonlinear response above 50 mM (Figure 3.8c-d).

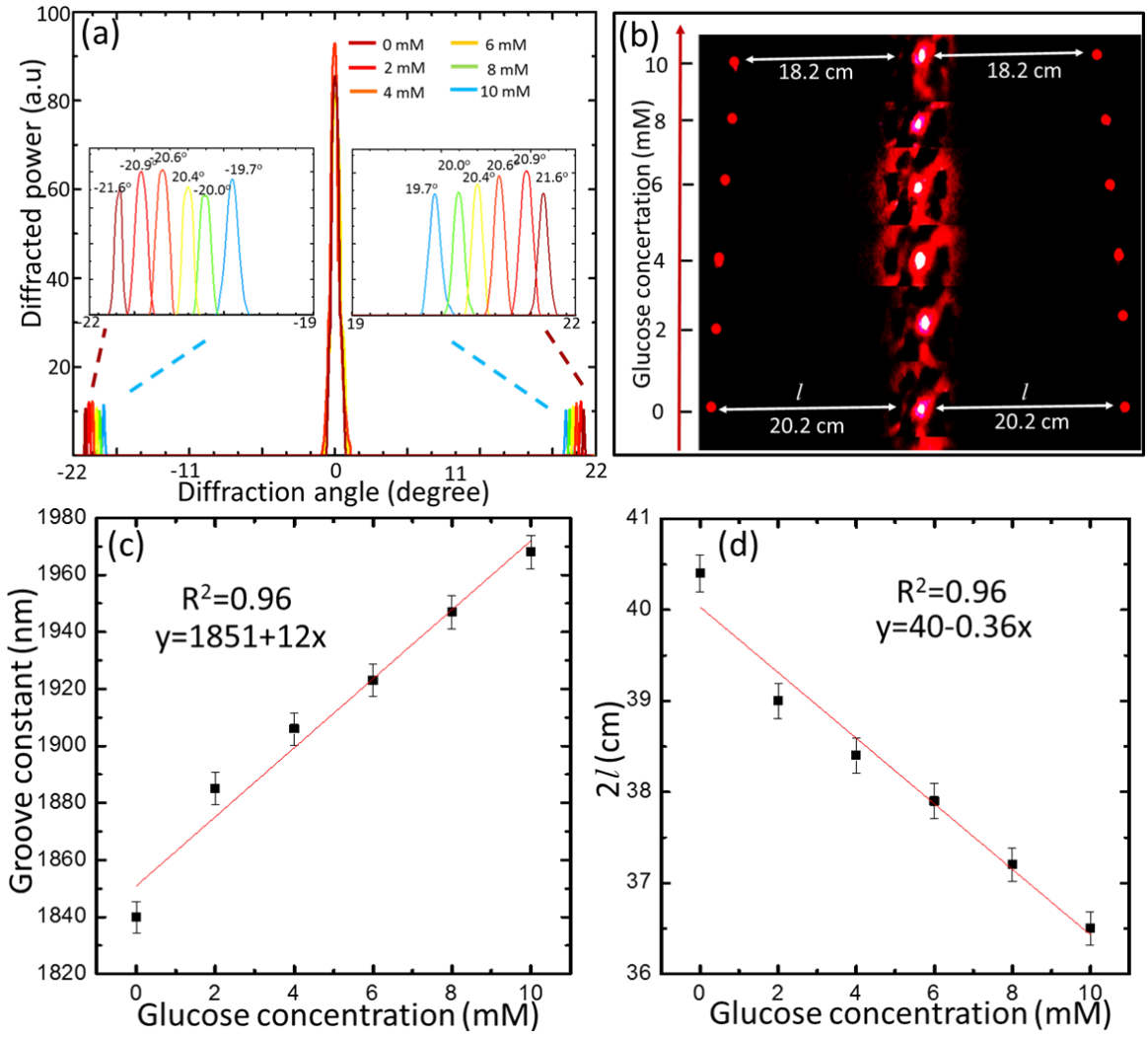

Figure 3.7. Low glucose concentration sensing *via* recording the diffraction images of the PS sensor in transmission mode. (a) Transmitted diffraction pattern for the PS sensor in glucose concentrations range of 0-10 mM, (b) Images of the diffraction pattern on the screen for the PS sensor immersed in various concentrations of glucose solutions, (c) Dependence of the periodic constant of the PS sensor on glucose concentrations (0-10 mM) in PBS buffer (ionic strength, 150 mM, pH 7.4 at 24°) as probed by a red laser beam in normal incidence configuration. (d) Dependence of the interspace of the first order diffraction spots ($2l$) on glucose concentrations (0-10 mM). The scale bars show standard error (n=3).

The sensitivity of the sensor for glucose can be given by the slope of the linear correlation of the periodic constant versus the glucose concentration, $S = \frac{\Delta\Lambda}{\Delta M}$, where $\Delta\Lambda$ is the change in the periodic constant, and ΔM is the change in glucose concentration. For low glucose

concentrations (0-10 mM), which is the most significant range, the sensitivity of the PS sensor was ~12.8 nm/mM, that resulted in a decrease of 4 cm between the first order spots, while the image screen was placed at 50 cm away from the sensor. Within the range of 10-50 mM, the sensor's sensitivity decreased to ~ 4.5 nm/mM, and this behavior agrees with the previously reported work [17, 18].

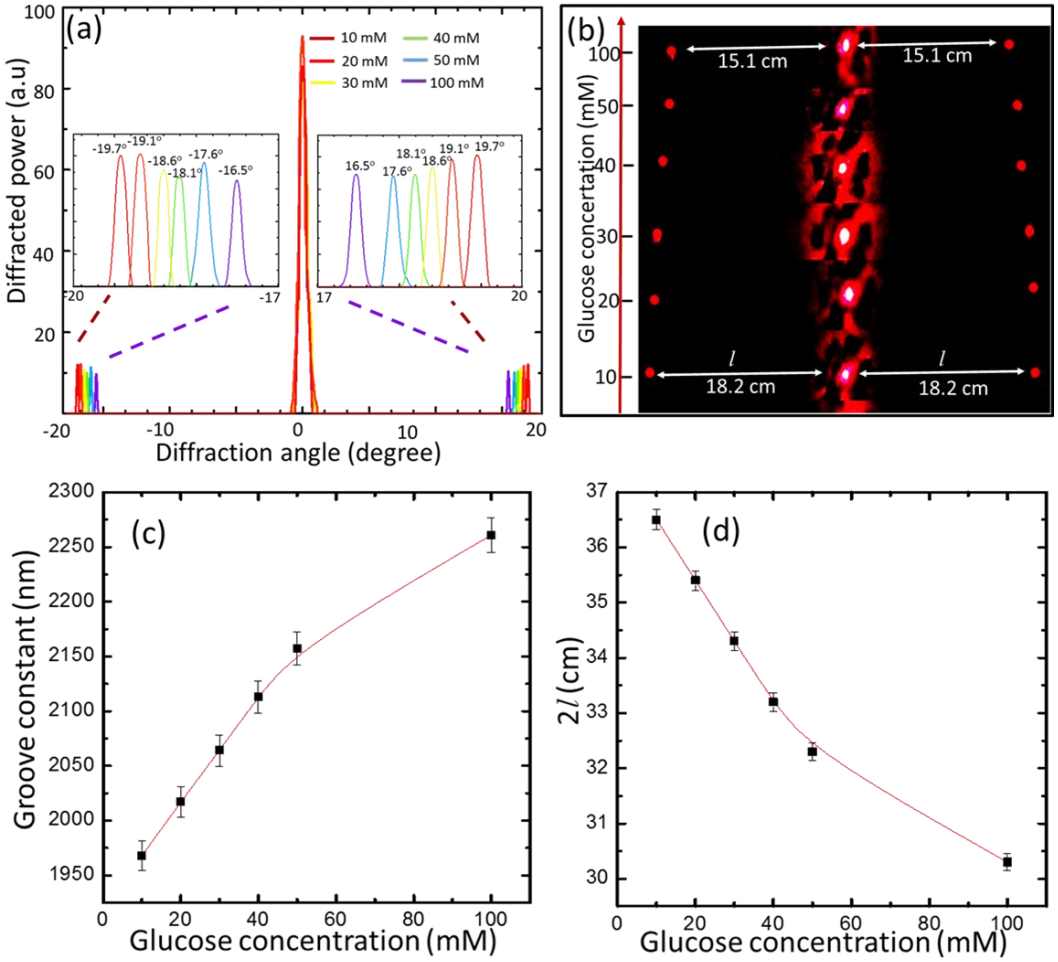

Figure 3.8. Detecting of high glucose concentrations *via* recording the diffraction images of the PS sensor in transmission mode, (a) Transmitted diffraction of the sensor in high glucose concentrations from 10 to 100 mM, (b) Images of the diffraction pattern on a screen for the sensor immersed in high glucose concentrations, (c) The periodic constant of the sensor *versus* high glucose concentrations (10 to 100 mM) in a PBS buffer of ionic strength 150 mM, pH 7.4 at 24 °C, (d) The interspace between the first order spots for the sensor in high glucose concentrations. The scale bars show standard error (n=3).

One dimesional holographic and 3D crystalline colloidal array (PCCA) glucose sensors exhibit a 300 nm wavelength shift over the glucose range from 0 to 50 mM [20, 27]. The periodic contant of the PS sensor increased by 310 nm for the same glucose concentration range. Diffraction measurements from holographic and PCCA sensors are a relatively complex process, requiring measurements in dark to prevent the ambient light interference, high-cost fiber optics, and spectrophotometers [33]. In contrast, readout and quantitative measurements of the glucose concentration by the PS sensor only requires a screen, a laser pointer, and a camera, which renders this approach simple, low-cost, and practical. Comparing the sensitivity of the PS sensor with the 2D-sensors, the PS offers nearly double their sensitiviy. For example, in 2D glucose sensors, the particle spacing shifted by 7 nm per mM glucose concentration in the range from 0 to 10 mM, but the periodic constant of the PS sensor shifted by 12 nm per mM [24]. The higher sensitivity of the PS sensor as compared to the 2D-array sensors can be attributed to the larger active surface area resulting from the repliated photonic microstructres on the sensor's surface. In contrast, the existing 2D arrays involve an inactive polysterene particles monlayer that covers one of the sensor's surfaces, which reduces the sensing active area.

The swelling kinetics of the PS sensor upon glucose binding has been studied for low (2 mM) and high (10 mM) glucose concentrations (Figure 3.9). The change of the periodic constant of the sensor was recorded every 5 min for each concentration. The sensor exhibited rapid response to glucose and reached complexation equilibrium in 25 min and 20 min for low and high glucose concentrations, respectively (Figure 3.9a-b). The low glucose concentration (2 mM) took a longer time to reach saturation (25 min) which agreed with the previously

reported work [33, 34]. In recent studies, the saturation time for the 3PBA-modified PCCAs was 40 min for 10 mM glucose concentration which was double the saturation time (20 min) for our PS sensor [20]. Also, the saturation time for 3PBA-holographic sensors was recorded to be 120 min for low glucose concentration and more than 50 min for high glucose concentrations [33]. The rapid response for low and high glucose concentrations is one of the advantageous characteristics of the PS sensor that can be explained by increasing the surface-to-volume ratio due to printing the PS on the top of the glucose-responsive hydrogel matrix. To investigate the stability and reusability of the sensor, the response of the sensor during three cycles was recorded (Figure 3.9c). The sensor was examined for 60 min, then reset by a buffer solution of pH 4.6 for 10 s and 60 min in PBS buffer before the next cycle. The periodic spacing swelled to become 1905±3 nm from its original value 1840 nm in each cycle and by resetting, the periodic constant shrunk to its pristine value around 1840±3 nm each time.

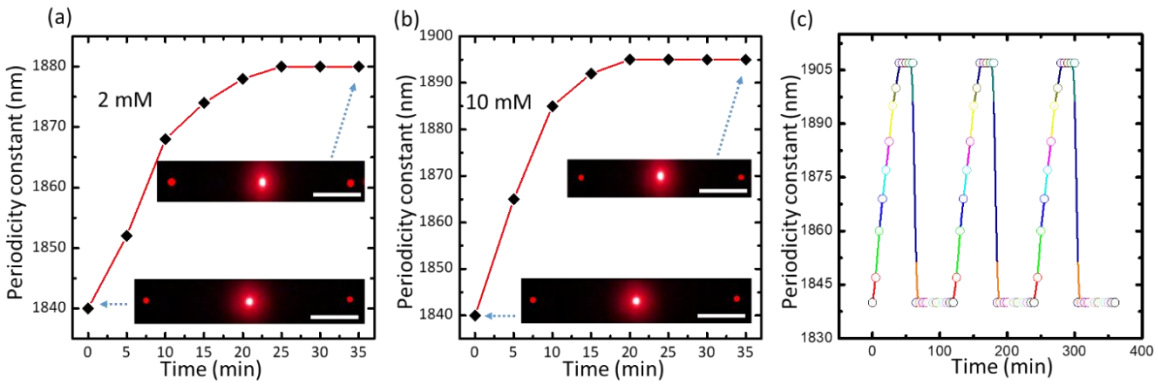

Figure 3.9. Response kinetics of the PC sensor (a) the swelling kinetics of the sensor in PBS buffer of 2 mM glucose (b) 10 mM glucose (pH 7.4 and ionic strength 150 mM). Scale bar= 10 cm. (c) The periodicity constant versus time for 10 mM glucose concentration during three cycles as the sensor was reset for 10 s in pH 4.6 then 60 min in PBS buffer in each cycle.

Back diffraction measurements were employed to confirm the PS sensor can sense glucose by this method as well. The sensor was placed on a horizontal mirror and illuminated by a broadband source at 38°. The back diffracted light was collected by a spectrophotometer fixed on a precision rotation stage (Figure 3.10a). Figure 3.10b illustrates the experimental data for diffracted light plotted against wavelength for glucose concentrations 10-50 mM. The diffracted wavelength shifted from 470 to 504 nm upon glucose concentration from 10 to 50 mM.

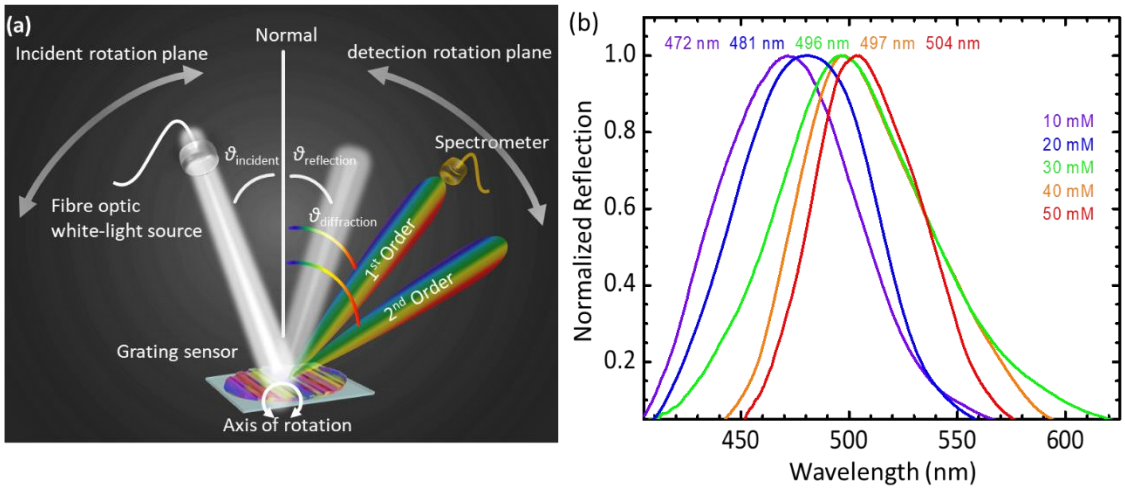

Figure 3.10. Sensing glucose by measuring the diffracted light in the reflection mode. (a) Schematic of the setup used for measuring the diffraction in the reflection mode. (b) Light diffraction *versus* wavelengths for the PS sensor in various glucose concentrations from 10 to 50 mM.

The utility of the PS glucose sensor was demonstrated in the form of a point-of-care wearable sensor; the sensor was attached to a commercial contact lens and the glucose concentration was measured by a smart phone app (Figure 3.11a-c). As shown in Figure 3.11b, the sensor exhibits a rainbow light effect on the contact lens surface under normal room light conditions.

For the constrained sensor on the contact lens surface, the glucose concentration was monitored by recording the reflected power of the first order spot (P_1). The constraint offered by the contact lens does not allow the grating spacing to change; however, the groove depth of the sensor increases with glucose complexing leading to changes in the diffraction efficiency (P_1/P_o). The contact lens was illuminated with a low power monochromatic light of wavelength 532 nm and the reflected power of the first-order spot was recorded by a power meter and a smart phone's photodetector. Continuous monitoring of the reflected power in response to glucose concentrations (0-50 mM) was carried out (Figure 3.11d-g). As the contact lens was used as the substrate platform for the sensor, this allowed us to cut down the sensor thickness to be around ~ 2 μm, which offered a fast response time near 3 s, and reached the equilibrium state in 12, 4, 4, 2, 2, 1.5 min for glucose concentrations 10, 20, 30, 40, 50, and 100 mM, respectively (Figure 3.12a-f). The response and saturation times for the contact lens based PS sensor are impressive as compared to the recently published report, where an equilibrium time of ~20 min was recorded [31].

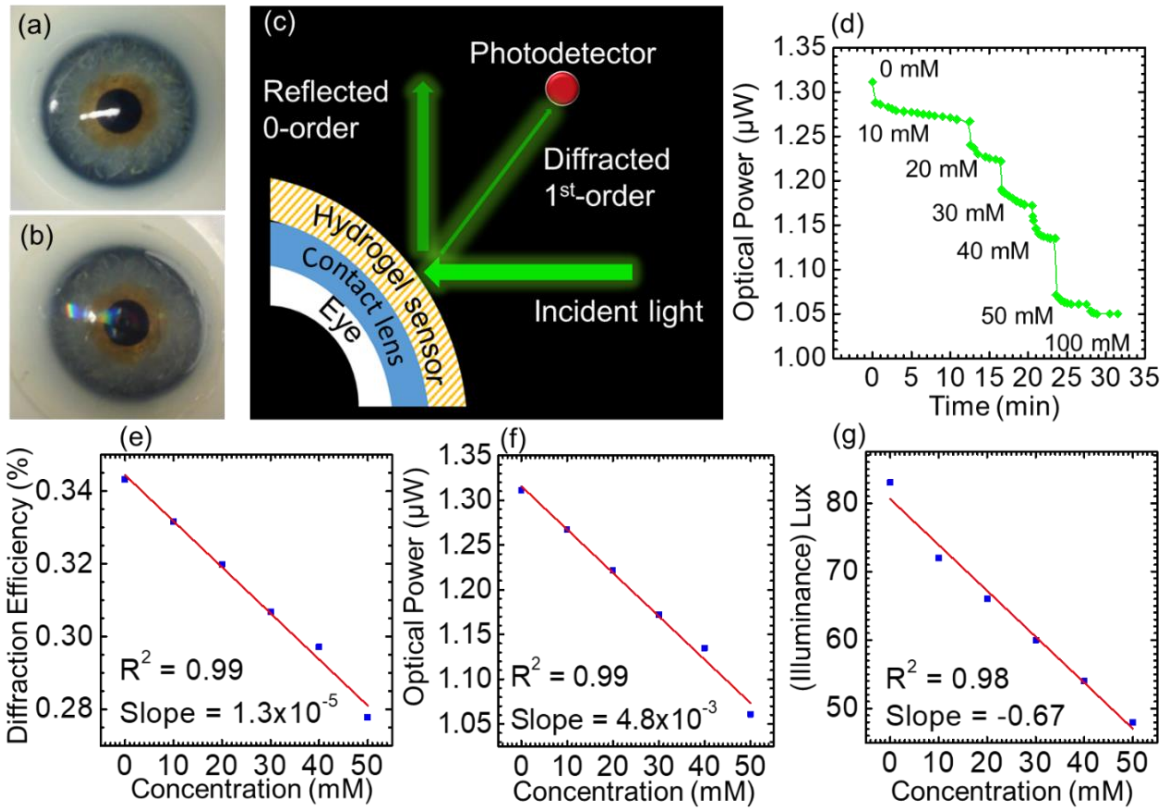

Figure 3.11. Contact lens integrated glucose sensor; (a) A photograph for a commercial contact lens on an artificial eye model, (b) A photograph of the PS sensor attached to the contact lens and placed on the eye model, (c) Schematic diagram of the measurement setup, (d) The reflected optical power of the diffracted first-order at various glucose concentrations (0-50 mM) versus time measured using the optical power meter, (e) Diffraction efficiency of the sensor versus glucose concentrations (0-50 mM), (f) The optical power of the first-order spot reflected from the sensor against glucose concentrations, (g) Reflected illuminance recorded by a smartphone against glucose concentration.

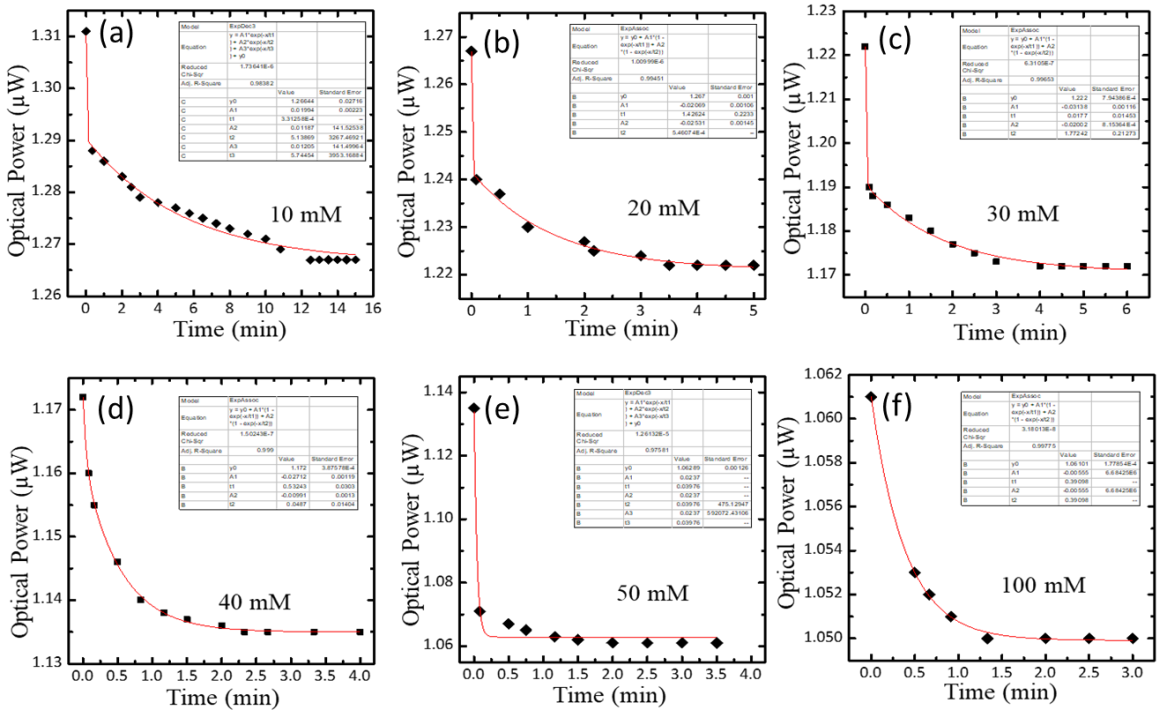

Figure 3.12. The kinetic swelling of the contact lens attached sensor in different glucose concentrations from 10 mM to 100 mM in continuous monitoring mode (a-f).

The effect of the mechanical strain on the output signal of the contact lens sensor was also studied (Figure 3.13). The contact lens integrated with the PS sensor was exposed to an extension force and the change in the output signal was recorded by an optical power meter. The mechanical strain was monitored against the reflected power for the first-order spot. 2.2% change in the mechanical strain, affected the output signal by 3.0%. In the present work, it was found that increasing the glucose concentration from 0 to 50 mM decreased the output power by ~20% (1.31 to 1.05 µW). Therefore, 2.2% change in the mechanical strain caused 13% interference in the output reading when the sensor monitored a glucose concentration of 50 mM. This interference percentage increases at lower glucose concentrations. For example, for 10 mM glucose concentration, the interference is expected to be ~40%. Therefore, the sensor is not recommended for patients who suffer from eye diseases that

change the intraocular pressure. The PS glucose sensor attached to a contact lens had advantages as compared to the previously proposed electrochemical and fluorescent glucose sensors attached to contact lenses. The PS contact lens sensor was easy and quick to be fabricated and its readout method does not require high-cost or complex equipment. Moreover, the sensor's cost was reasonable and the response was rapid. On the contrary, the electrochemical sensors attached to contact lenses are associated with significant fabrication complexity. A significant challenge of this electrochemical technology concerns the limitations in miniaturization of electronics in contact lenses. Additionally, the capability to transmit power and receive data from a contact lens remains a hurdle. Furthermore, fluorescent sensors have many disadvantages such as photobleaching and the pH/oxygen of the environment can interfere with the dye's response. In addition, the potential toxicity of the dyes and their potential accumulation in the cells is a major safety concern. Moreover, the sensor's materials are expensive, and the readout is complicated as it requires an expensive appliance (spectrofluorometer) and a dedicated monochromatic light source.

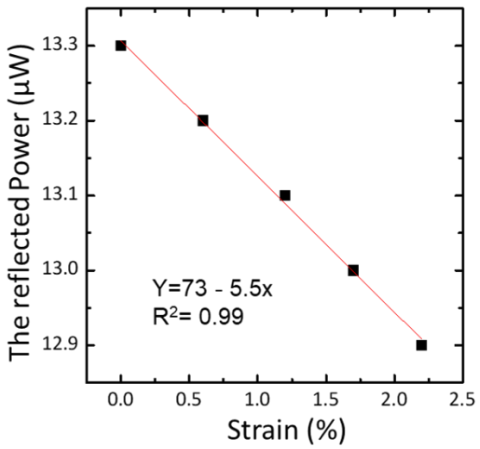

Figure 3.13. The reflected power from the contact lens sensor versus the change in strain.

3.4 Materials and Methods

3.4.1 Materials

Acrylamide (AA), *N*,*N*'-methylenebisacrylamide (BIS), 3-(acrylamido) phenylboronic acid (3-APBA), dimethyl sulfoxide (DMSO), 2,2-diethoxyacetophenone (DEAP), β-D-(+) glucose, and Phosphate buffer saline (PBS) were purchased from Sigma Aldrich and used without further purification.

3.4.2 Fabrication of the hydrogel sensor

The acrylamide hydrogel film was synthesized by the free radical polymerization utilizing DEAP as the photoinitiator and BIS as the crosslinker. The monomer solution was prepared from AA (78.5 mol %), BIS (1.5 mol %), 3-APBA (20 mol %), and DEAP in DMSO. The suspended monomer solution was stir-mixed for 10 min at 24 °C. Monomer solution (100 μl) was drop cast directly onto the master photonic microstructure (600 lines mm^{-1}). A hydrophobic glass slide was placed on top of the solution to obtain a layer having uniform thickness. Photopolymerization process was initiated with a UV lamp (Black Ray, 365 nm) and the sample was exposed to UV light for 5 min. The resulting periodic microstructure hydrogel was peeled off from the master PS and washed three times with deionized water and kept in dry condition in dark prior to experiments.

3.4.3 Photonic Device Characterization

The PS hydrogel sensor and the original photonic microstructure were investigated by an optical microscopy (Zeiss, 100× objective lens). Upon illumination with blue (405 nm), green (532 nm), and red (650 nm) lasers, the diffraction of monochromatic light by the PS sensor

in 40% relative humidity and fully hydrated conditions were recorded to investigate effect of swelling on the PS diffraction pattern. The setup was fixed on an optical bench and composed of a 3D movable holder for the sample and the light source, and a screen on which the diffraction pattern was projected. A digital camera was fixed near by the screen, where the diffraction fringes for each blue, green, and red laser were captured. These images were analyzed by ImageJ program to measure the zero-first order interspace and the absolute diffraction efficiency. Transmission spectra of the sensor at various polarization angles were recorded by a UV-Vis spectrometer attached to an optical microscope (Zeiss, 5× objective lens). The PS sensor was illuminated by a broadband white light source, where light passed through a linear polarizer and propagated through the sensor. The transmitted light passed through another linear polarizer which could be rotated from 0° to 90°. A 20× tube lens collected the transmitted light at imaging side of the microscope which was coupled with a photodetector to measure the spectra.

Angle-resolved measurements for the sensor were acquired by collecting the back diffracted light while the sensor was positioned on an aluminum mirror and was illuminated by a halogen light source (Ocean Optics HL-2000). The incident angle of the white light was fixed at 38° and the back diffracted light was collected by rotating the detector.

In order to characterize the response of the PS sensor to the variation in glucose concentration, the sensor was equilibrated in PBS buffer (7.4 pH, 24° C, ionic strength, 150 mM) for 2 h. Glucose concentrations from 0 to 100 mM were prepared in the same PBS buffer. The sensor's cross-section was measured under the optical microscope (5× lens) in different glucose concentrations.

The diffraction measurements by a monochromatic light in transmission mode was utilized for visual detection of the glucose concentrations.

3.5 Conclusion

A PS glucose sensor was developed and integrated with a contact lens to operate in the physiological conditions. The whole fabrication processes of the PS-contact lens sensor involving polymerization, functionalization, printing the PS, and attaching the sensor to the contact lens were carried out in one step, requiring a short time of near 5 minutes. The volumetric change resulting from glucose binding to the hydrogel sensor was monitored by two different strategies; for the free standing PS sensor, the periodic constant through measuring the zero-first order interspace (*l*), and for the contact lens based sensor, the diffraction efficiency or the power of the first-order spot. The PS sensor that is constrained on the contact lens has advantages of presenting rapid response time (3 s), short saturation time (4 min), and high sensitivity. Thus, a rapid and highly sensitive glucose sensor was developed, which offers simple quantitative readouts. Contact lens based on PS sensor may find applications in quantitative glucose measurements at point-of-care settings.

References

1. L. Olansky and L. Kennedy, "*Finger-stick glucose monitoring*," Diabetes care, 2010. **33** (4): p. 948-949.
2. J. J. Norman, M. R. Brown, N. A. Raviele, M. R. Prausnitz, and E. I. Felner, "*Faster pharmacokinetics and increased patient acceptance of intradermal insulin delivery using a single hollow microneedle in children and adolescents with type 1 diabetes*," Pediatric diabetes, 2013. **14** (6): p. 459-465.
3. K. Ul Hasan *et al.*, "*A miniature graphene-based biosensor for intracellular glucose measurements*," Electrochimica Acta, 2015. **174**: p. 574-580.
4. G. S. Wilson and Y. Hu, "*Enzyme-based biosensors for in vivo measurements*," Chemical Reviews, 2000. **100** (7): p. 2693-2704.
5. S. P. Nichols, A. Koh, W. L. Storm, J. H. Shin, and M. H. Schoenfisch, "*Biocompatible materials for continuous glucose monitoring devices*," Chemical Reviews, 2013. **113** (4): p. 2528.
6. J. Wang, "*Electrochemical glucose biosensors*," Chemical Reviews, 2008. **108** (2): p. 814-825.
7. A. Heller and B. Feldman, "*Electrochemical glucose sensors and their applications in diabetes management*," Chemical Reviews, 2008. **108** (7): p. 2482-2505.
8. P. Choudhary *et al.*, "*Real-time continuous glucose monitoring significantly reduces severe hypoglycemia in hypoglycemia-unaware patients with type 1 diabetes*," Diabetes care, 2013. **36** (12): p. 4160-4162.
9. J.-W. van Dijk and L. J. van Loon, "*Exercise Strategies to Optimize Glycemic Control in Type 2 Diabetes: A Continuing Glucose Monitoring Perspective*," Diabetes Spectrum, 2015. **28** (1): p. 24-31.
10. A. R. Maurizi and P. Pozzilli, "*Do we need continuous glucose monitoring in type 2 diabetes?*," Diabetes/metabolism research and reviews, 2013. **24** (10).
11. L. Monnier, C. Colette, C. Boegner, T. Pham, H. Lapinski, and H. Boniface, "*Continuous glucose monitoring in patients with type 2 diabetes: Why? When? Whom?*," Diabetes & metabolism, 2007. **33** (4): p. 247-252.
12. J. Durner, "*Clinical chemistry: challenges for analytical chemistry and the nanosciences from medicine*," Angewandte Chemie International Edition, 2010. **49** (6): p. 1026-1051.
13. D. Rodbard, "*Continuous glucose monitoring: a review of successes, challenges, and opportunities*," Diabetes technology & therapeutics, 2016. **18**: p. 2-13.
14. A. Kikuchi *et al.*, "*Glucose-sensing electrode coated with polymer complex gel containing phenylboronic acid*," Analytical chemistry, 1996. **68** (5): p. 823-828.
15. Y.-J. Lee, S. A. Pruzinsky, and P. V. Braun, "*Glucose-sensitive inverse opal hydrogels: analysis of optical diffraction response*," Langmuir, 2004. **20** (8): p. 3096-3106.
16. A. Matsumoto, S. Ikeda, A. Harada, and K. Kataoka, "*Glucose-responsive polymer bearing a novel phenylborate derivative as a glucose-sensing moiety operating at physiological pH conditions*," Biomacromolecules, 2003. **4** (5): p. 1410-1416.
17. V. L. Alexeev, S. Das, D. N. Finegold, and S. A. Asher, "*Photonic crystal glucose-sensing material for noninvasive monitoring of glucose in tear fluid*," Clinical Chemistry, 2004. **50** (12): p. 2353-2360.
18. V. L. Alexeev *et al.*, "*High ionic strength glucose-sensing photonic crystal*," Analytical chemistry, 2003. **75** (10): p. 2316-2323.

19. S. A. Asher *et al.*, "*Photonic crystal carbohydrate sensors: low ionic strength sugar sensing*," Journal of the American Chemical Society, 2003. **125** (11): p. 3322-3329.
20. C. Zhang, M. D. Losego, and P. V. Braun, "*Hydrogel-based glucose sensors: effects of phenylboronic acid chemical structure on response*," Chemistry of Materials, 2013. **25** (15): p. 3239-3250.
21. C. Zhang, G. G. Cano, and P. V. Braun, "*Linear and fast hydrogel glucose sensor materials enabled by volume resetting agents*," Advanced Materials, 2014. **26** (32): p. 5678-5683.
22. M. Honda, K. Kataoka, T. Seki, and Y. Takeoka, "*Confined stimuli-responsive polymer gel in inverse opal polymer membrane for colorimetric glucose sensor*," Langmuir, 2009. **25** (14): p. 8349-8356.
23. D. Nakayama, Y. Takeoka, M. Watanabe, and K. Kataoka, "*Simple and precise preparation of a porous gel for a colorimetric glucose sensor by a templating technique*," Angewandte Chemie, 2003. **115** (35): p. 4329-4332.
24. F. Xue, Z. Meng, F. Wang, Q. Wang, M. Xue, and Z. Xu, "*A 2-D photonic crystal hydrogel for selective sensing of glucose*," Journal of Materials Chemistry A, 2014. **2** (25): p. 9559-9565.
25. J.-T. Zhang, N. Smith, and S. A. Asher, "*Two-dimensional photonic crystal surfactant detection*," Analytical chemistry, 2012. **84** (15): p. 6416-6420.
26. J.-T. Zhang, L. Wang, X. Chao, and S. A. Asher, "*Periodicity-controlled two-dimensional crystalline colloidal arrays*," Langmuir, 2011. **27** (24): p. 15230-15235.
27. S. Kabilan *et al.*, "*Holographic glucose sensors*," Biosensors and Bioelectronics, 2005. **20** (8): p. 1602-1610.
28. M.-C. Lee, S. Kabilan, A. Hussain, X. Yang, J. Blyth, and C. R. Lowe, "*Glucose-sensitive holographic sensors for monitoring bacterial growth*," Analytical chemistry, 2004. **76** (19): p. 5748-5755.
29. E. G. Loewen and E. Popov, *Diffraction gratings and applications*. New York Marcel Dekker Inc. , 1997.
30. Y. Egawa, R. Miki, and T. Seki, "*Colorimetric sugar sensing using boronic acid-substituted azobenzenes*," Materials, 2014. **7** (2): p. 1201-1220.
31. A. K. Yetisen *et al.*, "*Glucose-Sensitive Hydrogel Optical Fibers Functionalized with Phenylboronic Acid*," Advanced Materials, 2017. **29** (15): p. 1606380-1606391.
32. M. Elsherif, M. U. Hassan, A. K. Yetisen, and H. Butt, "*Glucose Sensing with Phenylboronic Acid Functionalized Hydrogel-Based Optical Diffusers*," ACS nano, 2018. **12**: p. 2283-2291.
33. A. K. Yetisen *et al.*, "*Reusable, robust, and accurate laser-generated photonic nanosensor*," Nano letters, 2014. **14** (6): p. 3587-3593.
34. M. Ben-Moshe, V. L. Alexeev, and S. A. Asher, "*Fast responsive crystalline colloidal array photonic crystal glucose sensors*," Analytical chemistry, 2006. **78** (14): p. 5149-5157.

Chapter 4: Glucose Sensing with Phenylboronic Acid Functionalized Hydrogel Based Optical Diffusers

This chapter of the alternative format thesis is published in journal of ACS Nano. The publishing details and authors contributions are outlined below.

Mohamed Elsherif**, Mohammed Umair Hassan, Ali K. Yetisen, and Haider Butt*, Glucose Sensing with Phenylboronic Acid Functionalized Hydrogel Based Optical Diffusers, **ACS Nano**, 2018, 12, 2283−2291.

Authors Contributions

M.E. and H.B. conceived the project idea. **M.E**. designed the project, carried out experiments, analyzed results and wrote the article. H.B. supervised experiments and led the project. M.U.H and A.K.Y. revised the manuscript and provided intellectual contributions throughout the project.

Keywords: diffraction; photonic microstructures; glucose sensor; phenylboronic acid; contact lenses

4.1 Abstract

Phenylboronic acids (PBAs) have emerged as synthetic receptors that can reversibly bind to cis-diols of glucose molecules. The incorporation of phenylboronic acids in hydrogels offer exclusive attributes as the binding process with glucose induces osmotic pressure resulting in volumetric changes in the hydrogel matrix. However, their practical applications are hindered because of complex readout approaches and their time-consuming fabrication processes. Here, we demonstrate a replica mould method to fabricate light diffusing microstructures on surfaces of hydrogel films functionalized with phenylboronic acid derivatives. The microstructures function as a light diffuser as they scatter the incident light beam at different angles resulting in a diffused profile of light spot in the forward and backward directions. The signature of the dimensional modulation due to the volumetric expansion of the hydrogel altered the diffusion efficiency of the hydrogel. The spatial profile and the maximum optical power of the diffused light passed through the sensor were measured to determine the variation in glucose concentrations at physiological conditions. The sensor was integrated into a commercial contact lens and placed over an artificial eye. Artificial stimulation of variation in glucose concentration allowed quantitative measurements using a smartphone's photodiode. The developed sensing platform offers low-cost, rapid fabrication, and easy detection scheme as compared to other optical sensing counterparts. The presented detection scheme may have applications in wearable real-time biomarker monitoring devices at point-of-care settings.

4.2 Introduction

Glucose sensors based on various optical phenomena have been extensively explored [1-8]. Optical glucose sensors can be classified into four groups according to the optical transducer/phenomena: surface Plasmon resonance (SPR), fluorescence, surface enhanced Raman scattering (SERS), and photonic band gap sensors. For instance, plasmonic sensors were investigated for glucose sensing due to their high sensitivity to the change in the surrounding dielectric constant. The readout of these sensors depended on detecting the change in the resonant absorbed wavelength with glucose concentrations. An enzyme responsive plasmonic nanoshell system was reported to sense glucose through enzyme complexation [1]. Aggregation and dissociation of gold nanoparticles coated with dextran were also utilized to sense glucose. The nanoparticles aggregate with concanavalin A induced by glucose led to a change in plasmonic absorption [9].

SERS surfaces were adopted for glucose sensing as they enhanced the scattered Raman signals by the molecular adsorption, and the enhancement factor can reach up to 10^{11} fold [10]. The intensity of Raman spectra can be used to quantify glucose concentrations. For example, a template of mercaptophenyl boronic acid (MBA) and silver/gold nanoparticles with graphene oxide nanomaterial was developed to enzymatically sense glucose [2]. Gold nanostar silica core-shell nanoparticles were prepared with glucose oxidase as a SERS substrate for label-free glucose detection [11]. In-situ gold nanoparticles were created in porous and stable metal-organic framework and this system was decorated with glucose and lactate oxidases for *in vivo* detection of glucose and lactate [12]. However, the fabrication of SERS and SPR glucose sensors require high vacuum and advanced technologies such as

atomic layer deposition and e-beam deposition, making the process costly and complicated. In addition, the readout methods of both systems require a customized setup of high-cost optical fibers or a Raman spectrometer.

Fluorescent sensors for continuously monitoring of glucose have also been reported. For example, PBA containing fluorophores was employed in a wearable device for continuous glucose monitoring. The employed charge transfer mechanism induced spectral changes in the presence of glucose. The fluorescence wavelength and the intensity shifted with glucose complexation [3]. Fluorescent sensors suffer from photobleaching of the fluorophore and variations in the illumination source causes over/underestimation of the glucose concentrations.

Hydrogels of integrated photonic band gap (PBG) structures have been functionalized and designed to undergo a reversible change in their physical dimension in response to external stimuli such as glucose, pH, ionic strength, temperature, humidity, solvent composition, and biomolecule binding [4, 13-23]. The PBG sensors are sensitive to hydrogel's volumetric change and convert this change into readable optical information. The PBG hydrogel sensors can be classified into three types according to the dimensions of the refractive index periodicity: 1D, 2D, and 3D photonic bandgap sensors. In such sensors, the reading out can be recorded by colorimetric, and spectral shift measurements [5-7, 24-28].

Phenylboronic acid functionalized hydrogel is a glucose-responsive system due to their affinity to diol-containing molecules [5, 13]. The complexation of PBA immobilized in the hydrogel matrix with glucose molecules causes volumetric change (Figure 4.1). Self-assembly methods have been utilized for the formation of 3D-PBG structure and 3D inverse

opal (IO) PBG structure combined with PBA modified hydrogel for glucose sensing [29]. The PBA functionalized 3D-PBG and -IO hydrogel sensors based on the polymerized acrylamide around 3D sacrificial charged polystyrene particles, have been shown to sense glucose concentrations and their optical signals obeyed Bragg's law [30]. Due to their intrinsic periodicity, these 3D-PBG sensors diffract light of certain wavelengths at specific incident angles. Thereby, at a particular point in space, spectral shifts are observed because of the change in the periodic constant induced by the swelling/shrinking of the hydrogel as a response to the external stimuli (Figure 4.1).

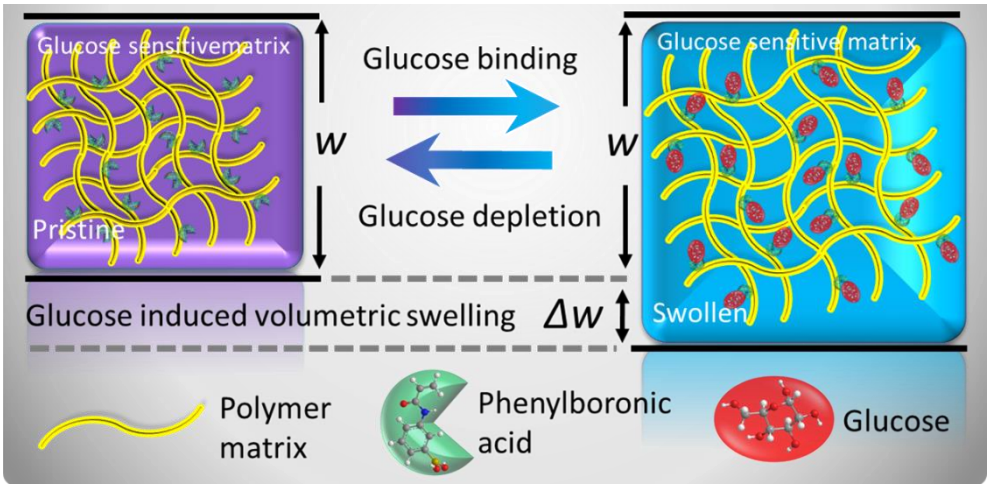

Figure 4.1. Schematic illustration of volumetric transition upon glucose introduction into or depletion from the glucose-sensitive hydrogel matrix.

The construction of such 3D-PBG hydrogel sensors requires non-ionic hydrogel precursors to avoid disordering in the charge-stabilized 3D polystyrene particles [5]. These 3D crystalline colloidal array particles were fabricated by self-assembly and this process lasts two weeks which is time-consuming. 3D-IOs structure from templates have also been transferred to the hydrogel during the polymerization of monomers – once polymerized, the 3D-IOs were removed by chemical etching, yielding a periodic porous polymer [31]. The

3D-IO method also suffers from the high defect density and prone to damage during template etching. A limited range of detection is also a significant drawback of 3D-PBG hydrogel sensors.

1D-PBG hydrogel glucose sensors have been fabricated based on the diffusion of silver nanoparticles into glucose-responsive hydrogels, followed by laser treatment to form composite layers separated by hydrogel layers modulating the refractive index in one dimension [32]. The fabrication of the 1D-PBG sensor process requires many stages and these sensors also have a limited field of view, making readouts very complicated. 2D-PBG sensors based on colloidal crystal arrays (CCA) have also been realized [18]. Although these sensors were sensitive to glucose in the physiological concentration range, they had limitations in their fabrication [33]. These sensors require a well-ordered monolayer of particles, demanding optimization, and functionalization with phenylboronic acid post-polymerization [15]. In addition, reading out requires setups of expensive optical fibers fixed on rotating stages, dark rooms and spectrophotometers connected to a computer. Table 4.1 presents a comparison of various types of glucose sensors summarizing the working principle, advantages, disadvantages, and the detection ranges.

In this work, we developed an optical glucose sensor that achieves the crucial need of fast and economical fabrication process and a simple readout method. We introduced a transducer (light diffusing microstructures) that was easy to imprint on the surface of the glucose-responsive hydrogel through a UV gel curing process, facilitating and accelerating the fabrication process. The volumetric change of the hydrogel in response to various glucose concentrations modulated the dimensions of the light diffusing microstructures and hence the

scattering/diffusion efficiency of the sensor. As a result, the beam profile and the maxima optical power for the transmitted and reflected beams changed. The readouts were taken using an optical powermeter and with a smartphone app as well. Therefore, this sensor offers advantages in terms of its fast and facile preparation, and simple readouts within physiological conditions.

Table 4.1. Different categories of the optical glucose sensors and their working principle, merits, and drawbacks.

Type	**Working principle**	**Advantages**	**Disadvantages**	**Range (mM)**	**R.**
SPR	Shift of the SPR peak due to change of the refractive index result in the enzyme - glucose reaction.	i) Selective for glucose over fructose, lactate, and galactose	i) Require expensive tools for reading out and a customized setup ii) Multiple stages and complex fabrication process	0-2	1
SERS	Enhancement of the Raman signal due to enzyme-glucose reaction.	i) Selective for glucose in the presence of proteins ii) Highly sensitive for glucose in the physiological range	i) Fabrication process is time-consuming and complicated ii) Reading out requires expensive tool (Raman probe).	5-100	2
Fluorescent	The fluorescent wavelength shifts, or the spectra intensity emitted changes with PBA-glucose complexation.	i) Very sensitive for low glucose concentrations ii) function at the physiological conditions.	i) Photobleaching of the fluorophores ii) variations in the illumination source causes over/underestimation of the glucose concentration.	0-140	3

3D-photonic structure sensor	Change in the diffracted Wavelength due to the volumetric shift that result from glucose complexation. The diffracted wavelength follows Bragg's law.	i) Sensitive for low glucose concentrations ii) Visual detection, as the color of the sensor changes with various glucose concentrations	i) Time-consuming and complicated fabrication process ii) Requires long time to reach to the equilibrium	0-40	4
3D-inverse opal sensor	Change in the diffracted wavelength due to the volumetric changes following glucose complexation. The detected wavelength follows Bragg's law.	i) Sensitive for physiological glucose concentrations ii) Visual detection	i) Fragile ii) long response time and saturation time iii) complex fabrication process	0-100	5
2D-photonic structure sensor	Change in the Debye ring diameter due to volumetric changes following glucose complexation.	i) Sensitive for low glucose concentrations ii) Visual detection	i) Complex fabrication process that requires many stages ii) Non practical reading out method iii) Does not function at the physiological pH	0-40	6
1D-photonic crystal sensor	Change in the diffracted wavelength based on glucose-induced volumetric modification.	i) Sensitive for glucose at low and high concentrations ii) Visual detection	i) Complex fabrication process ii) long response and saturation times	0-12	7

2.5D-photonic structure sensor	Change in the diffraction angles lead to increase the interspace among the diffraction spots	i) facile detection. ii) Simple fabrication process	i) Not sensitive for low glucose concentrations ii) Takes long time to reach to the equilibrium/saturation	10-200	8
Light diffuser sensor	Change in the profile/ power of the transmitted and reflected light with glucose-boronate complexation	i) Visual detection ii) Simple and easy readout using a smartphone app iii) Fast fabrication process iv) Detect a wide range of glucose concentrations	i) Takes long time to reach to saturation	0-100	present

4.3 Results and Discussion

Light diffusing microstructures (LDMs) were mirror replicated on the hydrogel network during photopolymerization by the replica mould method (Figure 4.2). Optical microscopy images confirmed successful transfer of the mirror replicated structure on the hydrogel layer (Figure 4.3a-b). Both the master holographic diffuser and the hydrogel sensor were illuminated with a broadband white light. The holographic diffuser exhibited a wider divergence/scattering angle, θ_d ~ 30°, as compared to the angle, θ_d ~15° obtained for the imprinted hydrogel matrix (Figure 4.3d). In addition, the maximum transmitted light intensity detected by using a photodetector for the master diffuser was ~ 2 times lower than that of the imprinted hydrogel matrix (Figure 4.3d). The holographic master had a higher divergence, which allowed less light (luminance) to reach the photodetector placed at the identical distance as compared to its mirror replica of the hydrogel matrix. The difference in

θ_d was expected because of the difference in the refractive indices between the master diffuser and the imprinted hydrogel matrix. The microstructured-hydrogel showed similar diffusing properties for monochromatic beams of various wavelengths; 405 nm, 532, and 650 nm (Figure 4.3e). However, the light dispersion properties of the imprinted hydrogel matrix weakened when it was exposed to highly humid conditions. In a fully hydrated condition, the hydrogel matrix exhibited a smaller θ_d angle, and higher maximum transmitted power than that in 40% relative humidity condition (Figure 4.3f). The 3PBA-functionalized hydrogel matrix as a glucose sensor swelled upon partial or full hydration, causing an initial size increase in the structural profile of the replicated microstructures, and decreasing the refractive index. This modification decreased the sensor's diffusing properties, and consequently, the divergence/scattering angles. Therefore, the decrease in the spot size in fully hydration conditions increased the maximum intensity of the diffused light when recorded at the center of the spot. For subsequent experiments, the sensor's reference was set according to its fully hydrated condition.

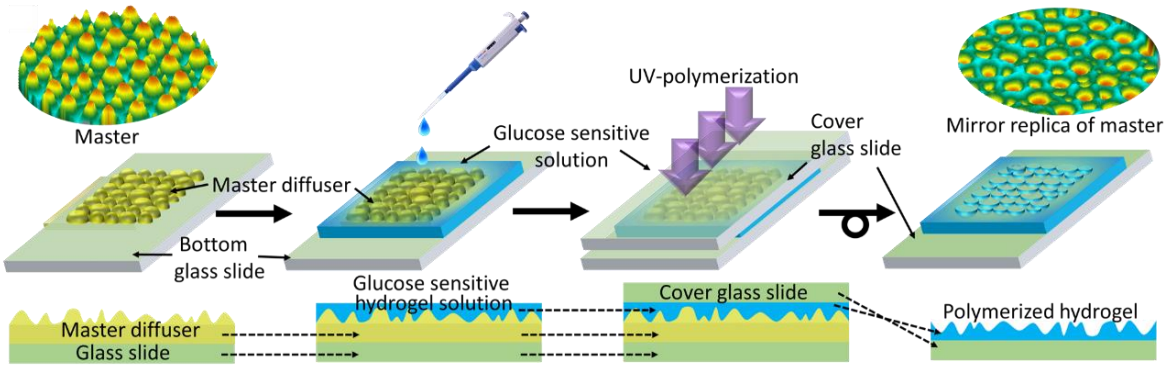

Figure 4.2. Schematic for the fabrication process of hydrogel-based optical glucose sensor: a diffuser master replica is drop-cast with a glucose-sensitive solution which is polymerized using UV-light. After polymerization, the master PS was removed and the imprinted glucose-sensitive hydrogel is obtained on the glass slide.

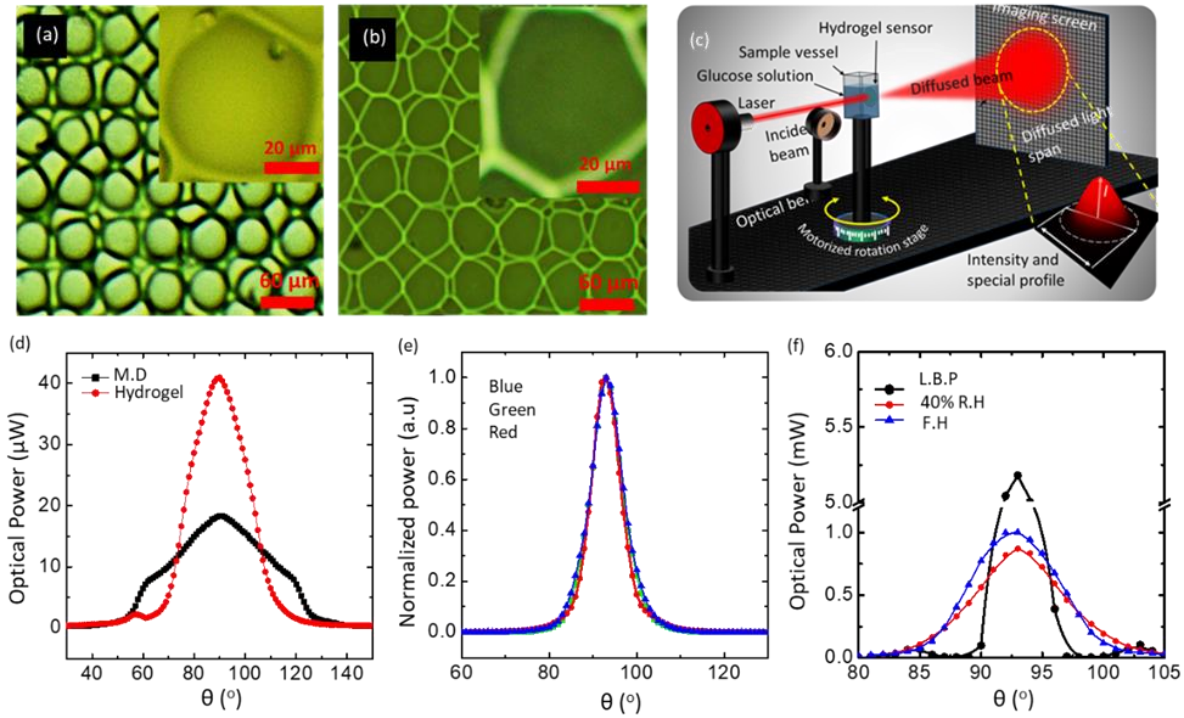

Figure 4.3. Microscopic images and profiles of the light transmitted beams through the diffusers: (a-b) microscopic images of the master diffuser and the hydrogel sensor, (c) Schematic of the setup that was utilized to investigate the profiles of the light beam passed through the master diffuser and the imprinted hydrogel sensor, (d) Profile of the white light beam transmitted through the master diffuser and the hydrogel, (e) Profiles of three different laser beams; blue (405 nm) , green (532 nm), and red (650 nm), transmitted through the hydrogel sensor which was in 40% relative humidity condition (40% R.H), (f) Profiles of the white light beam (L.B.P) when it does not pass through the sensor, and the beam profile when it transmitted through the hydrogel sensor in 40 % relative humidity (40% R.H) and fully hydrated conditions (F.H).

LDMs-based hydrogel sensors were tested in different glucose concentrations in transmission mode using a monochromatic light (Figure 4.4). The sensing was carried out by measuring the maximum transmitted power, and recording the profile/diameter of the diffused light after passing through the hydrogel sensor. The sensor was equilibrated in PBS solution (pH 7.4, ionic strength 150 mM, and 24 °C) for 2 h; and each measurement for different glucose concentration (M) within the range $0 \leq M \leq 100$ mM was carried out after 90 min to the last preceding sensing trial. An incident monochromatic light beam of λ=532

nm was used and the sensing measurements were performed in the transmission mode. Figure 4.3c illustrates the schematic of the experimental setup utilized in sensing experiments. In addition to the swelling caused by water diffusion inside the optical hydrogel sensor, glucose swelled the sensor due to the formation of anionic boronate-glucose 1:1 complexation in the hydrogel matrix that increased the boronate anions, leading to increasing Donnan osmotic pressure, and hence, causes a positive volumetric shift. The dimensional shift in the light diffusing microstructures (LDMs) engraved on the sensor's surface altered the overall scattering/divergence of the beam and this is the principal of sensing. The change of the optical parameters could be correlated to the variation in the glucose concentration. Increasing glucose concentration initially increased the maximum transmitted light power, P_{tmax}, and shrank the diameter of the diffused light spot on the imaging screen (Figure 4.4). Upon increasing the glucose concentration, $0 \leq M \leq 100$ mM, the maximum transmitted light power P_{Tmax} and the diameter underwent a slower corresponding shift – the sensor response saturated at high concentrations, below which the response was fairly linear. The sensitivity at the glucose concentration range (0-50 mM) was ~ 12.7 μW mM^{-1} (~ 2.3% mM^{-1}) where the maximum transmitted power (P_{Tmax}) increased from the primary value of 550 μW to reach 1190 μW. However, at the higher glucose range, from 50 mM to 100 mM the sensitivity decreased to be 4.2 μW mM^{-1} as the output signal reached up to 1400 μW. The sensitivity of the proposed sensor was around 22 fold higher than that of the recently reported work as for the glucose concentration range of 0-100 mM, the LDMs sensor showed 152% change in the maximum transmitted power compared to the 7% attenuation of the transmitted light that was previously reported [34]. The decrease in the sensitivity at higher glucose concentrations may be due to the decrease in the available boronate binding sites and decreasing elasticity

of the hydrogel matrix that competed against the volumetric swelling process and glucose complexation. The visual shift of the diffused spectra was also very clear, that could be seen by the naked eye (Figure 4.4d).

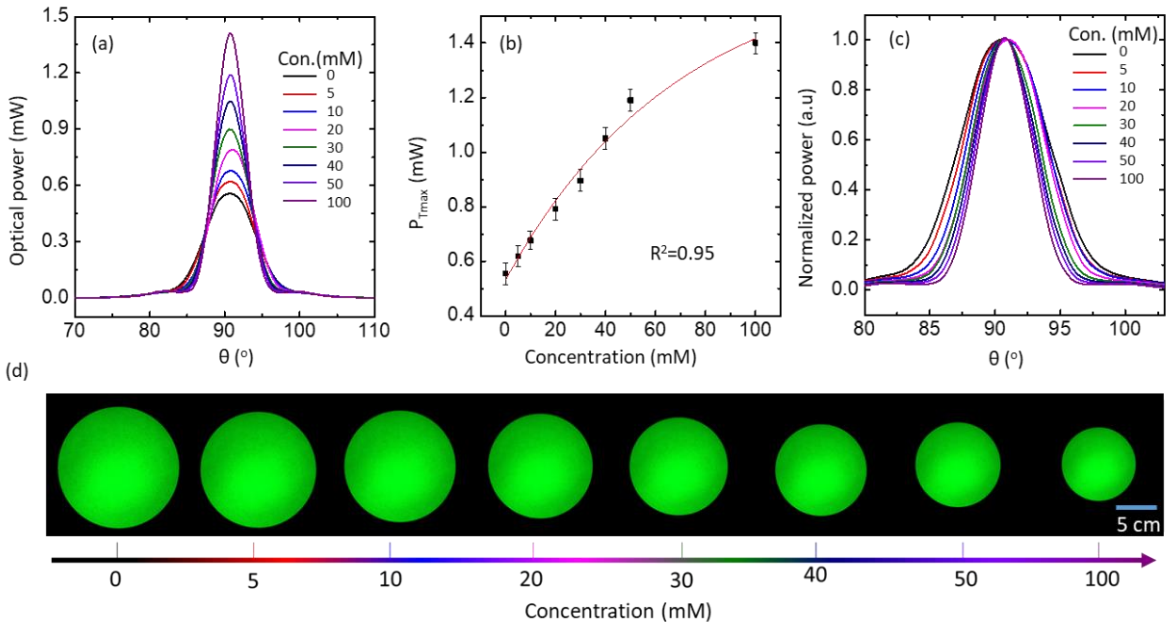

Figure 4.4. Quantification of glucose concentrations LDMs hydrogel sensor: (a) The transmitted optical power, *P*, behavior for the green laser beam *versus* the forward scattering angle at glucose concentration within the range of 0-100 mM, (b) Peak transmitted light power, $P_{Tmax,}$ as a function of glucose concentration. (c) Normalized transmitted light power for different glucose concentrations *versus* the forward scattering angle showing the change in the diameter of the diffused spot (captured on imaging screen), and (d) Photographs of diffused monochromatic light spots after passing through the sensor submerged in different glucose concentration solutions. The scale bars show standard error (n=3).

Interrogation the sensor by white light beams was also carried out in the same glucose concentration range, $0 \leq M \leq 100$ mM (Figure 4.5). Photographs of the diffused spots on a screen 40 cm away from the sensors were captured for visual detection. Increase in the glucose concentration decreased the light scattering angles and increased the maximum power of the transmitted beam. The sensor's sensitivity based on the optical output signals was 6.3 μW mM^{-1} (2.25% mM^{-1}) within the glucose range of 0-50 mM as the maximum

transmitted power increased from the primary value of 280 µW to reach 595 µW. The sensitivity decreased to be ~ 2.6 µW mM^{-1}, in the glucose range of 50-100 mM. The light diffuser-based sensor was able to quantify glucose within a wider detection range as compared to its other counterparts based on the visual detection scheme (1D, 2D, and 3D PBG sensors).

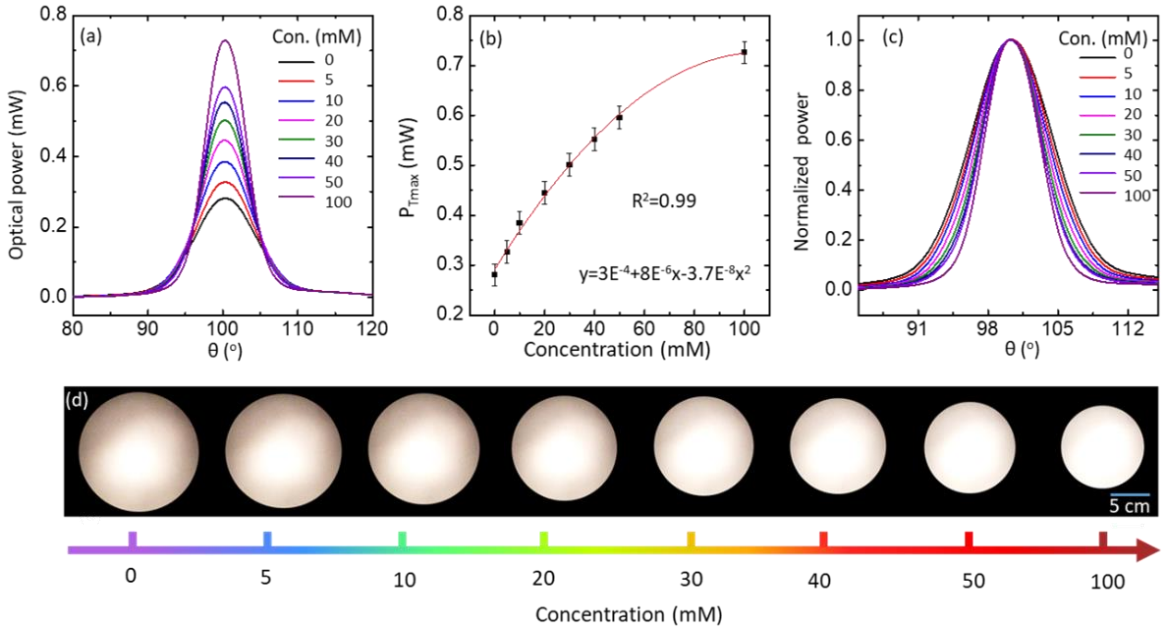

Figure 4.5. Quantification of glucose with a broadband light source for the concentration range of $0 \leq M \leq 100$ mM. (a) The transmitted optical power versus θ_d of the hydrogel sensor, recorded at different glucose concentrations. (b) $P_{T\max}$ plotted against various glucose concentrations. (c) Normalized transmitted power of the broadband light *versus* the scatter angle, showing the change in the diffused spot diameter with increasing glucose concentrations. (d) Photographs of diffused broadband light spots after passing through the sensor submerged in different glucose concentration solutions. The scale bars show standard error (n=3).

The swelling dynamics of the sensor were studied for 10 mM, and 50 mM glucose concentrations (Figure 4.6a-b). Upon exposure to glucose solution, the binding equilibrium reached to saturation in 60 and 50 min for low and high glucose concentrations, respectively. These saturations times are expected to cut down to the third at the physiological temperature

37 ^{o}C. According to swelling kinetics of the sensor at room temperature when the sensor was immersed in glucose concentration of 10 mM, the sensor provided a readout rate of 0.16 mM per min. The rapid response and quick saturation time are important steps toward the practical implementation of glucose continuous monitoring sensors. The stability and reusability of the sensor were investigated by recording the response of the sensor for four complete cycles (Figure 4.6c). The sensor's response for glucose concentrations was measured for ~ 100 min, followed by the reset using an acetate buffer of pH 4.6 for ~10 s and then for ~ 60 min in PBS buffer before commencing the next cycle for 10 mM glucose concentration. The increasing trend of $P_{T\max}$ remained identical throughout experiments with almost same saturation values for all the cycles.

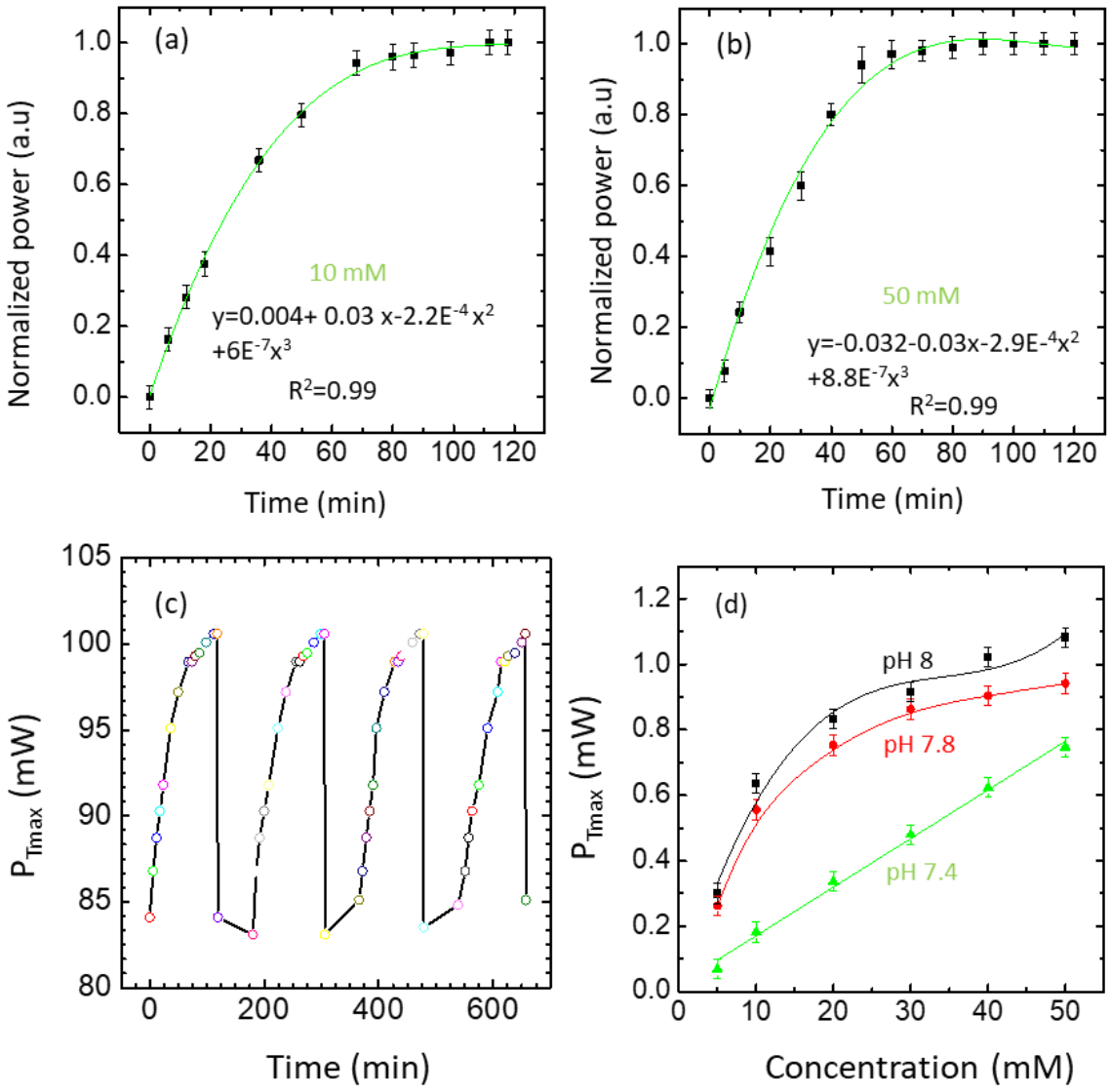

Figure 4.6. Kinetic swelling, reusability, and influence of pH on the sensitivity. (a) Maximum power of the transmitted diffused light (P_{Tmax}) *versus* time when the sensor was immersed in 10 mM glucose concentration over 120 min. (b) P_{Tmax} recorded over time for the sensor when it was submerged in 50 mM glucose concentration. (c) Switching of the sensor for various cycles against introduction or depletion of glucose (10 mM). (d) Quantification of glucose concentration at different pH values. The scale bars show standard error (n=3).

The effect of pH on the glucose detection was studied (Figure 4.6d). The sensitivity of the sensor increased with increasing pH. The highest sensitivity was recorded for pH 8, while at the physiological pH (7.4), a relatively lower glucose sensitivity was observed, consistent

with the previous studies [35, 36]. The utilized glucose recognition agent (3-acrylamido phenyboronic acid (3-APBA)) is a weak acid with a pK_a of 8.8 and it is existed in two configurations; planar trigonal structure and tetrahedral structure, and both structures react with glucose (Figure 3.6b). However, only the tetrahedral structure which is more abundant in the high pH medium can form a stable bond with glucose. As a result, the sensor exhibited superior sensitivity at higher pHs. Consequently, implication a PBA with a lower pK_a is expected to achieve better sensitivity at the physiological pH. Therefore, the pH has a significant effect on the sensor's response. In contrast, the temperature effect is expected to be much smaller as compared to pH. Based on literature, a slight decrease in the glucose sensitivity is expected when the temperature rises from 25 to 37 ^{o}C.

To explain the higher sensitivity of the sensor at higher pH values, effect of pH on the sensor was examined (Figure 4.7a). We found that upon increasing the pH from 4 to 6, the hydrogel slightly swelled and consequently a slight increase in the maxima transmitted powers were recorded indicating an inconsequential increase in the anionic boronate ions. The sensor exhibited a linear and higher response between the pH values of 6 and 9, as the concentrations of boronate ions increased significantly. Therefore, the higher sensitivity at higher pH glucose solutions might be attributed to the increase in the concentration of the anionic boronate ions which have higher affinity to complexes with glucose forming a stable boronate anion. The sensitivity of the glucose sensor is not only affected by the pH of the glucose solution, but also by the ionic strength of the solution. It has been found that increasing the ionic strength of the aqueous solution increases the charged PBA in the

polymer matrix raising up the Donnan potential, leading to the improved swelling response of the sensor[6].

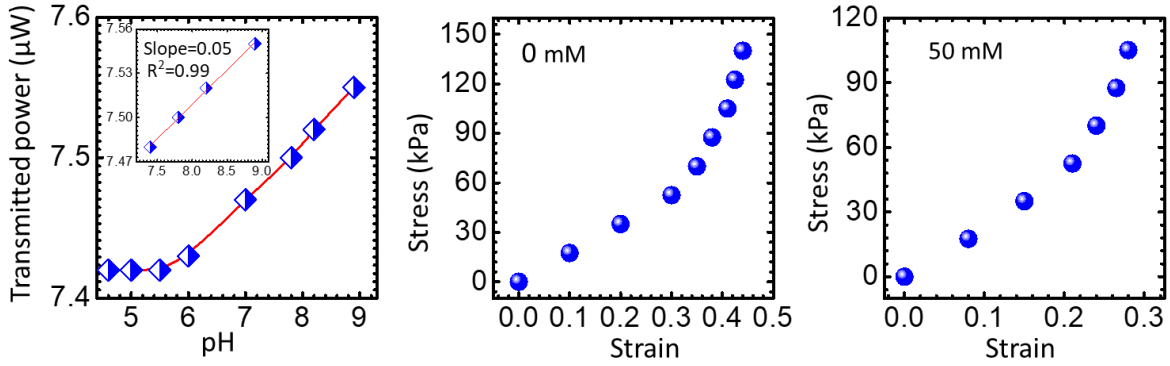

Figure 4.7. Influence of the solution's pH on the sensor and the mechanical properties of the hydrogel sensor; (a) pH of the aqueous solution versus the maxima transmitted power, the inset graph shows the linear relation in the pH range of 6-9, (b) Stress *versus* strain for the hydrogel sensor in absence of glucose, (b) Stress *versus* strain of the hydrogel sensor while the sensor was immersed and saturated in glucose concentration of 50 mM.

The effect of glucose complexation with the immobile PBA in the hydrogel matrix on the mechanical properties was also studied (Figure 4.7b-c). The Elasticity/Young's modulus for the sensor in absence of glucose was ~ 175 kPa and increased to be ~ 218 kPa for the glucose concentration of 50 mM. The stiffness of the sensor increased from ~ 0.49 to 0.61N/m, indicating a decrease in the flexibility. Increasing the sensor stiffness with glucose complex results from increasing of the cross-link density in the hydrogel matrix, and this explains the decreased sensitivity of the sensor at high glucose concentrations.

To show the sensor utility in continuous glucose monitoring, we attached it to a commercial contact lens (Figure 4.8a-b). Light intensity measurements were obtained in reflection mode (with the incident and reflection angles of 45° with respect to the normal) using a smartphone photodiode. The inbuilt light sensor in the smartphone was utilized to capture the

backscattered light (at a distance of 12 cm) and record the illuminance. Illuminance defines the amount of light falling onto a given surface area and the its SI unit is the lux. Illuminance and luminance terms are quite confusing and most often used incorrectly interchanged. However, luminance is the light intensity emitted from a surface per unit area in a certain direction. Also, it can be defined as a photometric measure of the luminous intensity per unit area traveling in a given direction. For measuring the illuminance, we used 'Smart Tools' android app which is freely available from Google app store. Upon continuous application of different glucose solutions on the sensor surface, the changing luminance against varying glucose concentration (0-50 mM) was measured. The sensor was sensitive to the glucose concentration in the range of 5 mM and upward. The recorded optical signal increased from 61 Lux to 75 Lux upon increasing glucose concentration up to 50 mM (Figure 4.8b). The sensitivity of the stimuli- responsive hydrogel-based sensors depend on the thickness and are inversely proportional. We anticipate that the sensitivity might improve to work in the tear range (0.26-0.9 mM) with further optimization to the sensor's thickness and decreasing the resolution of the light diffusing microstructures. These modifications can improve the sensor's active surface area and as a result, minimal swelling of the sensor will alter the transmitted and reflected beam profiles [37]. It is known that the transduction mechanism used to monitor the volumetric modulation is an important factor that affects the sensitivity, for example, a 2D photonic structure-based glucose sensor showed a quick response time; however, the transduction mechanism posed the limit of detection to ~ 10 mM [8].

We anticipate no harm due to illuminating the eyes for few seconds with a white light source as the ophthalmologists examine the patient's eyes by ophthalmoscopes that are provided by

light pointers. The data file can be stored for global recognition and can be remotely sent to the physician for better health and care facilities. In contrast to other sophisticated electrochemical sensing schemes for glucose sensing, optical sensors incorporated in contact lenses do not require an electrical power supply, significantly simplifying the operation and readout system with already available photodiode light sensors in smartphones [38].

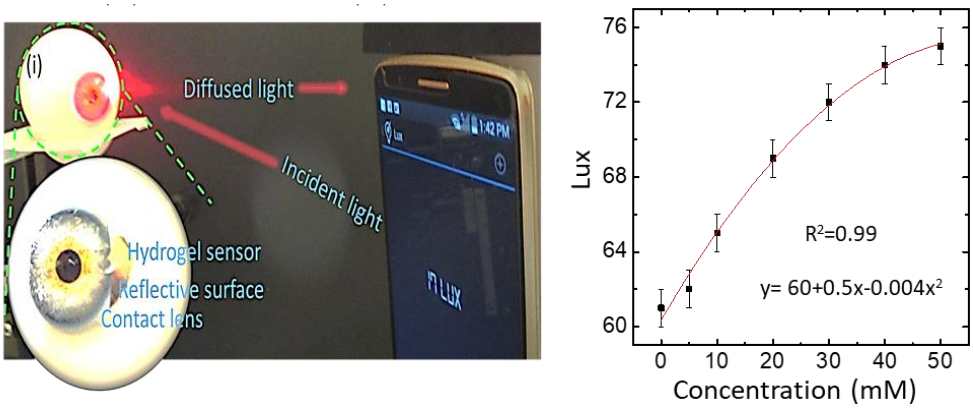

Figure 4.8. LDMs glucose sensor integrated on a contact lens. (a) Experimental setup: photograph of an artificial eye with attached contact lens and sensor, (b) Quantification of glucose sensing using a smartphone camera taken at 12 cm. The scale bars show standard error (n=3).

4.4 Materials and methods

Acrylamide (AA), *N*,*N*'-methylenebisacrylamide (BIS), 3-(acrylamido) phenylboronic acid (3-APBA), dimethyl sulfoxide (DMSO), 2,2-diethoxyacetophenone (DEAP), β-D-(+) glucose, and phosphate buffered saline (PBS) were purchased from Sigma Aldrich and used without further purification. A master diffuser of a model number ED1-C50 -MD was purchased from Thorlabs and was replicated on the stimuli-responsive hydrogels. The diffuser's surface consisted of a variety of randomly distributed microlenses, which provide excellent control over the light beam profile and the light intensity distribution. Each microlens is individually specified with respect to its surface profile and location on the

diffuser's surface. The microlens distribution removes-zero-order bright spots and diffraction artifacts from the output to retain the best properties. The master diffuser was fabricated by a laser writing system developed by RPC photonics. A thick layer of a photoresist material is exposed to the laser beam in a raster scan mode and the intensity of the scanning laser beam is modulated producing a deeply textured engineered surface. The diffuser is made of ZEONORA[a], which has a refractive index of 1.53 and it is designed to diffuse the wavelength range of 380-1100 nm. The diameter of the diffuser is about 25.4 mm and its thickness is 1.5 mm.

The acrylamide hydrogel film was synthesized by the free radical polymerization utilizing DEAP as a photoinitiator and BIS as a crosslinker. The monomer solution was prepared from AA (78.5 mol %), BIS (1.5 mol %), 3-APBA (20 mol %), DEAP, and DMSO. The suspended monomer solution was stir-mixed for 10 min at 24 °C. The pre-polymerized solution (100 μl) was drop cast directly onto the light diffusing microstructures and a hydrophobic glass slide was placed on top of the solution to obtain a uniform thickness. The photopolymerization process was initiated with a UV-lamp (Black Ray, 365 nm) for 5 min. The light diffusing microstructures were mirror replicated on the hydrogel network during the photo-polymerization. Subsequently, the resulting replica hydrogel was peeled off the master diffuser, washed with deionized water and kept in the dry condition prior to further experiments.

The surface of the holographic diffuser (master) and the prepared hydrogel sensor were investigated using an optical microscope (Zeiss, 5x and 20x objective lens). For optical characterization, the setup comprised of a 3D translational stage (Thorlabs) with sample and

light source holders, and an optical power meter located at 12 cm from the sensor, all fixed on an optical bench. The master light diffuser and the hydrogel sensor were illuminated by monochromatic and broadband light sources at their normal and the transmitted diffused light spot were scanned by an optical power meter (Thorlabs, PM100A) for different sample orientations. The beam profile of the transmitted light was also studied using an imaging screen setup (by replacing the optical power meter with an imaging screen far 40 cm from the light diffuser). To measure the response of the optical hydrogel sensor against the variation in glucose concentrations, the hydrogel was equilibrated in PBS buffer (7.4 pH, 24° C, and ionic strength,150 mM) for 2 h, and optical transmission experiments were repeated under physiological conditions for different glucose concentrations. The sensing was also carried out on a sensor-integrated contact lens on an artificial eye by obtaining readouts with a smartphone camera and app.

4.5 Conclusion

We have demonstrated optical glucose sensors based on light diffusing microstructures (LDMs) integrated into a contact lens. The light diffusing microstructures were initially mirror-replicated onto a glucose-sensitive hydrogel. The replicated microstructures have various shapes and dimensions that exhibit scattering angles modification in response to the overall size modification of the hydrogel upon exposure to different glucose concentrations. The sensor was sensitive to glucose in the physiological conditions. More importantly, this optical sensor can be adapted as a minimally-invasive real-time measurement method at point-of-care settings. The developed sensor was also reversible and reusable and exhibited limited hysteresis over multiple cycles or glucose concentration increase and depletion. The

proposed proof-of-concept study may be vital for chronic diseases cases, especially for type 1 diabetics, where continuous glucose monitoring is a necessity for blood glucose management.

References

1. H. He, X. Xu, H. Wu, and Y. Jin, "*Enzymatic plasmonic engineering of Ag/Au bimetallic nanoshells and their use for sensitive optical glucose sensing*," Advanced Materials, 2012. **24** (13): p. 1736-1740.
2. V. K. Gupta *et al.*, "*A novel glucose biosensor platform based on Ag@ AuNPs modified graphene oxide nanocomposite and SERS application*," Journal of colloid and interface science, 2013. **406**: p. 231-237.
3. R. Badugu, J. R. Lakowicz, and C. D. Geddes, "*Noninvasive continuous monitoring of physiological glucose using a monosaccharide-sensing contact lens*," Analytical chemistry, 2004. **76** (3): p. 610-618.
4. V. L. Alexeev, S. Das, D. N. Finegold, and S. A. Asher, "*Photonic crystal glucose-sensing material for noninvasive monitoring of glucose in tear fluid*," Clinical Chemistry, 2004. **50** (12): p. 2353-2360.
5. Y.-J. Lee, S. A. Pruzinsky, and P. V. Braun, "*Glucose-sensitive inverse opal hydrogels: analysis of optical diffraction response*," Langmuir, 2004. **20** (8): p. 3096-3106.
6. F. Xue, Z. Meng, F. Wang, Q. Wang, M. Xue, and Z. Xu, "*A 2-D photonic crystal hydrogel for selective sensing of glucose*," Journal of Materials Chemistry A, 2014. **2** (25): p. 9559-9565.
7. S. Kabilan *et al.*, "*Holographic glucose sensors*," Biosensors and Bioelectronics, 2005. **20** (8): p. 1602-1610.
8. M. Bajgrowicz-Cieslak, Y. Alqurashi, M. I. Elshereif, A. K. Yetisen, M. U. Hassan, and H. Butt, "*Optical glucose sensors based on hexagonally-packed 2.5-dimensional photonic concavities imprinted in phenylboronic acid functionalized hydrogel films*," RSC Advances, 2017. **7** (85): p. 53916-53924.
9. K. Aslan, J. R. Lakowicz, and C. D. Geddes, "*Nanogold-plasmon-resonance-based glucose sensing*," Analytical biochemistry, 2004. **330** (1): p. 145-155.
10. E. Le Ru and P. Etchegoin, *Principles of Surface-Enhanced Raman Spectroscopy: and related plasmonic effects*. Elsevier, 2008.
11. I. Al-Ogaidi *et al.*, "*A gold@ silica core–shell nanoparticle-based surface-enhanced Raman scattering biosensor for label-free glucose detection*," Analytica chimica acta, 2014. **811**: p. 76-80.
12. Y. Hu *et al.*, "*Surface-enhanced raman scattering active gold nanoparticles with enzyme-mimicking activities for measuring glucose and lactate in living tissues*," ACS nano, 2017. **11** (6): p. 5558-5566.
13. V. L. Alexeev *et al.*, "*High ionic strength glucose-sensing photonic crystal*," Analytical chemistry, 2003. **75** (10): p. 2316-2323.
14. I. Cobo, M. Li, B. S. Sumerlin, and S. Perrier, "*Smart hybrid materials by conjugation of responsive polymers to biomacromolecules*," Nature materials, 2015. **14** (2): p. 143-159.

15. H. R. Culver, J. R. Clegg, and N. A. Peppas, "*Analyte-Responsive Hydrogels: Intelligent Materials for Biosensing and Drug Delivery*," Accounts of Chemical Research, 2017. **50** (2): p. 170-178.
16. A. K. Yetisen *et al.*, "*Reusable, robust, and accurate laser-generated photonic nanosensor*," Nano letters, 2014. **14** (6): p. 3587-3593.
17. A. K. Yetisen *et al.*, "*Light-directed writing of chemically tunable narrow-band holographic sensors*," Advanced Optical Materials, 2014. **2** (3): p. 250-254.
18. J. Huang, X. Hu, W. Zhang, Y. Zhang, and G. Li, "*pH and ionic strength responsive photonic polymers fabricated by using colloidal crystal templating*," Colloid and Polymer Science, 2008. **286** (1): p. 113-118.
19. M. Ilavský and J. Hrouz, "*Phase transition in swollen gels*," Polymer Bulletin, 1982. **8** (9): p. 387-394.
20. B. V. Slaughter, A. T. Blanchard, K. F. Maass, and N. A. Peppas, "*Dynamic swelling behavior of interpenetrating polymer networks in response to temperature and pH*," Journal of applied polymer science, 2015. **132** (24).
21. R. A. Barry and P. Wiltzius, "*Humidity-sensing inverse opal hydrogels*," Langmuir, 2006. **22** (3): p. 1369-1374.
22. A. Yetisen, M. Qasim, S. Nosheen, T. Wilkinson, and C. Lowe, "*Pulsed laser writing of holographic nanosensors*," Journal of Materials Chemistry C, 2014. **2** (18): p. 3569-3576.
23. S. Katayama, Y. Hirokawa, and T. Tanaka, "*Reentrant phase transition in acrylamide-derivative copolymer gels*," Macromolecules, 1984. **17** (12): p. 2641-2643.
24. Z. B. Zhao, H. Li, Q. L. Lu, Y. L. Li, and Y. Jiang, "*Multifunctional sensors based on silicone hydrogel and their responses to solvents, pH and solution composition*," Polymer International, 2017. **66** (4): p. 566-572.
25. J. Xu, C. Yan, C. Liu, C. Zhou, X. Hu, and F. Qi, "Photonic crystal hydrogel sensor for detection of nerve agent," in *IOP Conf. Ser.: Mater. Sci. Eng.* 167: IOP Publishing, p. 012024.
26. N. Hao *et al.*, "*Three-dimensional nitrogen-doped graphene porous hydrogel fabricated biosensing platform with enhanced photoelectrochemical performance*," Sensors and Actuators B: Chemical, 2017. **250**: p. 476-483.
27. A. Sabouri, A. K. Yetisen, R. Sadigzade, H. Hassanin, K. Essa, and H. Butt, "*Three-dimensional microstructured lattices for oil sensing*," Energy & Fuels, 2017. **31** (3): p. 2524-2529.
28. R. Ahmed, A. K. Yetisen, S. H. Yun, and H. Butt, "*Color-selective holographic retroreflector array for sensing applications*," Light: Science & Applications, Original Article, 2017. **6**: p. e16214.
29. S. A. Asher, J. Holtz, L. Liu, and Z. Wu, "*Self-assembly motif for creating submicron periodic materials. Polymerized crystalline colloidal arrays*," Journal of the American Chemical Society, 1994. **116** (11): p. 4997-4998.
30. D. Nakayama, Y. Takeoka, M. Watanabe, and K. Kataoka, "*Simple and precise preparation of a porous gel for a colorimetric glucose sensor by a templating technique*," Angewandte Chemie, 2003. **115** (35): p. 4329-4332.
31. M. Honda, K. Kataoka, T. Seki, and Y. Takeoka, "*Confined stimuli-responsive polymer gel in inverse opal polymer membrane for colorimetric glucose sensor*," Langmuir, 2009. **25** (14): p. 8349-8356.
32. S. Kabilan *et al.*, "*Glucose-sensitive holographic sensors*," Journal of Molecular Recognition, 2004. **17** (3): p. 162-166.

33. J. Tavakoli and Y. Tang, "*Hydrogel Based Sensors for Biomedical Applications: An Updated Review*," Polymers, 2017. **9** (8): p. 364.
34. A. K. Yetisen *et al.*, "*Glucose-Sensitive Hydrogel Optical Fibers Functionalized with Phenylboronic Acid*," Advanced Materials, 2017. **29** (15): p. 1606380-1606391.
35. Y. Zhang, Y. Guan, and S. Zhou, "*Synthesis and volume phase transitions of glucose-sensitive microgels*," Biomacromolecules, 2006. **7** (11): p. 3196-3201.
36. X. Zhang, Y. Guan, and Y. Zhang, "*Ultrathin hydrogel films for rapid optical biosensing*," Biomacromolecules, 2011. **13** (1): p. 92-97.
37. J. T. Baca, D. N. Finegold, and S. A. Asher, "*Tear glucose analysis for the noninvasive detection and monitoring of diabetes mellitus*," The ocular surface, 2007. **5** (4): p. 280-293.
38. K. Ul Hasan *et al.*, "*A miniature graphene-based biosensor for intracellular glucose measurements*," Electrochimica Acta, 2015. **174**: p. 574-580.

Chapter 5: Hydrogel Fiber Optic for Continuous Glucose Monitoring

This chapter of the alternative format thesis is published in journal of Biosensors and Bioelectronics. The publishing details and authors contributions are outlined below.

Mohamed Elsherif**, Mohammed Umair Hassan, Ali K. Yetisen, and Haider Butt*, Hydrogel Fiber Optic for Continuous Glucose Monitoring**, Biosensors and Bioelectronics**, 2019, 137, 25-32.

Authors Contributions

M.E. H.B conceived the project idea and designed the project. **M.E**. carried out experiments, analyzed results and wrote the article. H.B. supervised experiments and led the project. M.U.H and A.K.Y. revised the manuscript and provided intellectual contributions throughout the project.

Keywords: photonics; fiber optics; sensors; continuous glucose monitoring; boronic acids

5.1 Abstract

Continuous glucose monitoring facilitates the stringent control of blood glucose concentration in diabetic and intensive care patients. Optical fibers have emerged as an attractive platform; however, their practical applications are hindered due to lack of biocompatible fiber materials, complex and impractical readout approaches, slow response, and time-consuming fabrication processes. Here, we demonstrate the quantification of glucose by smartphone-integrated fiber optics that overcomes existing technical limitations. A glucose-responsive hydrogel was imprinted with light diffusing microstructures (LDMs) and was attached to a multimode silica fiber's tip during the photopolymerization, and subsequently interrogated for glucose sensing under physiological conditions. A smartphone and an optical power meter were employed to record the output signals. The functionalized fiber showed high sensitivity (0.37 % mM^{-1}), rapid response (30 s), and high glucose selectivity in the physiological glucose range. In addition, the fiber attained the glucose complexation equilibrium within 15 min. The lactate interference was examined and it was found minimal ~ 0.1% in the physiological range. A biocompatible hydrogel made of polyethylene glycol diacrylate was utilized to fabricate a flexible hydrogel fiber to replace the silica fiber, and the fiber's tip was functionalized with the glucose-sensitive hydrogel during the ultraviolet light curing process. The biocompatible fiber was quickly fabricated by the molding, the readout approach was facile and practical, and the response to glucose was comparable to the silica fiber. The fabricated optical fiber sensors may have applications in wearable and implantable point-of-care and intensive-care continuous monitoring systems.

5.2 Introduction

Stringent control of blood glucose concentration is essential in preventing hyper/hypoglycemia that may lead to serious diabetic complications including diabetic retinopathy, foot ulcers, diabetic nephropathy, and atherosclerosis [1-4]. Hyperglycemia may be found in intensive-care patients even in those without a clinical history of diabetes such as patients of high-degree burns, trauma, hypoxia, sepsis, and shock, where the stress of acute illness induces glucose production, insulin resistance, and relative insulin deficiency [5-12]. A strict blood glucose management for the patients with acute illness or in the intensive care unit (ICU) decreases the risk of morbidity and mortality [11-14]. Intensive glucose concentration management in ICUs has demonstrated a significant reduction in the overall medical care saving $1580 per adult patient [15-18]. Therefore, tight control of glycemia might provide favorable results in terms of clinical outcome and cost-effectiveness.

Commercial glucose monitoring systems are based on regular finger prick testing up to 3-5 times a day [12]. However, studies assessed the finger prick testing and it was inaccurate compared to blood venous samples; it was found that the postprandial glucose concentration in capillary blood is higher 35% than those in venous blood [19]. Therefore, an alternative noninvasive or minimally-invasive system would eliminate the inconvenience of the frequent blood sampling pain and aids to the strict control of the glucose concentration. To address this clinical need, implantable electrochemical sensors have been developed for short-term continuous glucose monitoring. However, these sensors have several drawbacks: (i) they are unstable *in vivo* due to the enzymatic reaction leading to the signal drift, (ii) their activity is

oxygen dependent, (iii) they are inaccurate in low glucose concentrations, and (iv) they cannot be used for long-term continuous glucose monitoring [20].

Fiber optic probes as minimally-invasive sensors have been developed for *in vivo* glucose monitoring to provide continuous quantitative analysis [19, 21]. For instance, surface plasmon resonance probes have emerged as a strong candidate; however, they suffer from complex fabrication, and convoluted readout processes [22-27]. Also, interferometric fiber probes have been developed for *in vivo* glucose sensing [28]. The readout approach of that probes was complicated and the output signals were processed to detect the volumetric response of the sensor attached to the fiber's tip. In addition, the silica fiber probe is not compatible with biological systems for implementation *in vivo* as it causes immune response resulting in inflammation and discomfort of patients [29-31].

Alternatively, hydrogel fibers were introduced as a promising technology for *in vivo* glucose sensing due to their biocompatibility and capability to incorporate functional groups for sensing [32]. Functionalizing the hydrogel fiber with glucose-recognition motif such as phenylboronic acid (PBA) derivatives modulates the optical properties of the fiber due to glucose-boronate complexation. For instance, a hydrogel fiber probe based on fluorescence has been reported for quantitative glucose measurements, in which the glucose recognition motif, diboronic acid, and the fluorescent dye (anthracene acid) were incorporated [20]. Despite the rapid response of the fluorescent fiber probe, it suffered from photobleaching of the fluorophore and it was not applicable to individuals with skin pigmentation, where the output signal was affected by epidermal thickness. Recently, polyacrylamide optical fibers were functionalized with 3-(acrylamido) phenylboronic acid [21]. The fiber diameter

increased in response to glucose leading to a change in the transmitted light intensity. The fiber required long time to reach equilibrium glucose complexation, and can be considered non-practical for *in vivo* glucose detection.

Here, we developed optical fiber probes for continuous glucose monitoring in physiological conditions. The glucose recognition agent (3-(acrylamido)-phenylboronic acid) was crosslinked with acrylamide to create glucose-responsive hydrogel and the light diffusing microstructures (LDMs) were imprinted on the hydrogel. The glucose-responsive hydrogel was chemically attached to the tip of a silica multimode fiber during the photopolymerization process. The functionalized fiber was interrogated for glucose quantification in transmission and reflection configurations. Upon glucose complexation with boronate anions immobilized in the hydrogel matrix, the fiber's attached hydrogel underwent a volumetric shift modifying the refractive index of the imprinted LDMs, subsequently, the scattering angles changed. Accordingly, the transmitted power, and the reflected power guided in the fiber changed. In addition, the hydrogel sensor was attached to the tip of a biocompatible hydrogel fiber. The biocompatible functionalized fiber was flexible and offered the convenience to be potentially implemented in biological tissues. The proposed glucose-responsive probe has additional advantages over the previously developed fiber probes, such as easy readout approach as it is compatible with smartphones and no output signal processing is required, rapid response (30 s) , short equilibrium time (15 min), low-cost, and glucose-selective.

5.3 Results and Discussion

The glucose-responsive hydrogel was fabricated, functionalized with the 3-APBA, and the light diffusing microstructures was replicated by the replica mould method during the photopolymerization (Figure 5.1a). The hydrogel sensor was attached to a commercial multimode silica fiber and an in-house made biocompatible fiber during the polymerization process (Figure 5.1b-c). Fabrication of the biocompatible fibers is shown in Figure 5.1d. The immobilized 3-APBA in the hydrogel matrix of the sensor has a high affinity to glucose molecules forming anionic boronate due to 1:1 complexation in the hydrogel network, increasing the osmotic pressure, and accordingly causing a volumetric shift [33]. The volumetric shift of the hydrogel modified the refractive index of the LDMs replicated on the hydrogel's surface leading to change the scattering angles, and consequently the maximum transmitted/reflected power that was correlated to the measured glucose concentration.

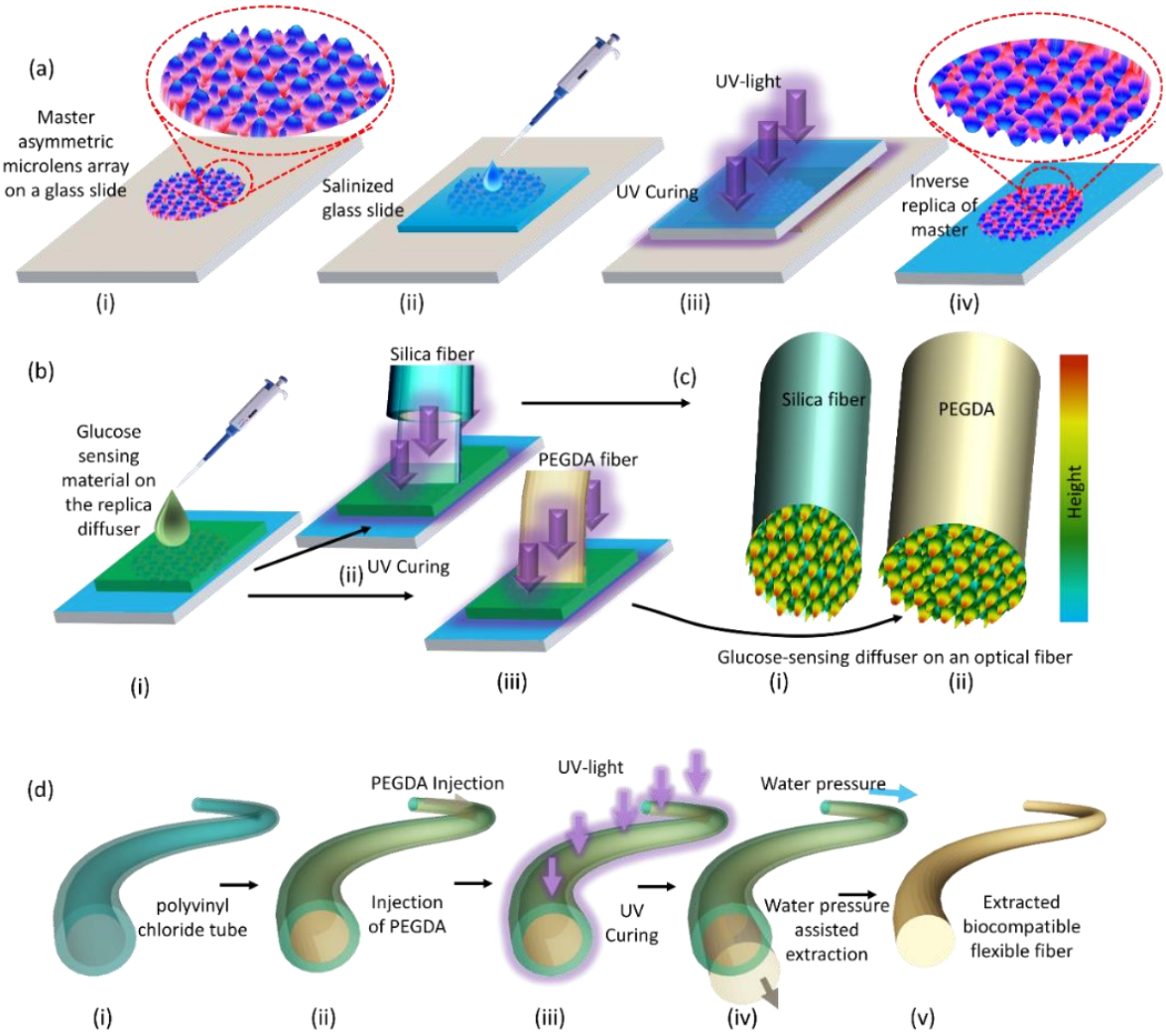

Figure 5.1. Fabrication of the glucose-responsive hydrogel, functionalizing the fibers, and fabrication of the hydrogel fiber. (a) Schematic shows the procedures of preparing the glass constrained glucose-responsive hydrogel replicated with light diffusing microstructures. (b-c) The functionalization process of the silica and the hydrogel fibers. (d) The fabrication process for the biocompatible hydrogel fiber.

The hydrogel sensor constrained on a glass substrate was examined in various glucose concentrations (0 to 50 mM). The sensor was equilibrated in PBS solution (pH 7.4, ionic strength 150 mM, and 24 °C) for 2 h before testing. A stock glucose solution (100 mM) was prepared in PBS buffer of pH 7.4 and diluted using the PBS solution to prepare the required

glucose concentrations. The sensor was submerged in glucose-free PBS buffer solution (1 ml) and illuminated with a green laser (532 nm) and the profile of the transmitted power (P_t) was recorded as a reference (Figure 5.2a). The glucose-free PBS buffer was replaced with a buffered glucose solution (1 ml, 5 mM), and the P_t was recorded after 15 min. The low glucose concentration (5 mM) was replaced with a higher concentration (10 mM) and the reading was recorded after 15 min, and this protocol was repeated until reaching 50 mM. The recorded P_t for the sensor in various glucose concentrations presented Gaussian shape profiles and the forward scattering angles decreased with increasing glucose concentrations (Figure 5.2b). The diffused light formed spots of smaller diameters on the screen -increasing the maximum optical transmitted power (P_{tmax}) with glucose concentration (Figure 5.2c). The P_{tmax} readings as a practical readout method were utilized to monitor the glucose concentrations. The sensor's response saturated with increasing glucose concentration; however, it presented a linear response within the range of 0-20 mM, which had a correlation coefficient, R^2 of 0.98 (Figure 5.2c). The P_{tmax} increased from 79.4 to 92.5 µW when glucose concentration increased from 0 to 20 mM and reached 99 µW when glucose concentration increased to 50 mM, presenting a sensitivity of 0.8 % mM^{-1} in the low glucose concentration range (0-20 mM) which is three time lower as compared to the free-standing condition (2.3 % mM^{-1}). The decrease of the sensitivity results from, in the free-standing condition both size and refractive index of the LDMs change upon glucose complexation but in the constrained condition only the refractive index of the LDMs changes. Again, the hydrogel sensor was examined for glucose sensing, but in this test, the sensor was illuminated by a broadband white light beam and the output signals, the maxima transmitted illuminance (L_t), were measured by a smartphone (Figure 5.2d). Thirdly, the sensor was interrogated in

reflection configuration. The sensor was illuminated by a monochromatic light (532 nm) at an incident angle of 45° and the maximum reflected powers (P_r) of the diffused spots were collected using an optical power meter (Figure 5.2e). The ambient light sensor of a smartphone was utilized to record the output signals to demonstrate the compatibility and the simplicity of the readout approach. The readout for the glucose-free buffer was 60 lux and jumped up to 69 upon increasing glucose concentrating from 0 to 20 mM and reached to 75 lux at 50 mM (Figure 5.2d). The relationship of the glucose concentration against the sensor's output signal was consistent with the experiment carried out using the monochromatic light and the optical power meter (Figure 5.2c). The sensor's response was linear for glucose concentration range of 0-20 mM with a sensitivity of 0.75 % mM^{-1} and saturated at higher glucose concentrations. The hydrogel sensor consistently detected glucose concentrations whether it was illuminated by a monochromatic light or a broadband white light and this is due to the ability of the LDMs to control the beam shape of the monochromatic and white light. In reflection configuration, the P_r increased with glucose concentration because of the positive volumetric shift of the hydrogel sensor that led to decrease the refractive index of the LDMs and consequently the light scattering efficiency of the sensor (Figure 5.2e). The sensor behavior was consistent with the experiments that were carried out in the transmission mode. The P_r increased from 4.6 µW to 5.33 µW upon increasing glucose concentration to 20 mM and reached 5.88 µW at 50 mM. The sensor's output signals saturated at high glucose concentration (30 mM) and the sensitivity was ~ 0.78 % mM^{-1} for glucose concentration within the range 0-20 mM.

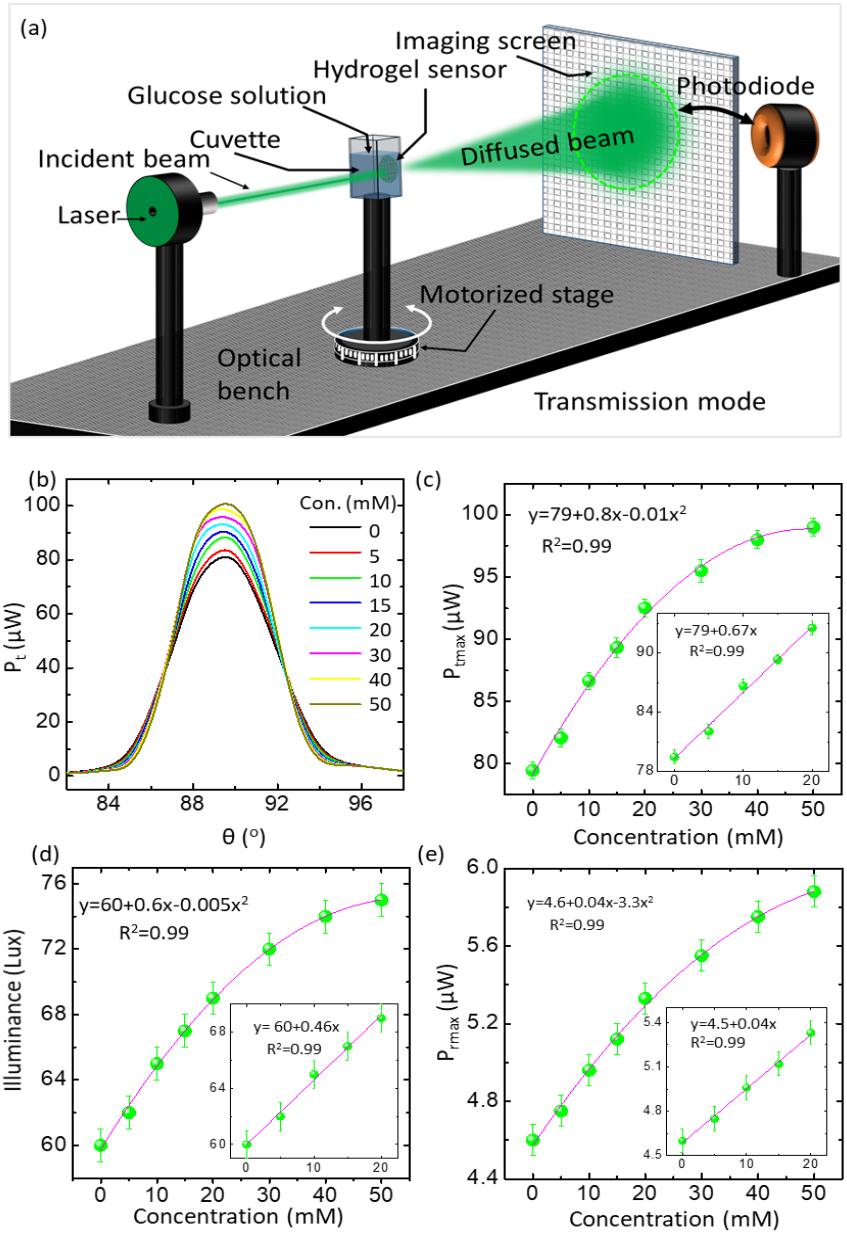

Figure 5.2. Quantification of glucose concentration by the hydrogel sensor. (a) Schematic of the setup for recording glucose concentrations in transmission mode. (b) The profile of the optical transmitted power passing through the sensor against glucose concentrations when the sensor was illuminated by a green laser (532 nm). (c) P_{tmax} of the sensor at various glucose concentrations (0-50 mM). The inset shows the glucose range of 0-20 mM. (d) The maximum transmitted illuminance (L_t) of the sensor versus glucose concentrations while the sensor was illuminated by the broadband white light beam, and the illuminance was recorded by an ambient light sensor of a smartphone. (e) The maxima reflected optical powers (P_{rmax}) of the hydrogel sensor for various glucose concentrations captured in reflection mode. The inset shows the glucose concentration range of 0-20 mM. The scale bars show standard error (n=3).

For *in vivo* or remote glucose sensing applications, the hydrogel sensor was attached to the tip of a multimode silica fiber having a diameter of 500 µm (Figure 5.3). The silica fiber with the functionalized tip was utilized for glucose detection in transmission and reflection configurations. In transmission mode, the fiber was coupled with a monochromatic light source (532 nm) at one end and the its functionalized end was immersed in the glucose solution stored in a plastic cuvette (Figure 5.3a). The photodetector (power meter or smartphone) was fixed below the cuvette to receive the optical fiber signal that pass through the glucose solution reaching the detector. The optical signals (maxima transmitted powers (P_{tmax})) were recorded for each glucose concentration over time. Optical microscopy images of the utilized silica fiber's cross-section and photos of the functionalized fiber illuminated by different monochromatic light sources are displayed in Figure 5.3b-d. The fabrication process of the functionalized silica fiber including preparing the hydrogel matrix, functionalizing the hydrogel with 3-APBA, imprinting the LDMs and attaching the hydrogel sensor to the fiber's tip was carried out in one stage lasting 5 min (Figure 5.1b). This facile and rapid fabrication approach is a great advantage of the developed sensor as compared to other fiber optic probes such as fluorescent and SPR based probes. The fiber probe was tested in glucose concentration range of 0-50 mM and the P_{tmax} values for each concentration over time were recorded at 24 °C (Figure 5.3e). When the glucose concentration was increased, the fiber's output signal (P_{tmax}) increased, showing a linear trend with a correlation coefficient R^2 of 0.99 for glucose concentration range of 0-20 mM. Upon increasing glucose concentration from 0 to 20 mM, P_{tmax} surged 44 µW, from 604 to 648 µW presenting a sensitivity of 0.36% mM^{-1} during this glucose range (Figure 5.3f). For high glucose concentrations from 20 to 50 mM, the P_{tmax} increased 30 µW, indicating declined sensitivity

(0.15 % mM^{-1}). The sensor's saturation at high glucose concentrations might be attributed to the limited available boronate binding sites and the reduced elasticity of the hydrogel matrix that competed against the volumetric swelling process [34]. The fiber probe interrogation results matched with the previous experiments carried out when the hydrogel glucose sensor was constrained on a glass substrate. The developed fiber probe showed a change of ~ 7% of its output signal when glucose concentration increased from 0 to 20 mM as compared to 7% change over the glucose range of 0-100 mM for fiber probe recently published [21].

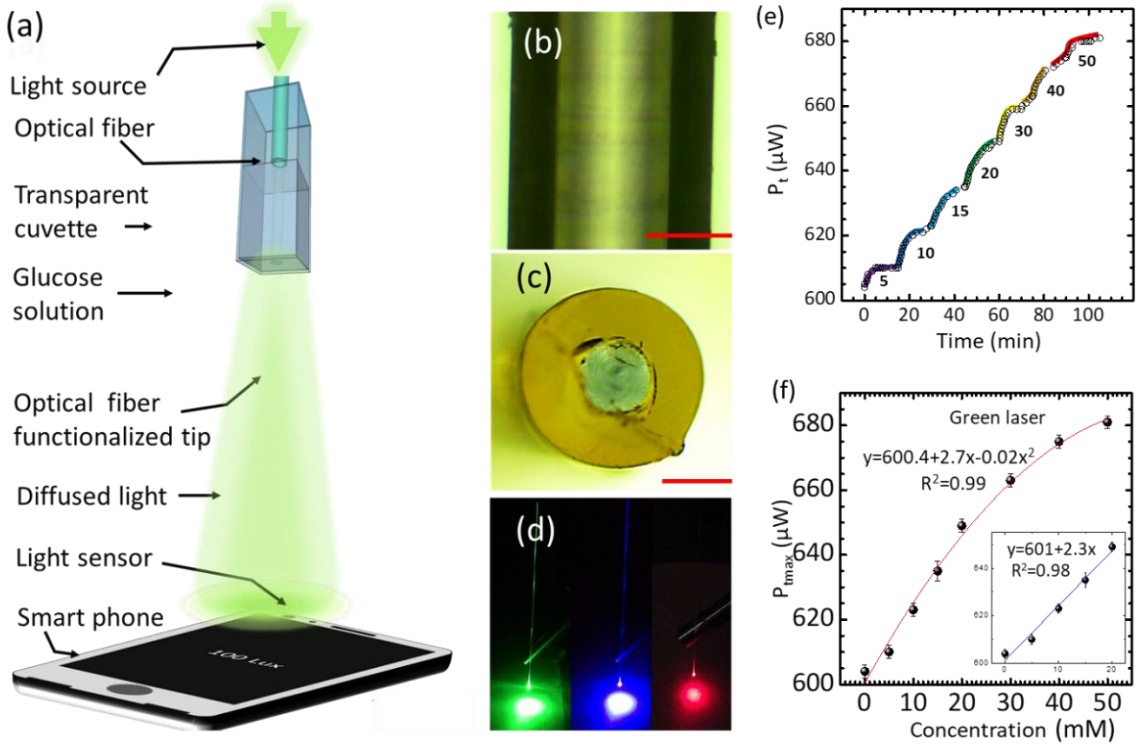

Figure 5.3. Continuous detection of glucose with functionalized silica fiber in transmission mode. (a) Schematic of the setup utilized to test the functionalized fiber in the transmission mode. (b-c) Optical microscopy images of the silica multimode fiber, scale bars 200 µm. (d) Photographs of the functionalized silica fiber coupled with blue, green, and red lasers. (e) The maximum optical transmitted power (P_{tmax}) of the functionalized fiber submerged in various glucose concentrations over time. (f) The P_{tmax} of the fiber against glucose concentrations (0-50 mM), while the fiber was coupled with a green laser and the readout was recorded by a power meter. The scale bars show standard error (n=3).

The optical fiber was coupled with a green laser and was re-interrogated for glucose sensing; however, in this test, a smartphone was employed to detect the output signals. The maximum transmitted illuminance (L_t) increased by 69 Lux, from 929 to 998 Lux with increasing glucose concentration from 0 to 20 mM. However, the growth of the output signal was 49 Lux when glucose concentration increased from 20 to 50 mM (Figure 5.4a). The trend of the recorded L_t against the glucose concentrations was comparable to results recorded by the optical power meter. The fiber probe's response was linear for glucose concentration range of 0-20 mM with a sensitivity of 0.37 % mM^{-1}, which declined at high concentrations as the sensor saturated. To test the feasibility of utilizing the broadband white light for sensing as it is safer than laser for human body implantation sensing, the functionalized fiber was coupled with a broadband white light source and re-examined for glucose concentrations within the range of 0-50 mM and the readout was collected by a smartphone and an optical power meter (Figure 5.4b-c). The trends of the output signals from the fiber probe immersed in various glucose concentrations were comparable whether the output signals were recorded by the smartphone or the optical power meter. The probe's response decreased at high concentrations and below 30 mM the response was linear with a sensitivity of 0.35 % mM^{-1}. The P_{tmax} increased from 100 to 107 µW in the glucose range of 0-20 mM-indicating a sensitivity almost same as the sensitivity when the probe was illuminated by a monochromatic light –meaning that the sensitivity of the probe does not depend on the light source. Advantageously, the probe's response to glucose concentrations was similar whether the coupled light source was a broadband white light or a monochromatic light source, and the smartphone was successfully employed for readouts and showed a reliable response. The readout approach was simple and low-cost whether the output signal was recorded by a

power meter or a smartphone and this one of the main advantages of the developed fiber probe as compared to the previous reported glucose probes [21, 22, 28]. For instance, interferometric, fluorescent, and SPR fiber probes require processing of the output signals, customized setups, and high-cost instruments such as spectrophotometers and fluorometers [24, 28].

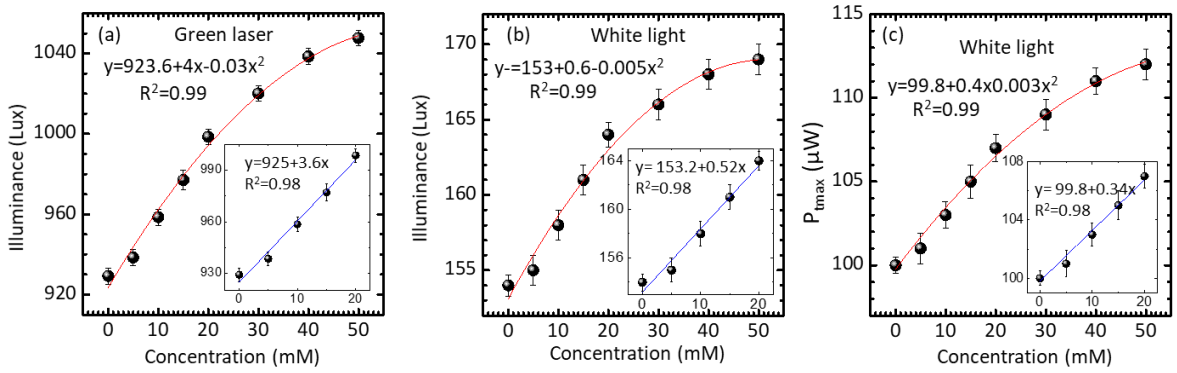

Figure 5.4. Interrogation of the fiber probe by the smartphone and the power meter as readout instruments. (a) The L_t of the fiber versus glucose concentrations were recorded while the fiber probe was coupled with a green laser and the readouts were captured by a smartphone. The inset shows the glucose concentration range of 0-20 mM. (b) The L_t of the fiber probe versus glucose concentrations while the fiber was coupled with a broadband light source and the output signals were captured by a smartphone. The inset shows the glucose concentration range of 0-20 mM. (c) The P_{tmax} of the optical fiber versus glucose concentrations while the fiber was coupled with a broadband light source and the output signals were recorded by an optical power meter. The inset shows the glucose concentration range of 0-20 mM. The scale bars show standard error (n=3).

The functionalized silica fiber was tested for glucose sensing within the concentration range of 0-50 mM, but this time in the reflection configuration, which is the desired mode for *in vivo* biosensing. In the reflection configuration, a three-terminal coupler 2×1 was utilized to connect the fiber with the white light source and the optical power meter (Figure 5.5a). The fiber was submerged in the glucose solution (1 ml) and the optical reflected power (P_r) was recorded by the power meter. Upon swelling of the hydrogel sensor fixed at the fiber's tip,

the P_r guided in the optical fiber increased (Figure 5.5b). In the reflection mode, the behavior of the output signal against glucose concentrations was comparable to the measurements in the transmission mode as the fiber response was linear within the concentration range of 0-20 mM with a correlation coefficient R^2 of 0.99, and the sensitivity decreased significantly above 20 mM. The optical reflected power was 318 nW for the glucose-free PBS buffer and increased to 338 nW at 20 mM concentration with a sensitivity of 0.31% mM^{-1} in this glucose range. For the high glucose concentration range of 20-50 mM, the output signal recorded an increment of 13 nW. Also, in the reflection mode configuration the fiber probe showed a higher sensitivity than in literature [21].

The boronic acids bind to *cis*-diol containing molecules and α- hydroxy acids. Fructose and galactose are monosaccharides present in human blood at low concentrations less than 0.1 mM [35, 36]. In addition, there are many other sugars in blood in the form of glycoproteins and macromolecular carbohydrates; however, they are not expected to significantly interfere with the probe's response as they may not diffuse into the hydrogel matrix and bind to PBA groups because of their large size [36]. Thus, the glucose selectivity during *in vivo* sensing was expected to be minimal; however, lactate is present in blood at a concentration of 0.36-0.75 mM in healthy adults and has a high affinity to bind with phenylboronic acid by its *α*-hydroxy group [21]. The potential interference of lactate on the probe's response was interrogated (Figure 5.5c). The lactate solutions were prepared in PBS buffer (pH 7.4) and the probe's response for lactate and glucose were recorded separately at human body temperature (37 °C) to determine the potential interference of lactate under the physiological conditions. The recorded output signals (P_{tmax}) of the fiber probe shifted significantly at high

lactate concentrations, but hardly any response was recorded at low lactate concentrations (1 mM). In contrast, the output signal of the fiber considerably shifted at low glucose concentrations within the physiological range (4-8 mM) and the fiber response saturated at higher concentrations [37, 38]. For lactate concentration of 5 mM, the output signal increased by 1.2% over 15 min as compared to 4% increase for the same concentration of glucose in the same interval. Therefore, the interference of the lactate according to its concentrations in blood would be 0.08-0.17%. However, the small molecular weight (Mw: 90 g mol^{-1}) of lactate molecule that accelerated its diffusion into the hydrogel matrix and its high affinity to bind with the pendant phenylboronic acid, it has a limited potential interference in the fiber's response [21, 39].

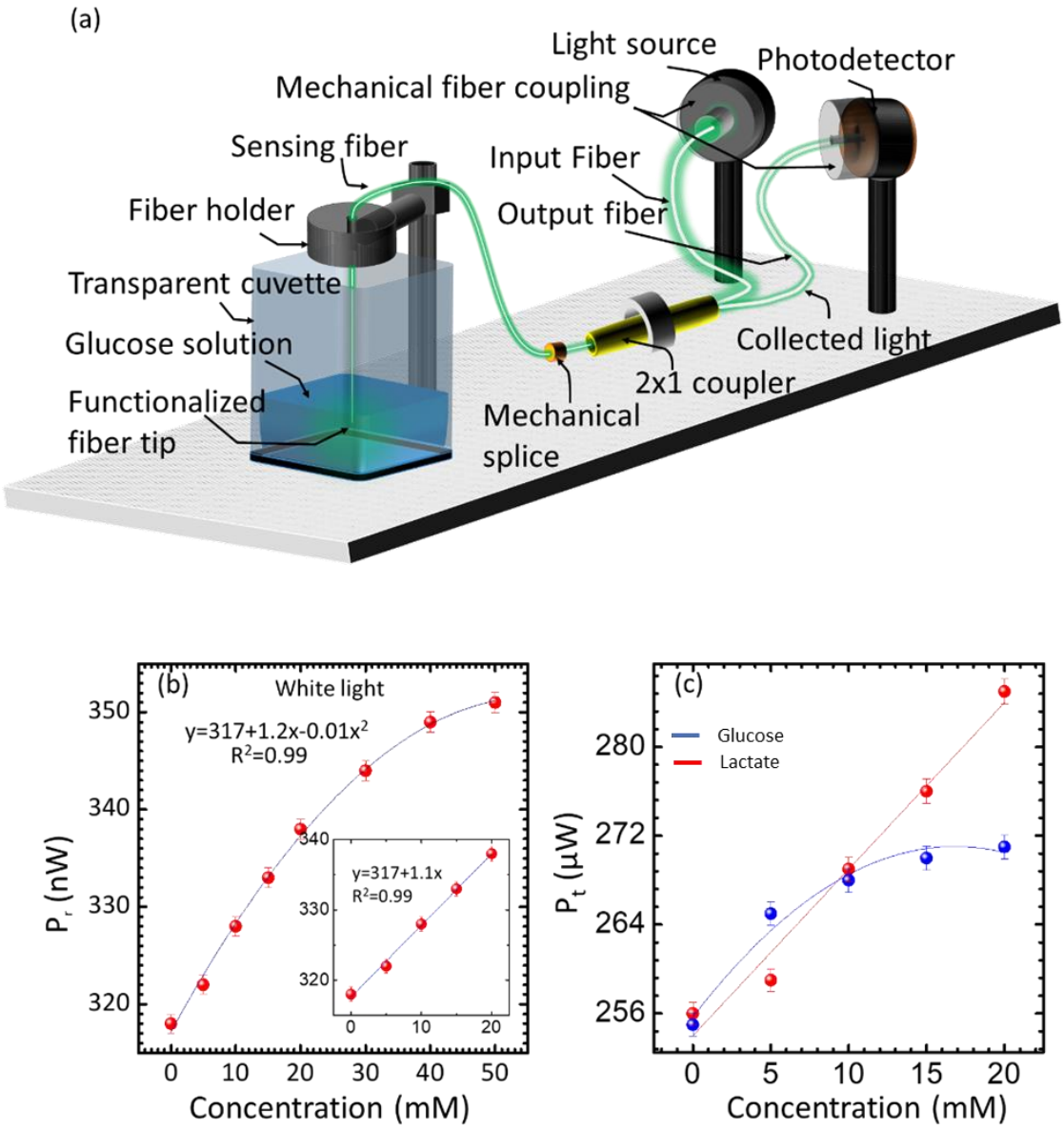

Figure 5.5. Testing the functionalized silica fiber for glucose sensing in reflection mode. (a) Schematic of the setup utilized for interrogating the fiber in reflection configuration. (b) The optical reflected power versus the glucose concentrations while the fiber coupled with a white light source and the output signal was captured by an optical power meter. (c) The lactate and glucose concentrations versus the P_t at human body temperature, 37 °C, the test was carried out in the transmission mode. The scale bars show standard error (n=3).

The swelling dynamics of the fiber probe was studied at 10 mM glucose concentration as the P_{tmax} was recorded over time. Upon exposure of the fiber to glucose solution, the binding equilibrium (glucose-boron complexation) saturated within 15 min and the response time

was 30 s (Figure 5.6a). This equilibrium time is one-third of that reported in previous studies, where the saturation time for the 3-APBA-modified optical fiber was 45 min [21]. For the diabetic patients, the readout rate required for monitoring glucose concentration is 0.078 $mM \cdot min^{-1}$, and the proposed probe provided a readout rate of 0.66 mM min^{-1}, which is 8-fold higher than the required speed [21]. The stability and reusability of the functionalized silica fiber were investigated by detecting the response of the fiber in four complete and continuous cycles (Figure 5.6b). The probe's response for 10 mM glucose concentration was monitored for 15 min, followed by the reset using an acetate buffer (pH 4.6) for ~10 s, and maintained in PBS for 15 min buffer before commencing the next cycle. When the fiber was immersed in buffer at pH 4.6, the hydrogel attached sensor shrank due to the decrease in the pH below the apparent pK_a value of the glucose-responsive hydrogel as the charged tetrahedral state of the 3-APBA transformed to uncharged trigonal planar form releasing the bound glucose molecules [21]. Upon immersing the functionalized tip into the PBS buffer of pH 7.4, the attached hydrogel returned to it is original volume, and consequently the LDMs were reset to its original geometry. These results are significant as the functionalized fiber exhibited reusability with limited hysteresis and had comparable sensitivity for each cycle. Furthermore, the effect of temperature on the fiber probe's response was investigated within the range of 10-45 °C (Figure 5.6c). Raising the solution's temperature induced shrinkage of the glucose-responsive hydrogel, enhancing the refractive index of the imprinted LDMs, and consequently the output signal decreased. Within the temperature range of 20-35 °C, the fiber probe's signal slightly shifted, but the output signals considerably changed below 20 °C and above 35 °C. The output signal shifted by 2% when the temperature increased from 10 to 20

°C, 0.5% within 20 to 35 °C, and 3.6% when the temperature increased to 45 °C (Figure 5.6c). The fiber's response to glucose must be calibrated at physiological conditions to avoid the temperature and pH interferences.

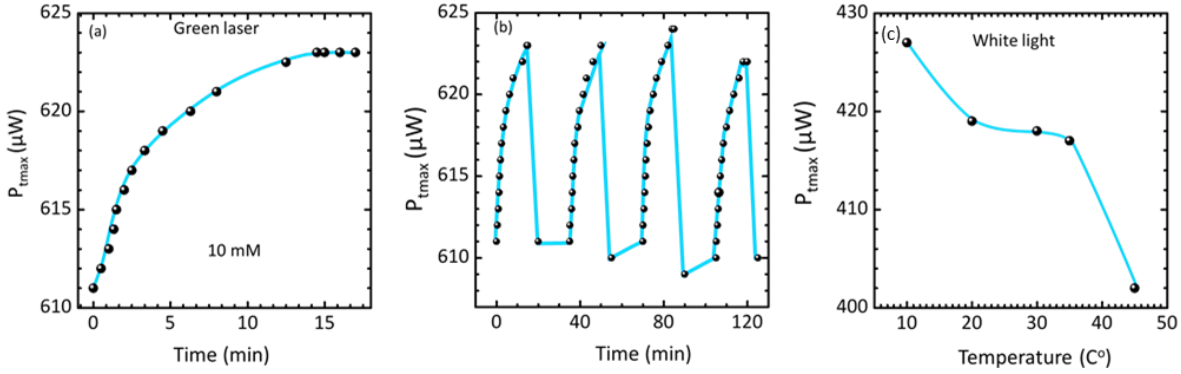

Figure 5.6. kinetic of swelling, reusability, and effect of temperature on the fiber probe. (a) The maximum transmitted power of the functionalized fiber immersed in 10 mM glucose concentration over time. (b) The fiber's output signal versus time at a glucose concentration of 10 mM for four cyles as the green laser laser pointer coupled with the fiber and the readings were recorded in transmission mode, the fiber was reset in acetate buffer (pH 4.6), and the transmitted power baseline was 611±1 µW and increased to 623±1 µW. (c) The solution's temperature *versus* the fiber's output signals, the test was carried out in the transmission mode

Silica fibers are not compatible with biological tissues to be implemented for *in vivo* sensing as they cause inflammation at the implantation sites and discomfort to patients. Therefore, a biocompatible hydrogel fiber was fabricated to replace the silica fiber. A biocompatible polymer, polyethylene glycol diacrylate (PEGDA) was utilized to fabricate hydrogel fibers because PEGDA counters the adsorption of proteins such as fibrinogen, albumin, and fibronectin that host the inflammatory cell interactions. Initially, polymerized PEGDA cubes of 1 cm side length were prepared at precursor concentrations of 5-90 vol% to determine the optimum concentrations for fabricating the hydrogel fiber (Figure 5.7a). The hydrogel attenuation for monochromatic light (532 and 650 nm), and broadband white light were

investigated (Figure 5.7b-c). For monochromatic and white light, increasing the PEGDA concentration from 5 to 60 vol% considerably reduced the light attenuation, and above 60 vol% a slight change was detected (Figure 5.7b-c). For monochromatic light, the attenuation was 22 dB cm^{-1} at the precursor concentration of 10 vol%, and decreased to ~1dB cm^{-1} when the precursor concentration reached 50 vol%. The attenuation decreased to ~0.4 dB cm^{-1} with increasing the precursor concentration to 90 vol%. These results confirmed that the optical properties of the PEGDA hydrogel depended on the precursor concentration which is consistent with the previous studies [40]. The attenuation of the broadband white light measurements showed higher attenuation for short wavelengths besides the significant dependence of the attenuation on the precursor concentration. Considering the mechanical and optical properties, the hydrogel fiber was made of PEGDA precursor concentration of 60 vol%. The tip of the hydrogel optical fiber was functionalized with the glucose-responsive hydrogel as in the case of the silica fiber. The hydrogel fiber with a length of 5 cm and a diameter of 950 μm, was coupled with a broadband white light source and an optical power meter by the 2×1 coupler. The functionalized hydrogel fiber probe was interrogated for glucose sensing in the reflection mode and the readings were recorded after 15 min for each glucose concentration. The output signal increased by 17 nW within the glucose concentrations range of 0-20 mM and by 10 nW upon glucose concentration change from 20-50 mM, presenting analogous response to the functionalized silica fiber (Figure 5.7d). The trend of the output signal was linear for the glucose concentration range of 0 to 20 mM and above this concentration the sensitivity decreased considerably. Notably, the sensitivity of the hydrogel fiber probe was ~ 0.25% mM^{-1} which is lower as compared to the silica fiber -this might be attributed to the higher light loss in the hydrogel fiber as compared to the silica

fiber, and this matter can be tackled by cladding the hydrogel fiber with a low-refractive index material such as calcium alginate [21].

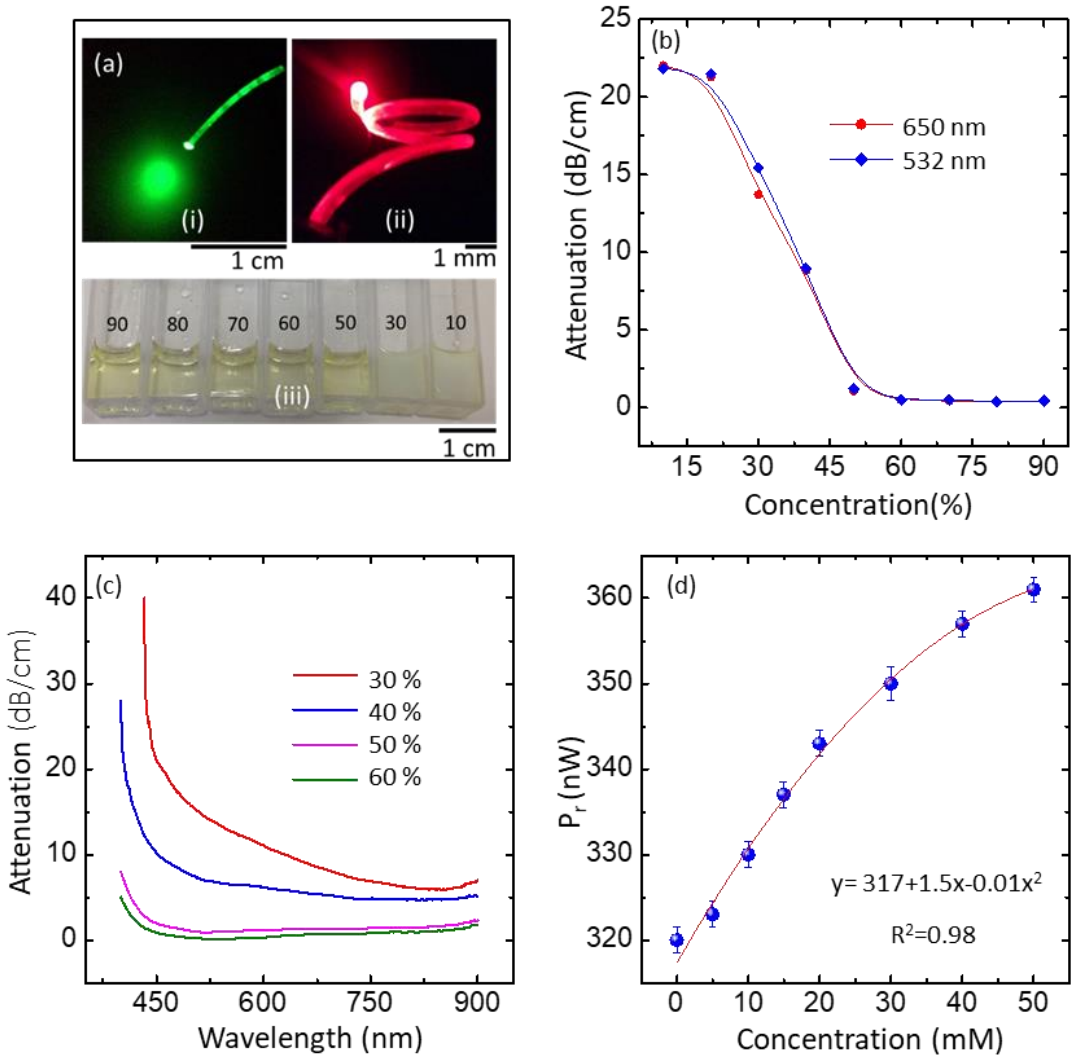

Figure 5.7. Hydrogel optical fiber sensors. (a) Photographs of the functionalized hydrogel optical fiber and the PEGDA hydrogel cubes of various precursor concentrations. (b) The attenuation of green and red laser beams (532 and 650 nm) versus the precursor concentration (PEGDA) (5-90 vol%). (c) The attenuation of the white light power by the hydrogels of 1 cm cube side *versus* the precursor concentrations. (d) Testing the biocompatible functionalized fiber for glucose detection in the reflection configuration. The optical reflected power values were recorded by the power meter versus glucose concentrations. The scale bars show standard error (n=3).

5.4 Materials and Methods

5.4.1 Materials

Polyethylene glycol diacrylate (PEGDA) (mw: 700 Da), acrylamide (AM) (98%), 3-(acrylamido)-phenylboronic acid (3-APBA) (98%), sodium L-lactate, *N*,*N*'-methylenebisacrylamide (99%), D-(+)glucose (99.5%), 2,2-dimethoxy-2-phenylacetophenone (DMPA) (99%), 2-hdroxy-2-methylpropiophenone (2-HMP) (97%), phosphate buffered saline tablets (PBS), dimethyl sulfoxide (DMSO) (99.9%), sodium phosphate monobasic (NaH_2PO_4), and sodium phosphate dibasic (NaH_2PO_4) were purchased from Sigma Aldrich and used without further purification.

5.4.2 Fabrication of the hydrogel sensor constrained on a glass slide

The precursor solution consisted of acrylamide (78.5 mol %), *N*, *N*'-methylenebisacrylamide (1.5 mol %), and 3-APBA (20 mol %) was mixed with DMPA (2% wt/vol) in DMSO and the monomer dilution was 1:2 wt/vol. The monomer solution (100 µl) was drop-cast on the LDMs (Thorlabs), and subsequently, was covered with a silanized glass piece, and was polymerized by UV lamp (365 nm) for 5 min. The polymerized sensor was washed with DI water/ethanol (1:1 v/v) and preserved in PBS solution at pH 7.4.

5.4.3 Functionalization of the silica and the hydrogel fibers

In order to functionalize the optical fiber with the glucose-responsive hydrogel, the fiber's tip was silanized and dipped in the glucose-sensitive solution (10 µl) that was drop-cast on the LDMs and was exposed to the UV light for 5 min. The functionalized fiber was preserved in the PBS solution at pH 7.4.

5.4.4 Fabrication of the biocompatible optical fiber

PEGDA monomer was mixed with 2-hydroxy-2-methylpropiophenone (2-HMP) (5 vol %) in DI water. The dilution of PEGDA in DI water was varied from 5 to 90 vol%. The prepared solution (200 µl) was injected into a polyvinyl chloride tube with an inner diameter of 1 mm and the tube was exposed to UV light (365 nm) for 30 min. The optical fiber was extracted from the tube by applying water pressure using a syringe. The optical fiber was washed with a mixture of ethanol and DI water (1:1, v/v).

5.5 Conclusion

We have developed fiber optic probes for continuous glucose monitoring based on functionalizing the tips of silica and biocompatible hydrogel fibers. The functionalization process was carried out during the photopolymerization of the glucose-responsive hydrogel. The PEGDA hydrogel was utilized to fabricate the biocompatible optical fiber that can potentially minimize the inflammation in the probe inserted site. The approach of the optical fiber's readout was simple, practical, and low-cost as it did not require data processing or costly equipment. The output signals were recorded by either a smartphone or an optical power meter, utilizing broadband white light or monochromatic light sources for illuminating the probe. Glucose quantification tests were attained in transmission and in reflection configurations, and effect of temperature on the fiber's response was examined. The silica fiber probe was highly sensitive (0.37% mM^{-1}) and selective for glucose than lactate within the physiological range as the interference of lactate was trivial (~0.1%). The developed probes presented significant optical, mechanical, and practical advantages than their previous counterparts in terms of ease fabrication process, rapid response (30 s), and practical

readouts. Therefore, the developed probes may find applications *in vivo* glucose monitoring systems at point-of-care and intensive care units. To realize broader applications, the proposed fiber probe can be functionalized with chelating agents and aptamers for continuously sensing a wide range of biomolecules such as proteins, DNA, and RNA in clinical samples.

References

1. G. The Action to Control Cardiovascular Risk in Diabetes Follow-On Eye Study and G. the Action to Control Cardiovascular Risk in Diabetes Follow-On Study, "*Persistent Effects of Intensive Glycemic Control on Retinopathy in Type 2 Diabetes in the Action to Control Cardiovascular Risk in Diabetes (ACCORD) Follow-On Study*," Diabetes care, 2016. **39** (7): p. 1089-1100.
2. J. S. Skyler *et al.*, "*Intensive glycemic control and the prevention of cardiovascular events: implications of the ACCORD, ADVANCE, and VA diabetes trials: a position statement of the American Diabetes Association and a scientific statement of the American College of Cardiology Foundation and the American Heart Association*," Circulation, 2009. **119** (2): p. 351-357.
3. M. P. Srinivasan, P. K. Kamath, N. M. Bhat, N. D. Pai, P. A. Manjrekar, and C. Mahabala, "*Factors associated with no apparent coronary artery disease in patients with type 2 diabetes mellitus for more than 10 years of duration: a case control study*," Cardiovascular Diabetology, 2015. **14**: p. 146.
4. O. Crofford, S. Genuth, and L. Baker, "*Diabetes Control and Complications Trial (DCCT): results of feasibility study*," Diabetes care, 1987. **10** (1): p. 1-19.
5. C. L. Thompson, K. C. Dunn, M. C. Menon, L. E. Kearns, and S. S. Braithwaite, "*Hyperglycemia in the hospital*," Diabetes Spectrum, 2005. **18** (1): p. 20-27.
6. G. Van Den Berghe *et al.*, "*Intensive insulin therapy in critically ill patients*," New England Journal of Medicine, 2001. **345** (19): p. 1359-1367.
7. L. S. Williams *et al.*, "*Effects of admission hyperglycemia on mortality and costs in acute ischemic stroke*," Neurology, 2002. **59** (1): p. 67-71.
8. G. Van den Berghe, "*Insulin therapy in critical illness*," International Diabetes Monitor, 2002. **14** (6): p. 1-6.
9. G. E. Umpierrez, S. D. Isaacs, N. Bazargan, X. You, L. M. Thaler, and A. E. Kitabchi, "*Hyperglycemia: an independent marker of in-hospital mortality in patients with undiagnosed diabetes*," The Journal of Clinical Endocrinology & Metabolism, 2002. **87** (3): p. 978-982.

10. V. M. Montori, B. R. Bistrian, and M. M. McMahon, "*Hyperglycemia in acutely ill patients*," Jama, 2002. **288** (17): p. 2167-2169.
11. S. J. Finney, C. Zekveld, A. Elia, and T. W. Evans, "*Glucose control and mortality in critically ill patients*," Jama, 2003. **290** (15): p. 2041-2047.
12. V. R. Kondepati and H. M. Heise, "*Recent progress in analytical instrumentation for glycemic control in diabetic and critically ill patients*," Analytical and bioanalytical chemistry, 2007. **388** (3): p. 545.
13. K. K. Haga *et al.*, "*The effect of tight glycaemic control, during and after cardiac surgery, on patient mortality and morbidity: A systematic review and meta-analysis*," Journal of cardiothoracic surgery, 2011. **6** (1): p. 3.
14. C. V. Doran, J. G. Chase, G. M. Shaw, K. T. Moorhead, and N. H. Hudson, "*Automated insulin infusion trials in the intensive care unit*," Diabetes technology & therapeutics, 2004. **6** (2): p. 155-165.
15. A. G. Rapsang and D. C. Shyam, "*Blood sugar control in the intensive care unit: time to relook*," Southern African Journal of Anaesthesia and Analgesia, 2014. **20** (4): p. 1-5.
16. J. S. Krinsley and R. L. Jones, "*Cost analysis of intensive glycemic control in critically ill adult patients*," CHEST Journal, 2006. **129** (3): p. 644-650.
17. G. Van den Berghe, P. J. Wouters, K. Kesteloot, and D. E. Hilleman, "*Analysis of healthcare resource utilization with intensive insulin therapy in critically ill patients*," Critical care medicine, 2006. **34** (3): p. 612-616.
18. J. S. Krinsley and R. L. Jones, "*Cost analysis of intensive glycemic control in critically ill adult patients*," Chest, 2006. **129** (3): p. 644-650.
19. C. Yang, C. Chang, and J. Lin, "*A comparison between venous and finger-prick blood sampling on values of blood glucose*," International Proceedings of Chemical, Biological and Environmental Engineering, 2012. **39**: p. 206-210.
20. Y. J. Heo, H. Shibata, T. Okitsu, T. Kawanishi, and S. Takeuchi, "*Long-term in vivo glucose monitoring using fluorescent hydrogel fibers*," Proceedings of the National Academy of Sciences, 2011. **108** (33): p. 13399-13403.
21. A. K. Yetisen *et al.*, "*Glucose-Sensitive Hydrogel Optical Fibers Functionalized with Phenylboronic Acid*," Advanced Materials, 2017. **29** (15): p. 1606380-1606391.
22. D. Li *et al.*, "Glucose measurement using surface plasmon resonance sensor with affinity based surface modification by borate polymer," in *Solid-State Sensors, Actuators and Microsystems (TRANSDUCERS), 2015 Transducers-2015 18th International Conference on*: IEEE, p. 1569-1572.
23. S. Cao *et al.*, "*Highly sensitive surface plasmon resonance biosensor based on a low-index polymer optical fiber*," Optics express, 2018. **26** (4): p. 3988-3994.
24. D. Li *et al.*, "*Affinity based glucose measurement using fiber optic surface plasmon resonance sensor with surface modification by borate polymer*," Sensors and Actuators B: Chemical, 2015. **213**: p. 295-304.
25. S. K. Srivastava, V. Arora, S. Sapra, and B. D. Gupta, "*Localized surface plasmon resonance-based fiber optic U-shaped biosensor for the detection of blood glucose*," Plasmonics, 2012. **7** (2): p. 261-268.
26. S. Singh and B. D. Gupta, "*Fabrication and characterization of a surface plasmon resonance based fiber optic sensor using gel entrapment technique for the detection of low glucose concentration*," Sensors and Actuators B: Chemical, 2013. **177**: p. 589-595.

27. T.-J. Lin and M.-F. Chung, "*Detection of cadmium by a fiber-optic biosensor based on localized surface plasmon resonance*," Biosensors and Bioelectronics, 2009. **24** (5): p. 1213-1218.
28. S. Tierney, B. M. H. Falch, D. R. Hjelme, and B. T. Stokke, "*Determination of Glucose Levels Using a Functionalized Hydrogel– Optical Fiber Biosensor: Toward Continuous Monitoring of Blood Glucose in Vivo*," Analytical chemistry, 2009. **81** (9): p. 3630-3636.
29. T. T. Ruckh and H. A. Clark, "Implantable nanosensors: toward continuous physiologic monitoring," vol. 86, ed: ACS Publications, 2013, pp. 1314-1323.
30. A. Heller and B. Feldman, "*Electrochemical glucose sensors and their applications in diabetes management*," Chemical Reviews, 2008. **108** (7): p. 2482-2505.
31. S. Vaddiraju, D. J. Burgess, I. Tomazos, F. C. Jain, and F. Papadimitrakopoulos, "*Technologies for continuous glucose monitoring: current problems and future promises*," Journal of diabetes science and technology, 2010. **4** (6): p. 1540-1562.
32. M. Choi, J. W. Choi, S. Kim, S. Nizamoglu, S. K. Hahn, and S. H. Yun, "*Light-guiding hydrogels for cell-based sensing and optogenetic synthesis in vivo*," Nature photonics, 2013. **7** (12): p. 987.
33. I. Hisamitsu, K. Kataoka, T. Okano, and Y. Sakurai, "*Glucose-responsive gel from phenylborate polymer and poly (vinyl alcohol): prompt response at physiological pH through the interaction of borate with amino group in the gel*," Pharmaceutical research, 1997. **14** (3): p. 289-293.
34. M. Elsherif, M. U. Hassan, A. K. Yetisen, and H. Butt, "*Glucose Sensing with Phenylboronic Acid Functionalized Hydrogel-Based Optical Diffusers*," ACS nano, 2018. **12**: p. 2283-2291.
35. T. D. James, K. S. Sandanayake, and S. Shinkai, "*A glucose-selective molecular fluorescence sensor*," Angewandte Chemie International Edition in English, 1994. **33** (21): p. 2207-2209.
36. S. Kabilan *et al.*, "*Holographic glucose sensors*," Biosensors and Bioelectronics, 2005. **20** (8): p. 1602-1610.
37. G. Boeckxstaens, M. Horowitz, H. Bermingham, and R. Holloway, "*Physiological variations in blood glucose concentration affect oesophageal motility and sensation in normal subjects*," Neurogastroenterology & Motility, 1997. **9** (4): p. 239-246.
38. V. Thomé-Duret *et al.*, "*Use of a subcutaneous glucose sensor to detect decreases in glucose concentration prior to observation in blood*," Analytical chemistry, 1996. **68** (21): p. 3822-3826.
39. M. Bajgrowicz-Cieslak, Y. Alqurashi, M. I. Elshereif, A. K. Yetisen, M. U. Hassan, and H. Butt, "*Optical glucose sensors based on hexagonally-packed 2.5-dimensional photonic concavities imprinted in phenylboronic acid functionalized hydrogel films*," RSC Advances, 2017. **7** (85): p. 53916-53924.
40. M. Choi, M. Humar, S. Kim, and S. H. Yun, "*Step-index optical fiber made of biocompatible hydrogels*," Advanced Materials, 2015. **27** (27): p. 4081-4086.

Chapter 6: Real-Time Optical Fiber Sensors Based on Light Diffusing Microstructures

This chapter of the alternative format thesis is published in journal of Lap on a Chip. The publishing details and the authors contributions are outlined below.

Mohamed Elsherif**, Rosalia Moreddu, Mohammed Umair Hassan, Ali K. Yetisen, and Haider Butt*, Real-Time Optical Fiber Sensors Based on Light Diffusing Microstructures, **Lab on a Chip**, 2019, 2019, 19, 2060-2070.

Authors Contributions

M.E. and H.B conceived the project idea. **M.E.** performed the experiments and wrote the manuscript. H.B. led the study. M.U.H, A.K.Y. and R.M. made intellectual contributions and edited the article.

Keyword: Photonics; sensors; diffusers; fiber optics; hydrogels

6.1 Abstract

Applications of fiber optics are impeded in implantable medical diagnosis due to incompatibility with biological tissues, and immune reaction *in vivo*. The utilization of biocompatible materials to construct a photonic sensing platform can reduce the immune response in *in vivo* medical diagnostics. Here, we develop real-time optical fibers functionalized with stimuli-responsive polymers. Light diffusing microstructures (LDMs) were replicated on stimuli-sensitive hydrogels as stand-alone sensors and were chemically attached to the tips of silica and biocompatible optical fibers. Quantitative measurements were carried out using a smartphone to demonstrate the ease, simplicity, and practicality of the readout approach. To demonstrate the utility in real-time sensing, the fiber probe was investigated in various concentrations of ethanol, propan-2-ol, and dimethyl sulfoxide, and showed immediate response. Also, another fiber probe was developed and showed a rapid response to pH in the acidic region with a sensitivity of 20% pH^{-1}. To develop biocompatible probes for biosensing applications, LDM imprinted polymer were attached to the tip of a hydrogel optical fiber. The optical fiber probe in the refection configuration showed a sensitivity of 7.5% pH^{-1} in the acidic region. The developed hydrogel fiber probes may have application in gastric pH, point-of-care diagnostics, continuous biomarker monitoring, and critical care sensing devices.

6.2 Introduction

Optical fiber sensors offer unique features such as immunity to electromagnetic interference, remote sensing, miniaturization, and small volumes of samples [1-7]. Fiber sensors based on stimuli-responsive hydrogels can detect a wide variety of parameters with high sensitivity and rapid response time [8-10]. The hydrogels have the ability to undergo volumetric changes as a response to external stimuli including pH, temperature, ionic strength, and electric field or to certain analytes such as glucose, lactate, proteins, and DNA [11-19]. Therefore, optical fiber sensors can be utilized in diverse fields such as industrial biotechnology, environmental monitoring, and biosensing [20-26].

Fiber optic sensors based on optical techniques, such as interferometry, detect the volumetric response of the fiber's tip that has a stimuli-responsive hydrogel attached to it. The interferometric technique enables accurat detecion of volumetric changes in the hydrogels; however, it requires a complex readout instrumentation and high-quality polymer stimuli-responsive films [3]. Additionally, the interferometry necessitates highly coherent light sources that significantly increase the cost of the fiber probe interrogation setup [3].

Surface plasmon resonance phenomenon (SPR) was employed with fiber optics for remote sensing applications. The plasmonic fiber probe based on stimuli-responsive hydrogel includes a plasmonic-metal layer or-nanoparticles covering the unclad core region of the optical fiber, followed by the hydrogel layer [27]. Plasmonic fiber probes have been used for a broad range of sensing applications such as for pH, glucose, and metal ions [28-30]. Complexity of the fabrication and the readout approach, and the technical limitations such as

low penetration of the evanescent waves to the analyte-responsive medium impeded the commercialization of these probes at a large scale.

Fiber optic probes based on amplitude absorbance measurements suffer from poor spectral peak, and are influenced by the intensity fluctuation of the light source, making the readouts impractical. Moreover, these probes require a precise position of the stimuli-responsive hydrogel coatings and light launching angle [3, 31]. For instance, an unclad region of the optical fiber was coated with a silica layer trapping a pH responsive-dye [31]. The intensity of the transmitted light changed based on the pH of the fiber surrounding solution. The fiber illumination angle was critical to initiate high intensity evanescent waves at the sensing region to achieve a reasonable absorption of the guided light in the fiber, making the probe impractical [31].

Therefore, it is highly desirable to develop fiber optic probes for remote sensing and for implantable biosensing applications that have less limitations in terms of fabrication, readouts, and practicality.

Detection of alcohol concentration is significant in industrial biotechnology, drug discovery, fermentation, and food production [32-34]. Numerous electrochemical sensors have been developed for ethanol measurements, mostly based on enzymes such as alcohol oxidase and alcohol dehydrogenase [35-39]. For instance, an electrochemical sensor was developed for the quantification of ethanol in blood plasma based on ethanol dehydrogenase (EDH) and nicotinamide adenine dinucleotide (NAD^+) [40]. High overpotential that might increase the interference with the composition of the sample was demanded. Selvam et.al, demonstrated

a wearable ethanol sensor to monitor alcoholic consumption in human sweat. The sensor showed a long response time of near 30 min. [41]

Also, hydrogel-based alcohol sensors have been reported [42-44]. For example, ethanol-responsive hydrogel made of polyacrylamide matrix was demonstrated [45]. The hydrogel presented a negative volumetric shift in ethanol aqueous solutions. The volumetric shifts were converted into measurable output voltages by integrating the hydrogel with a piezoresistive pressure sensor. The sensor was not reproducible as two sensors made of the same hydrogel showed different sensitivities. In addition, the hydrogel equilibrium time exceeded 90 min. Existing enzymatic-based sensors suffer from instability and signal drift in long-term usage due to the unreliable nature of the enzymes and the electroactive interferences from the sample. Additionally, they are difficult to be sterilized and have limited dynamic range that does not allow direct measurements in undiluted samples [32]. Hence, robust alcohol sensors are needed to quantitatively measure a wide range of samples in real-time.

Here, we developed fiber optic probes for remote sensing of alcohol and pH. The developed probes do not require high-quality films, coherent light sources, high-cost instrumentation, output signal processing, or complex fabrication process as the case in the previous reported fiber probes. Light diffusing microstructures (LDMs) that function as a light diffuser were imprinted on stimuli-responsive hydrogels and chemically-attached to the tips of optical fibers. The fabricated fiber optic probes were investigated for quantitative sensing of alcohols and pH in aqueous solutions in transmission mode. In addition, sensing tests were carried out in reflection mode to test the applicability of the developed probes for implantable sensing

applications. The introduced fiber optic probes overcome technical limitations of the existing fiber optic probes in terms of ease of fabrication, practicality, portability, and simple readout approach.

6.3 Results and discussion

Light diffusing microstructures were imprinted on both alcohol and pH responsive-hydrogels during the UV curing process to create stand-alone and fiber integrated sensors (Figure 6.1a-c). The stand-alone alcohol sensor was prepared to be constrained on a glass slide. The sensor was investigated in alcohol concentration range of 0-50 vol% after being equilibrated in DI water. The sensor was submerged in DI water (1 ml) and illuminated with a green laser of wavelength 532 nm. The profile of the optical transmitted power (P_t) was recorded by an optical power meter and was taken as the reference. The DI water was replaced with an aqueous ethanol solution (2 vol%, 1 ml), and the P_t was recorded again. The ethanol solution (2 vol%) was replaced by a higher ethanol concentration (4 vol%), and the reading was recorded; this protocol was repeated until reaching 50 vol% (Figure 6.2). The same procedure was followed to examine the sensor's sensitivity for propan-2-ol and DMSO.

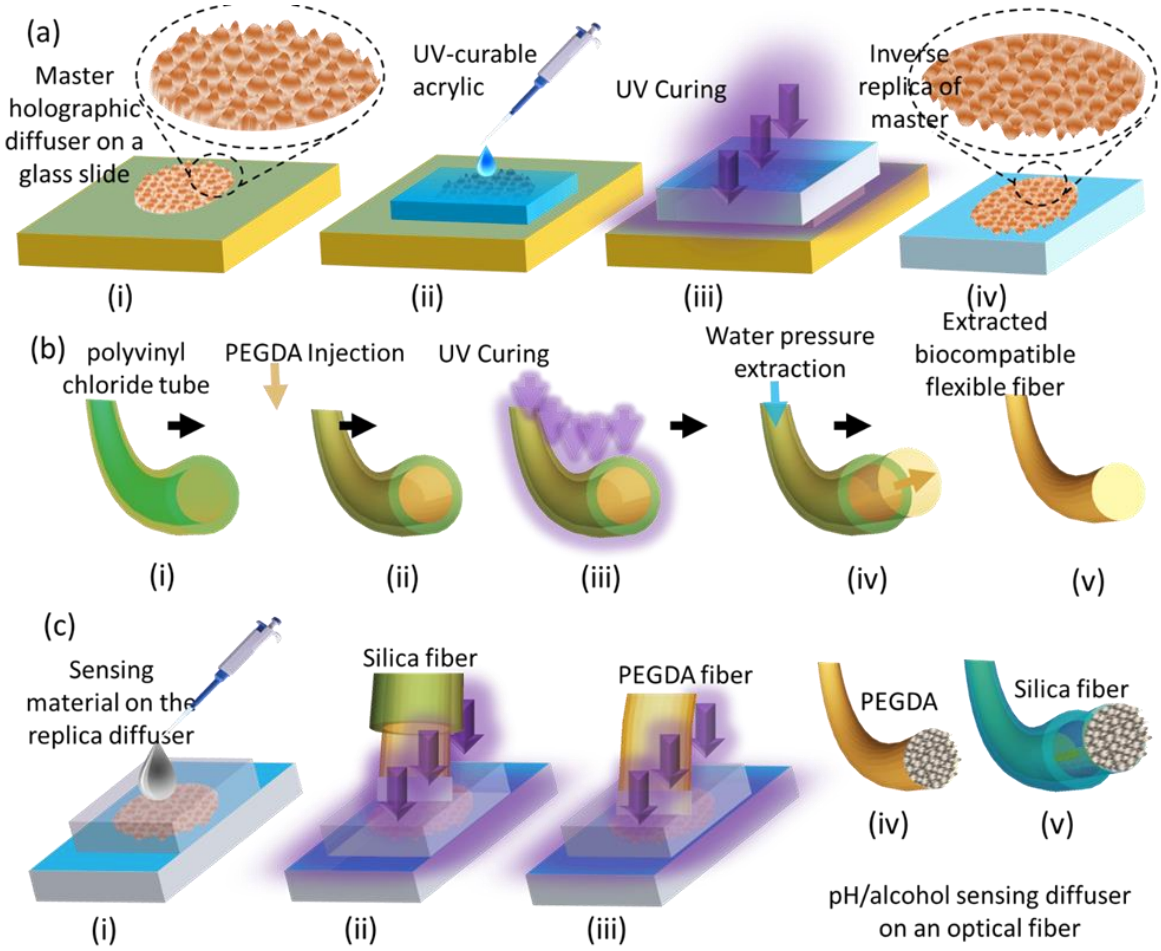

Figure 6.1. Fabrication of the hydrogel-based LDMs sensor, the hydrogel fiber, and attachment of hydrogel sensor to the optical fiber's tip. (a) Schematic for the fabrication of the hydrogel sensor constrained on a glass substrate and imprinted with the LDMs. The monomer solution was pipetted on the master of the LDMs and was covered with a silanized glass slide, and the monomer solution was exposed to UV-light for curing. (b) Schematic of the biocompatible optical fiber fabrication. The monomer solution was injected into a tube mold and polymerized by UV-light, and the polymerized fiber was extracted by applying water pressure. (c) Schematic shows the functionalization process of the optical fiber's tip. A droplet of 20 µl of the monomer solution was drop casted on the microlens array and the silanized optical fiber tip was contacted with the droplet and cured for 60 min.

The optical transmitted power of the diffused spot passed through the sensor exhibited Gaussian profile. The maximum optical transmitted powers (P_{tmax}) increased with increasing alcohol concentration (Figure 6.2a-c). This trend was due to decreasing scattering angles resulting from decreasing the diffusion efficiency of the LDMs that led to concentrate the

transmitted power on a smaller solid angle, and hence a smaller circular area on projection screen/photodiode sensor. The P_{tmax} readings as a practical readout method were utilized to monitor the alcohol concentrations. The sensor responded to all the presented alcohols; however, it was more sensitive to DMSO as compared to propan-2-ol and ethanol, this may be due to DMSO was more able to penetrate the hydrogel network (Figure 6.2d). The ability of alcohol to penetrate into the hydrogel matrix increases as the alkyl chain length increases [32]. The sensor's response against ethanol was nonlinear presented an increase of the optical signal of ~ 4 µW vol%$^{-1}$ for low ethanol concentration range of 0-10 vol%, which increased to ~ 6 µW vol%$^{-1}$ for higher concentration range of 10 to 40 vol%, and reached ~ 9.2 µW vol%$^{-1}$ for the 40-50 vol% range (Figure 6.2d). On the contrary, the sensor's response to propan-2-ol was linear, presenting a sensitivity of ~ 7.3 µW vol^{-1} across the entire concentration range of 0-50 vol%. The sensor's response to DMSO was nonlinear for the entire tested concentration range (0-50 vol%). The sensitivity increased from ~ 8 µW vol%$^{-1}$ for the 0-10 vol% range to ~ 12 µW vol%$^{-1}$ within the concentration range 10-40 vol%, and to ~ 13 µW vol%$^{-1}$ in the high concentration range 40-50 vol% (Figure 6.2d). The sensor's response for ethanol and propan-2-ol was consistent with previous studies [32]. The sensitivity of the hydrogel to alcohols could be controlled by varying the content of the cross linker; hence, the elasticity of the hydrogel film could be tuned [32]. Unlike the diffraction and chromophore-based systems, the developed sensor was able to cover the entire alcohol concentration range 0-50 vol%.

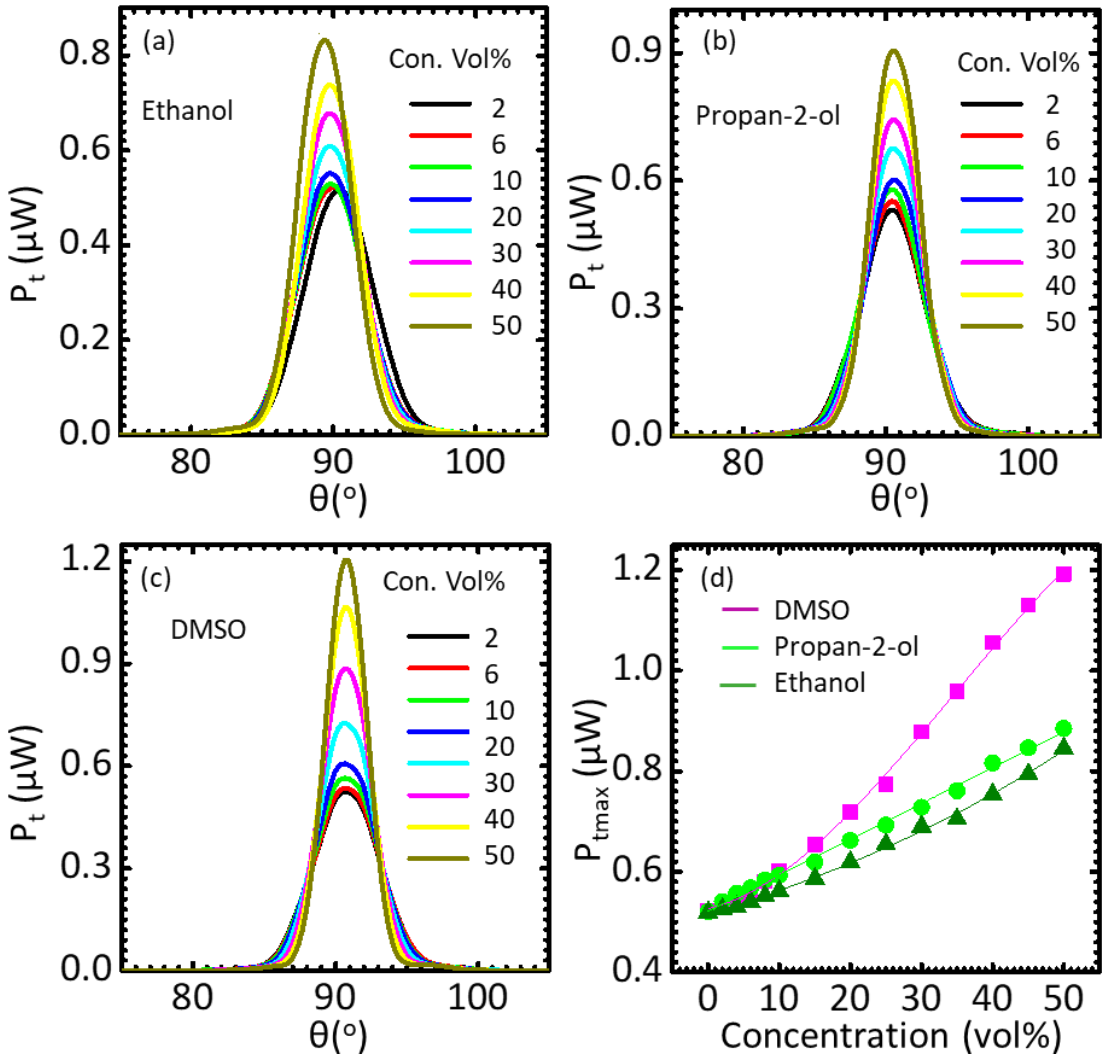

Figure 6.2. Interrogation of the alcohol sensor attached chemically to a glass slide. (a,b, & c) The spatial optical profile of the transmitted diffused light beam through the alcohol sensor while the sensor was tested in ethanol, propan-2-ol, and DMSO, respectively. (d) The maximum transmitted power (P_{tmax}) of the laser beam passing through the alcohol sensor submerged in various alcohol concentrations.

For the remote sensing applications, the alcohol hydrogel sensor was chemically attached to the tip of a multimode silica fibers of a diameter of 500 µm. The fabrication of the fiber optic probe including preparing the alcohol-responsive polymer, replicating of the LDMs, and attaching of the sensor to the tip of the optical fiber were achieved through a simple and single step process. Unlike the fiber probes based on surface Plasmon resonance (SPR) or

the interferometric spectroscopy, the fabrication process was facile and rapid. Many complex steps were avoided; these include pretreatment of the optical fiber, depositing the adhesive layer and the metal thin layer (plasmonic coating), immobilizing the hydrogel on the metal layer, and stringent requirements such as high-quality films [3, 46].

The fiber optic probe was tested for alcohol detection in transmission and reflection configurations. Optical microscope images of the silica fiber and photos of the fiber probe guiding different laser beams are displayed in chapter 5. A green laser (532 nm) was coupled with the functionalized silica fiber and the output signals (P_{tmax}) were recorded by either an optical power meter or a smartphone. Upon increasing the alcohol concentration, the probe exhibited a linear response against propan-2-ol, and showed nonlinear behaviors against ethanol and DMSO. All results matched with the previous experiments carried out while the sensor was constrained on a glass substrate. The fiber probe showed the highest sensitivity to DMSO as compared to propan-2-ol and ethanol. Starting from the identical P_{tmax} values of 390 µW at 0 vol%, the P_{tmax} recorded by the optical power meter showed an increase of ~ 246, 273, and 500 µW at 50 vol% against increasing the concentration of ethanol, propan-2-ol, and DMSO, respectively (Figure 6.3a). The average sensitivity of the fiber probe through the alcohol concentration range of 0-50 vol% was calculated to be 1.2% vol^{-1}, 1.4% vol^{-1}, and 2.5% vol^{-1} for ethanol, propan-2-ol, and DMSO, respectively. Similarly, the maximum transmitted luminance (L_t) recorded by the smartphone showed an increase of ~ 181, 202, and 370 Lux at 50 vol% concentrations of ethanol, propan-2-ol, and DMSO, respectively (Figure 6.3b). Output signal trends recorded by the smartphone and the optical power meter were analogous, confirming the reliability of the smartphone-based readout

method. One of the main advantages of the proposed technique is that it facilitates the direct readout process as no complex data processing is required, and no bulky instruments like computers were necessary, making the probe compact and simple. Additionally, the proposed fiber probe cuts down the cost of the sensor by introducing cost-effective and portable instruments for recording the output signals. Another advantage of the proposed probe is its low limit of detection (LOD) (2%, v/v) compared to many other types of fiber optic probes those depend on; interferometry, surface Plasmon resonance, Fresnel reflectometry, and total internal reflection phenomena [47-51]. For instance, tapered fiber probe showed LOD of 5% (v/v) [48]. Also, LOD of ethanol was recorded to be 10% (w/w) for Fabry-Perot fiber probe [47]. Fiber probe based on surface Plasmon resonance presented LOD of 10% (v/v) [49]. In addition, fiber probe based on Fresnel reflectometry principal showed LOD of 30% (v/v) for ethanol [51]. An alcohol fiber probe based on the change in the total internal reflection presented LOD of 10% (v/v) [50]. Even, colorimetric-responsive hydrogel based on inverse opal structure, which made of the same alcohol- responsive hydrogel (HEMA), showed LOD of 5 % (v/v) for ethanol detection[43].

The reusability of the fiber probe was examined by exposing the fiber probe to ethanol solution (5%, v/v) for six cycles (Figure 6.3c). The fiber probe was modulated over several cycles with limited random memory retention. The response time was in few seconds and the equilibrium time was near 60 s; however, it varied depending on the alcohol type and alcohol concentration. These results were consistent with the previous studies [32, 52].

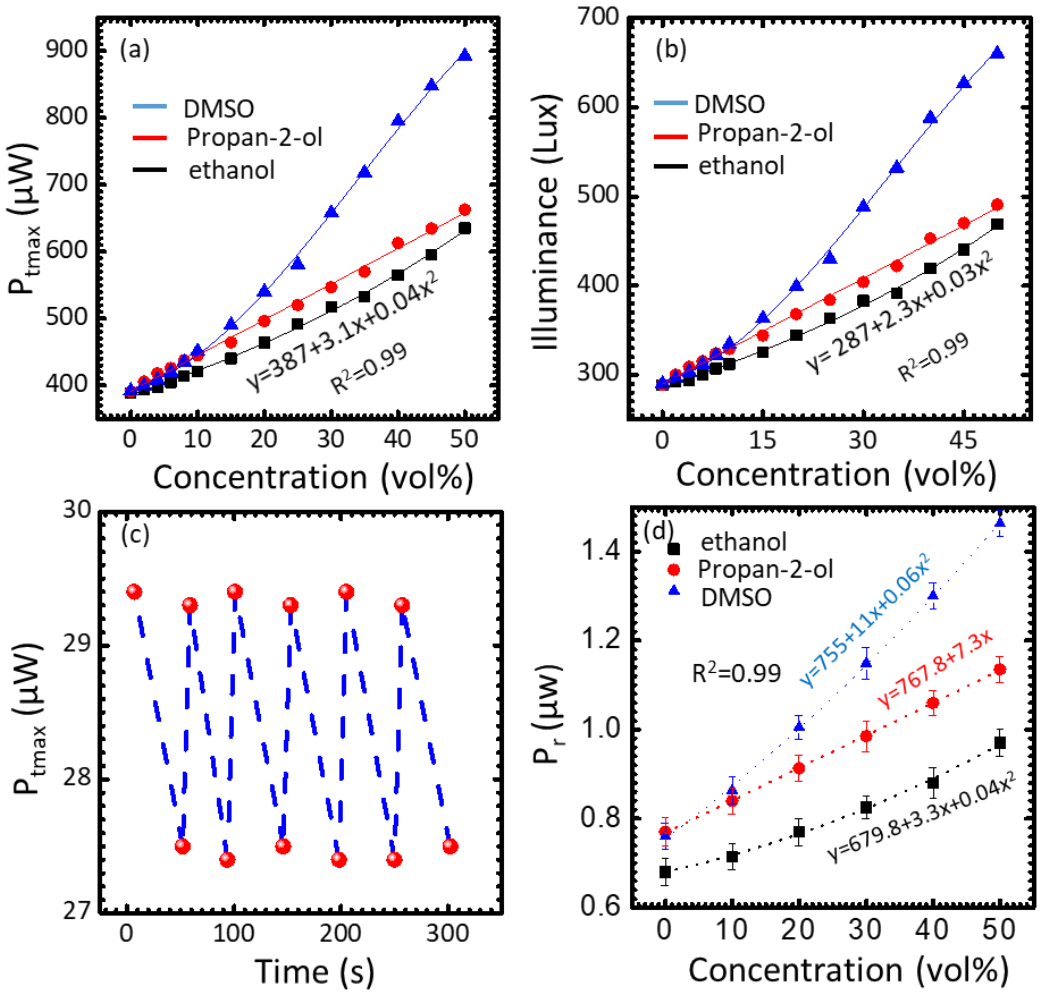

Figure 6.3. Testing the fiber probe in the transmission and reflection configurations. (a) The maxima optical transmitted power (Ptmax) from the functionalized fiber probe versus alcohol concentrations while the probe was illuminated with a green laser (532 nm) and the output signals recorded with an optical power meter. (b) The illuminance of the fiber probe detected by a smartphone while the probe was submerged in various alcohol concentrations- the probe was illuminated by a white light source. (c) The maximum transmitted power (Ptmax) of the fiber probe tested in ethanol (5% v/v) and DI water for 6 cycles versus time. (d) The reflected power through the fiber probe versus alcohol concentrations. The scale bars show standard error (n=3).

The reflection configuration is the ideal mode for implantable and remote sensing, and it was employed in this work to test the probe sensing performance. A broadband white light source was coupled with one of the terminals at the bifurcated of a 2×1 coupler and the reflected

power was collected from the second terminal at the same side using an optical power meter. The functionalized tip of the probe was submerged in various alcohol concentrations. With increasing alcohol concentration, the hydrogel functionalized tip underwent a positive dimensional shift which increased the reflected power guided in the probe. At 50 vol% of ethanol, propan-2-ol, and DMSO concentrations, maximum increases of ~ 290, 365, and 703 nW were recorded, respectively (Figure 6.3d). The recorded sensitivity was 0.8% vol^{-1}, 0.94% vol^{-1}, and 1.85% vol^{-1} for ethanol, propnan-2-ol, and DMSO, respectively. Notably, the trend of the output signals in reflection configuration was comparable with the trend in transmission configuration as the response of the fiber probe was linear for propan-2-ol and nonlinear for ethanol and DMSO, in addition to the highest sensitivity was for DMSO and the least was for ethanol.

Continuous monitoring pH of blood and brain tissue in critically ill patients and in traumatic brain injury is a primary medical exigency [53-57]. The pH of the brain tissues indicates the tissue viability and it decreases during brain insult from the normal pH 7.4 to 6.8 [58]. Additionally, continuous monitoring of the brain tissue pH might be useful in the treatment of comatose neurosurgical patients [58, 59]. For these purposes, electrochemical sensors have been developed [60-63]. Hydrogel-based fiber optic probes may present unique advantages over electrochemical sensors as they are biocompatible for in *vivo* sensing and safe as no electrical currents are passed [64]. The hydrogel pH sensor imprinted with the LDMs and constrained on a glass slide was tested in the transmission mode in various pH solutions (4.3-8.8) of ionic strength 150 mM at 24 °C. The sensor was submerged in pH solution (1 ml) and illuminated with a laser beam (532 nm) and P_t was recorded by an optical

power meter. The sensor's volume positively shifted upon increasing the pH of the tested solution due to the Donnan's potential resulting from ionization of the carboxyl group and dissolving of the carboxylates [43]. Consequently, the sensor's diffusion efficiency decreased- increasing P_{tmax} on account of the scattering angles (Figure 6.4a). Initially, the pH sensor significantly responded to pH in the range of 5.0 to 7.0 and hardly any response was detected in the alkaline region. The output signal increased by ~ 1.7 µW, as it increased from 4.2 µW to 5.9 µW when pH increased from 5.0 to 7.0 (Figure 6.4b). When the pH was changed from 4.3 to 5.0, the sensor's output signal changed by ~ 8%, from 3.84 to 4.15 µW, consistent with the previous study for the pH sensor based on polyHEMA [43]. The hydrogel pH sensor showed a similar response in reflection mode as compared to the transmission mode, where the output signal significantly increased by 250 nW with increasing pH from 5.0 to 7.0, and no response was recorded above pH 7.0 (Figure 6.4c). The output signal increase by 20 nW when pH was increased from 4.3 to 5.0. The decrease of the sensor's sensitivity in the reflection mode may be attributed to the readout setup, where the sensor was illuminated at 45° and the detector was fixed at the same angle. The hydrogel sensor was chemically attached to the tip of a silica optical fiber following the same protocol utilized to attach the alcohol sensor. The sensing investigations were carried out in both transmission and reflection modes (Figure 6.5). The response of the fiber probe to pH was comparable with the response of the constrained pH hydrogel sensor attached to the glass substrate (Figure 6.5a). The trends of the output signals recorded by the smartphone and the power meter were similar (Figure 6.5a-b). The fiber probe was highly sensitive in the pH range from 5.0 to 7.0 and displayed negligible response above pH 7.0. The recorded L_t by the smartphone showed a significant change in the same range, recording a sensitivity of 20% pH^{-1}. The

response of the pH fiber probe in the reflection configuration was analogous to the transmission mode (Figure 6.5c). An increase of 115 nW was measured in the output signal during increasing the pH from 5.0 to 7.0, with a sensitivity of ~57 nW pH^{-1} or 11% pH^{-1}. Based on the pH-response of the proposed probe, it can be employed for monitoring gastric pH which has a physiological range of 1-7, and for milk quality application as the milk pH lies in the range of 4.6-6.7 [65, 66]. However, the sensitivity of the probe and the sensing range can be tailored by varying the ionizable co-monomer and its concentration. For example, to increase the sensitivity in the alkaline pH, the hydrogel network can be co-polymerized with 2- (dimethylamino) ethyl methacrylate (pK_a=8.4) [67].

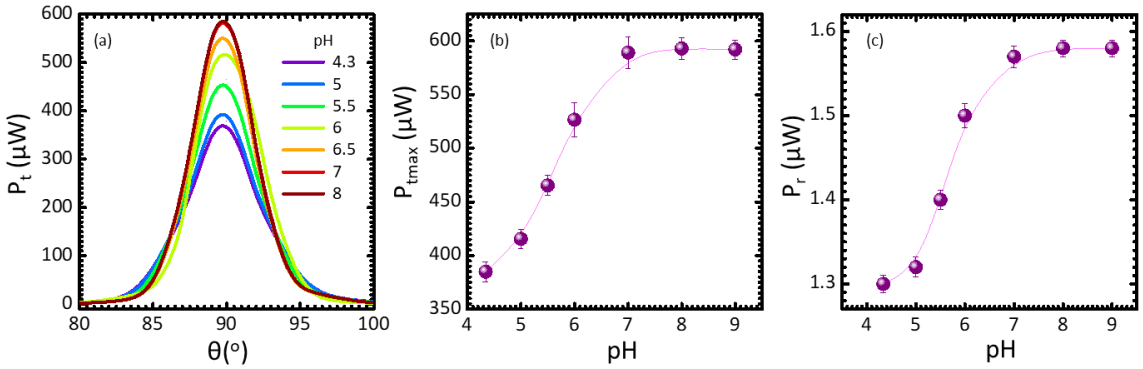

Figure 6.4. Interrogation of the pH-hydrogel sensor attached chemically on a glass slide. (a) The spatial optical profiles of the transmitted diffused light passing through the sensor while the sensor was submerged in various pH solutions and was illuminated by a green laser beam, 532 nm at 24 °C. (b) The maxima transmitted power for the beam passing through the pH-sensor submerged in various pH solutions. (c) The maximum optical reflected power from the pH-sensor exposed to various pH solutions and was illuminated by a green laser beam. The scale bars show standard error (n=3).

A key challenge of the pH-sensitive fiber probes for the real-time measurements in biological applications is the swelling and shrinkage kinetics. The response time of the fiber probe depends on the concentration of the ionizable monomer (AA) and the ionic strength of the examined solution. The response time is directly proportional to the ionizable monomer and

inversely proportional to the buffer concentration [68]. The developed fiber probe showed a rapid response as it reached the equilibrium within 60±10 s when the pH was changed from 5.5 to 6.0 and the output signal varied up to ~17.6 µW (Figure 6.5d). Additionally, the fiber probe was examined for reusability by exposing it to consecutive swelling/shrinkage for three cycles and no hysteresis was observed (Figure 6.5e). This behavior was consistent with the previous studies of polyHEMA-*co*-AA where the hydrogel sensor did not present a significant hysteresis in a high ionic strength solution [68].

For the implantable biosensing applications, the silica fiber probe was replaced with a biocompatible fiber as the silica fiber causes inflammation in the implantation site and increases the risk of infection. The biocompatible fiber was made of polyethylene glycol diacrylate, functionalized with the pH-responsive hydrogel, and was examined for pH sensing in physiological conditions (Figure 6.5f). The trend of the output signals against pH was comparable with the response of the silica fiber probe. The response of the biocompatible fiber probe was considerable in the pH range of 5.0 to 7.0, and reached a plateau above pH 7.0. The sensitivity of the probe was ~7 nW pH^{-1} or 7.5 % pH^{-1} in the pH range of 5.0 to 7.0 which is lower as compared to the silica fiber probe due to inefficient light guiding of the biocompatible core bare fiber. This can be overcome by decreasing the guided light loss which can be achieved by covering the fiber core with a biocompatible clad having a low refractive index [69].

In contrast to optic fiber probes based on the interferometric techniques, the developed probes do not require high quality films, coherent light sources, and complex and bulky readout setups [3, 23]. As compared to the SPR probes that require multistage and

complicated fabrication process, output signal processing and costly instrumentations for the readout setup, the proposed probe is easy to fabricate (single stage process), low-cost, and portable [27]. Unlike the fluorescent probes, the measurement of the optical power is not prone to photobleaching [3, 69]. The developed fiber optic probes can be functionalized with stimuli-responsive hydrogels to sense proteins, nucleic acids, and to be utilized in drug delivery applications [69].

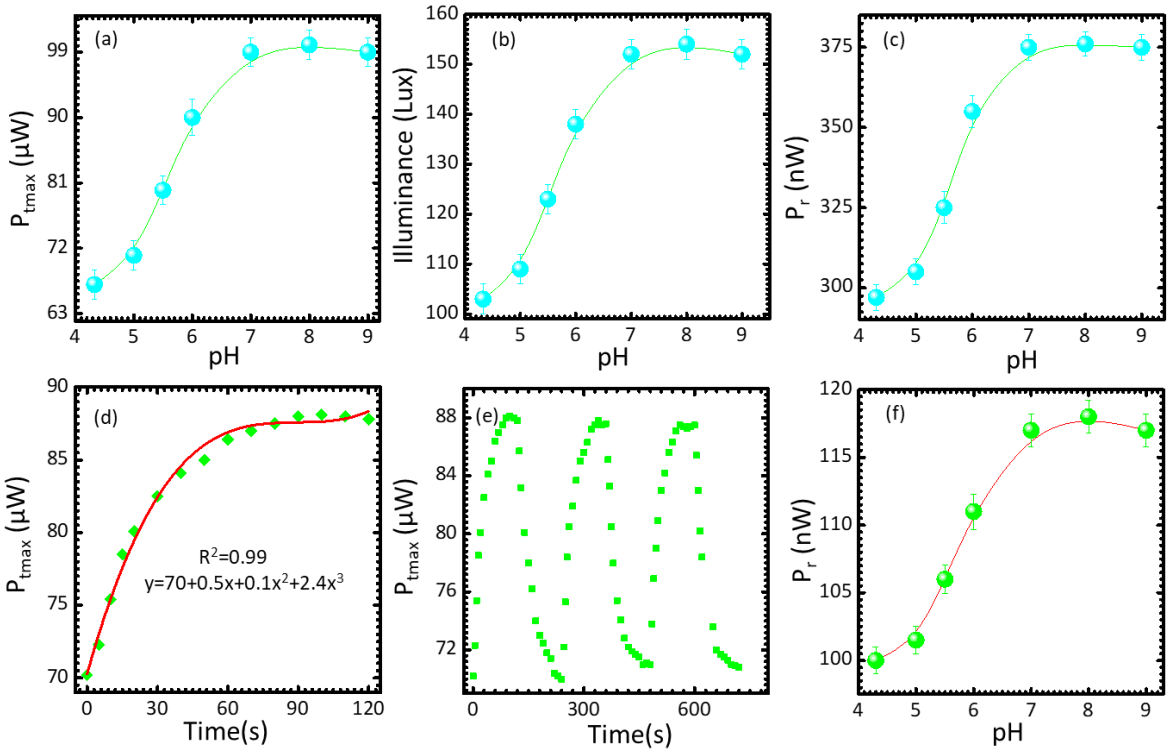

Figure 6.5. Interrogation of the pH-fiber probe in the transmission and reflection configurations. (a) The maximum transmitted power of the fiber probe recorded when it was submerged in various pH solutions. (b) The maximum illuminance emitted from the fiber probe recorded by a smartphone against the pH solutions. (c) The reflected power in the probe recorded by the power meter when the probe was soaked in various pH solutions. (d) Kinetic swelling of the pH-fiber probe when it was soaked in pH 6.0 solution and P_{tmax} was recorded. (e) The maximum transmitted power of the fiber tested in two different pH solutions for 3 cycles versus time. (f) The reflected power in the biocompatible fiber probe versus pH of aqueous solutions. The scale bars show standard error (n=3).

6.4 Materials and methods

6.4.1 Materials

Ethylene glycol dimethacrylate (EGDMA) (98%), 2-hydroxyethyl methacrylate (HEMA) (97%), 2,2-dimethoxy-2-phenylacetophenone (DMPA) (99%), polyethylene glycol diacrylate (PEGDA) (mw: 700 Da), 2-hdroxy-2-methylpropiophenone (2-HMP) (97%), dimethyl sulfoxide (DMSO) (99.9%), ethanol, propan-2-ol, sodium phosphate monobasic (NaH_2PO_4), sodium phosphate dibasic (NaH_2PO_4), and acrylic acid (AA) were purchased from Sigma Aldrich and used without further purification.

6.4.2 Hydrogel alcohol sensor fabrication

The precursor consisted of HEMA (92.5 mol %) and EGDMA (7.5 mol %) was mixed with DMPA (2% wt/vol) in propan-2-ol. The monomer solution (20 µl) was drop cast on the light diffusing microstructures (LDMs) and covered with a silanized glass piece, and cured by a UV lamp (365 nm) for 1 h. The polymerized sensor was washed with DI water/ethanol (1:1, v/v) and preserved at 24 °C.

6.4.3 Hydrogel pH sensor fabrication

The precursor consisted of HEMA (91.5 mol%), EGDMA (2.5 mol%), and acrylic acid (6 mol%), was mixed with DMPA in propan-2-ol (2%, wt/vol). The monomer solution (20 µl) was pipetted on the LDMs and covered with a salinized glass piece, and cured by the UV lamp (365 nm) for 1 h. The polymerized sensor was washed with DI water/ethanol (1:1, v/v) and preserved at 24 °C.

6.4.4 Hydrogel optical fiber fabrication

PEGDA monomer was mixed with 2-hydroxy-2-methylpropiophenone (2-HMP) (5 vol %) in DI water. The dilution of PEGDA in DI water was varied from 5 to 90 vol%. The prepared solution (200 µl) was injected into a polyvinyl chloride tube having an inner diameter of 1 mm and the tube was exposed to UV light (365 nm) for 30 min. The optical fiber was extracted from the tube by applying water pressure using a syringe. The optical fiber was washed with a mixture of ethanol and DI water (1:1, v/v). The tip of the fiber was functionalized with the pH-sensitive hydrogel by dipping the tip in a pH-sensitive solution (10 µl) that was pipetted on the LDMs and was exposed to UV light for 1 h. To create a probe, the tip of the fiber was silanized and dipped in either alcohol or pH-sensitive solutions during the curing process. The functionalized tip was washed in DI water/ethanol (1:1, v/v) and preserved at 24 °C.

6.4.5 Testing the hydrogel sensor constrained on the glass slide

The stimuli-responsive hydrogel imprinted with the LDMs and attached chemically on the glass slide was submerged in 1 ml of the tested solution in a plastic cuvette fixed on a rotating stage. White a light source or a laser pointer was fixed on the same rotating stage to illuminate the sensor. P_t, and P_{tmax} were recorded by a photodiode that was fixed and immobile on the optical bench. Also, the smartphone was fixed to pick up the maximum transmitted luminance (L_t) exploiting the ambient light sensor of smartphone for sensing measurements.

6.4.6 Testing the fiber probe in the transmission mode

The fiber probe was coupled with a white light source/laser pointer at one end and the other end that is functionalized was soaked in the tested solution container. Below the tested solution container, the photodiode detector/smartphone was fixed to collect the P_t/L_t.

6.4.7 Testing the fiber probe in the reflection mode

The fiber probe was coupled with the seven fibers terminal of 2×1 coupler. The light source was connected to the coupler terminal to deliver the light in one of the seven fibers and the photodiode was connected to the coupler terminal of six fibers. Therefore, one fiber was illuminating the sensing probe and the six fiber were collecting the reflected light in the probe to be guided into the photodetector.

6.5 Conclusions

Fiber optic probes were developed for remote sensing and implantable biosensing applications. Alcohol -and pH-responsive hydrogels were imprinted with light diffusing microstructures during the UV-curing process and were attached to the tips of the optical fibers. Firstly, the alcohol and pH hydrogel sensors constrained on glass slides were interrogated in the transmission and reflection configurations. An optical power meter and a smartphone were employed for recording the output signals. Both showed an analogous trend confirming the reliability of using the smartphones to simplify the readout approach. Secondly, the fiber optic probes based on alcohol and pH-responsive hydrogels showed similar responses to their hydrogel sensor counterparts constrained on glass slides whether they were examined in the transmission or the reflection modes. In addition, the

biocompatible fiber probe showed an analogous response to the silica fiber probe; however, the biocompatible fiber showed lower sensitivity, presumably due to light loss. The developed sensing technique shortcuts stages of the typical fabrication process of the fiber optic probes based on hydrogels and offers economical cost and portable readout strategy reducing the fiber probes cost. The developed sensors may have application in biological sensing, point-of-care diagnostics, as well as critical care devices for real-time measurements.

References

1. J. R. Epstein and D. R. Walt, "*Fluorescence-based fibre optic arrays: a universal platform for sensing*," Chemical Society Reviews, 2003. **32** (4): p. 203-214.
2. S. Jayawardhana, G. Kostovski, A. P. Mazzolini, and P. R. Stoddart, "*Optical fiber sensor based on oblique angle deposition*," Applied optics, 2011. **50** (2): p. 155-162.
3. J. Goicoechea, C. Zamarreño, I. Matias, and F. Arregui, "*Utilization of white light interferometry in pH sensing applications by mean of the fabrication of nanostructured cavities*," Sensors and Actuators B: Chemical, 2009. **138** (2): p. 613-618.
4. E. Sinchenko, W. K. Gibbs, C. E. Davis, and P. R. Stoddart, "*Characterization of time-resolved fluorescence response measurements for distributed optical-fiber sensing*," Applied optics, 2010. **49** (33): p. 6385-6390.
5. M. Mann, S. Mark, Y. Raichlin, A. Katzir, and S. Mordechai, "*Optimization of fiber-optic evanescent wave spectroscopy: a Monte Carlo approach*," Applied spectroscopy, 2009. **63** (9): p. 1057-1061.
6. M. Janotta, A. Katzir, and B. Mizaikoff, "*Sol-gel-coated mid-infrared fiber-optic sensors*," Applied spectroscopy, 2003. **57** (7): p. 823-828.
7. J. Wang and L. Wang, "*An optical fiber sensor for remote pH sensing and imaging*," Applied spectroscopy, 2012. **66** (3): p. 300-303.
8. N. Cennamo, G. D'Agostino, M. Pesavento, and L. Zeni, "*High selectivity and sensitivity sensor based on MIP and SPR in tapered plastic optical fibers for the detection of L-nicotine*," Sensors and Actuators B: Chemical, 2014. **191**: p. 529-536.
9. S. Tierney, B. M. H. Falch, D. R. Hjelme, and B. T. Stokke, "*Determination of glucose levels using a functionalized hydrogel– optical fiber biosensor: Toward continuous monitoring of blood glucose in vivo*," Analytical chemistry, 2009. **81** (9): p. 3630-3636.
10. J. Cong, X. Zhang, K. Chen, and J. Xu, "*Fiber optic Bragg grating sensor based on hydrogels for measuring salinity*," Sensors and Actuators B: Chemical, 2002. **87** (3): p. 487-490.
11. K. Lee and S. A. Asher, "*Photonic crystal chemical sensors: pH and ionic strength*," Journal of the American Chemical Society, 2000. **122** (39): p. 9534-9537.

12. A. Richter, D. Kuckling, S. Howitz, T. Gehring, and K.-F. Arndt, "*Electronically controllable microvalves based on smart hydrogels: magnitudes and potential applications*," Journal of microelectromechanical systems, 2003. **12** (5): p. 748-753.
13. J. C. Rueda, E. Campos, H. Komber, S. Zschoche, L. Häussler, and B. Voit, "*Synthesis and characterization of new pH-and thermo-responsive hydrogels based on N-isopropylacrylamide and 2-oxazolines*," Designed Monomers and Polymers, 2014. **17** (3): p. 208-216.
14. P. Preejith, C. Lim, A. Kishen, M. John, and A. Asundi, "*Total protein measurement using a fiber-optic evanescent wave-based biosensor*," Biotechnology letters, 2003. **25** (2): p. 105-110.
15. W. J. Yoo *et al.*, "*Measurements of spectral responses for developing fiber-optic pH sensor*," Optical review, 2011. **18** (1): p. 139-143.
16. M. Elsherif, M. U. Hassan, A. K. Yetisen, and H. Butt, "*Glucose Sensing with Phenylboronic Acid Functionalized Hydrogel-Based Optical Diffusers*," ACS nano, 2018. **12**: p. 2283-2291.
17. M. Elsherif, M. U. Hassan, A. K. Yetisen, and H. Butt, "*Wearable Contact Lens Biosensors for Continuous Glucose Monitoring using Smartphones*," ACS nano, 2018. **12**: p. 5452–5462.
18. F. K. Sartain, X. Yang, and C. R. Lowe, "*Complexation of L-Lactate with Boronic Acids: A Solution and Holographic Analysis*," Chemistry–A European Journal, 2008. **14** (13): p. 4060-4067.
19. A. Baeissa, N. Dave, B. D. Smith, and J. Liu, "*DNA-functionalized monolithic hydrogels and gold nanoparticles for colorimetric DNA detection*," ACS applied materials & interfaces, 2010. **2** (12): p. 3594-3600.
20. S. G. Ignatov, J. A. Ferguson, and D. R. Walt, "*A fiber-optic lactate sensor based on bacterial cytoplasmic membranes*," Biosensors and Bioelectronics, 2001. **16** (1-2): p. 109-113.
21. J. C. Carter *et al.*, "*Fabricating optical fiber imaging sensors using inkjet printing technology: A pH sensor proof-of-concept*," Biosensors and Bioelectronics, 2006. **21** (7): p. 1359-1364.
22. O. S. Wolfbeis, "*Fiber-optic chemical sensors and biosensors*," Analytical chemistry, 2008. **80** (12): p. 4269-4283.
23. J. Goicoechea, C. R. Zamarreño, I. Matias, and F. Arregui, "*Optical fiber pH sensors based on layer-by-layer electrostatic self-assembled Neutral Red*," Sensors and Actuators B: Chemical, 2008. **132** (1): p. 305-311.
24. D. A. Nivens, M. V. Schiza, and S. M. Angel, "*Multilayer sol–gel membranes for optical sensing applications: single layer pH and dual layer CO2 and NH3 sensors*," Talanta, 2002. **58** (3): p. 543-550.
25. B. Gupta and D. Sharma, "*Evanescent wave absorption based fiber optic pH sensor prepared by dye doped sol-gel immobilization technique*," Opt.Commun., 1997. **140**: p. 32-35.
26. N. Jiang *et al.*, "*Functionalized Flexible Soft Polymer Optical Fibers for Laser Photomedicine*," Advanced Optical Materials, 2018. **6** (3): p. 1701118.
27. B. D. Gupta and R. Kant, "*Recent advances in surface plasmon resonance based fiber optic chemical and biosensors utilizing bulk and nanostructures*," Optics & Laser Technology, 2018. **101**: p. 144-161.
28. S. K. Mishra and B. D. Gupta, "*Surface plasmon resonance based fiber optic pH sensor utilizing Ag/ITO/Al/hydrogel layers*," Analyst, 2013. **138** (9): p. 2640-2646.
29. H. Yuan *et al.*, "*Fiber-optic surface plasmon resonance glucose sensor enhanced with phenylboronic acid modified Au nanoparticles*," Biosensors and Bioelectronics, 2018. **117**: p. 637-643.

30. S. K. Mishra and B. D. Gupta, "*Surface plasmon resonance based fiber optic sensor for the detection of CrO 4 2− using Ag/ITO/hydrogel layers*," Analytical Methods, 2014. **6** (14): p. 5191-5197.
31. O. B. Miled, H. B. Ouada, and J. Livage, "*pH sensor based on a detection sol–gel layer onto optical fiber*," Materials Science and Engineering: C, 2002. **21** (1-2): p. 183-188.
32. A. G. Mayes, J. Blyth, M. Kyröläinen-Reay, R. B. Millington, and C. R. Lowe, "*A holographic alcohol sensor*," Analytical chemistry, 1999. **71** (16): p. 3390-3396.
33. M. Penza *et al.*, "*Alcohol detection using carbon nanotubes acoustic and optical sensors*," Applied Physics Letters, 2004. **85** (12): p. 2379-2381.
34. M. Morisawa and S. Muto, "*Plastic optical fiber sensing of alcohol concentration in liquors*," Journal of Sensors, 2012. **2012**: p. 11055-11060.
35. G. J. Lubrano, M. H. Faridnia, G. Palleschi, and G. G. Guilbault, "*Amperometric alcohol electrode with extended linearity and reduced interferences*," Analytical biochemistry, 1991. **198** (1): p. 97-103.
36. J.-K. Park, H.-J. Yee, and S.-T. Kim, "*Amperometric biosensor for determination of ethanol vapor*," Biosensors and Bioelectronics, 1995. **10** (6-7): p. 587-594.
37. B. Yon Hin and C. R. Lowe, "*Catalytic oxidation of reduced nicotinamide adenine dinucleotide at hexacyanoferrate-modified nickel electrodes*," Analytical chemistry, 1987. **59** (17): p. 2111-2115.
38. B. Leca and J.-L. Marty, "*Reusable ethanol sensor based on a NAD+-dependent dehydrogenase without coenzyme addition*," Analytica chimica acta, 1997. **340** (1-3): p. 143-148.
39. M. L. Castañón, A. M. Ordieres, and P. T. Blanco, "*Amperometric detection of ethanol with poly-(o-phenylenediamine)-modified enzyme electrodes*," Biosensors and Bioelectronics, 1997. **12** (6): p. 511-520.
40. G. Tian, X.-Q. Zhang, M.-S. Zhu, Z. Zhang, Z.-H. Shi, and M. Ding, "*Quantification of ethanol in plasma by electrochemical detection with an unmodified screen printed carbon electrode*," Scientific reports, 2016. **6**: p. 23569.
41. L. Wu, X. Zhang, and H. Ju, "*Detection of NADH and ethanol based on catalytic activity of soluble carbon nanofiber with low overpotential*," Analytical chemistry, 2007. **79** (2): p. 453-458.
42. Y. Nishiyama and M. Satoh, "*Swelling behavior of poly (acrylic acid) gels in aqueous ethanol–effects of counterion species and ionic strength*," Macromolecular rapid communications, 2000. **21** (4): p. 174-177.
43. X. Xu, A. V. Goponenko, and S. A. Asher, "*Polymerized polyHEMA photonic crystals: pH and ethanol sensor materials*," Journal of the American Chemical Society, 2008. **130** (10): p. 3113-3119.
44. K. Mukae *et al.*, "*Swelling of poly (N-isopropylacrylamide) gels in water-alcohol (C1-C4) mixed solvents*," The Journal of Physical Chemistry, 1993. **97** (3): p. 737-741.
45. J. Erfkamp, M. Guenther, and G. Gerlach, "*Hydrogel-Based Sensors for Ethanol Detection in Alcoholic Beverages*," sensors, 2019. **19** (5): p. 1199.
46. D. Li *et al.*, "*Affinity based glucose measurement using fiber optic surface plasmon resonance sensor with surface modification by borate polymer*," Sensors and Actuators B: Chemical, 2015. **213**: p. 295-304.

47. C. Moreno-Hernández, O. R. Quiroz, D. Monzón-Hernández, and J. Villatoro, "*Contactless optical fiber interferometric sensor to monitor water content in ethanol*," IEEE sensors journal, 2018. **18** (8): p. 3211-3217.
48. S. H. Girei, A. A. Shabaneh, H. Ngee-Lim, M. N. Hamidon, M. A. Mahdi, and M. H. Yaacob, "*Tapered optical fiber coated with graphene based nanomaterials for measurement of ethanol concentrations in water*," Optical review, 2015. **22** (3): p. 385-392.
49. M. Mitsushio and M. Higo, "*A gold-deposited surface plasmon resonance-based optical fiber sensor system using various light-emitting diodes*," Analytical Sciences, 2011. **27** (3): p. 247-247.
50. M. Morisawa and S. Muto, "*Plastic optical fiber sensing of alcohol concentration in liquors*," Journal of Sensors, 2012. **2012**.
51. E. Fujiwara, R. Takeishi, A. Hase, E. Ono, J. Santos, and C. Suzuki, "*Real-time optical fibre sensor for hydro-alcoholic solutions*," Measurement Science and Technology, 2010. **21** (9): p. 094035.
52. A. Yetisen, M. Qasim, S. Nosheen, T. Wilkinson, and C. Lowe, "*Pulsed laser writing of holographic nanosensors*," Journal of Materials Chemistry C, 2014. **2** (18): p. 3569-3576.
53. K. S. Bronk, K. L. Michael, P. Pantano, and D. R. Walt, "*Combined imaging and chemical sensing using a single optical imaging fiber*," Analytical chemistry, 1995. **67** (17): p. 2750-2757.
54. P. Muller, R. A. Peura, Y. Mendelson, S. Kun, and R. M. Dunn, "*In-vitro and in-vivo comparative analysis of four tissue pH monitoring systems*," Biomedical instrumentation & technology, 1998. **32** (6): p. 656-667.
55. M. Menzel, E. M. Doppenberg, A. Zauner, J. Soukup, M. M. Reinert, and R. Bullock, "*Increased inspired oxygen concentration as a factor in improved brain tissue oxygenation and tissue lactate levels after severe human head injury*," Journal of neurosurgery, 1999. **91** (1): p. 1-10.
56. B. Venkatesh and S.-P. Hendry, "*Continuous intra-arterial blood gas monitoring*," Intensive care medicine, 1996. **22** (8): p. 818-828.
57. B. Venkatesh, T. B. Clutton, and S. P. Hendry, "*A multiparameter sensor for continuous intra-arterial blood gas monitoring: a prospective evaluation*," Critical care medicine, 1994. **22** (4): p. 588-594.
58. B. A. McKinley, W. P. Morris, C. L. Parmley, and B. D. Butler, "*Brain parenchyma PO sub 2, PCO sub 2, and pH during and after hypoxic, ischemic brain insult in dogs*," Critical care medicine, 1996. **24** (11): p. 1858-1868.
59. S. A. Grant, K. Bettencourt, P. Krulevitch, J. Hamilton, and R. Glass, "*In vitro and in vivo measurements of fiber optic and electrochemical sensors to monitor brain tissue pH*," Sensors and Actuators B: Chemical, 2001. **72** (2): p. 174-179.
60. P. Takmakov, M. K. Zachek, R. B. Keithley, E. S. Bucher, G. S. McCarty, and R. M. Wightman, "*Characterization of local pH changes in brain using fast-scan cyclic voltammetry with carbon microelectrodes*," Analytical chemistry, 2010. **82** (23): p. 9892-9900.
61. B. J. Venton, D. J. Michael, and R. M. Wightman, "*Correlation of local changes in extracellular oxygen and pH that accompany dopaminergic terminal activity in the rat caudate–putamen*," Journal of neurochemistry, 2003. **84** (2): p. 373-381.
62. J. F. Cheer, K. M. Wassum, and R. M. Wightman, "*Cannabinoid modulation of electrically evoked pH and oxygen transients in the nucleus accumbens of awake rats*," Journal of neurochemistry, 2006. **97** (4): p. 1145-1154.

63. J. L. Ariansen *et al.*, "*Monitoring extracellular pH, oxygen, and dopamine during reward delivery in the striatum of primates*," Frontiers in behavioral neuroscience, 2012. **6**: p. 36.
64. S. A. Grant and R. S. Glass, "*A sol–gel based fiber optic sensor for local blood pH measurements*," Sensors and Actuators B: Chemical, 1997. **45** (1): p. 35-42.
65. E. J. Netto, J. I. Peterson, M. McShane, and V. Hampshire, "*A fiber-optic broad-range pH sensor system for gastric measurements*," Sensors and Actuators B: Chemical, 1995. **29** (1-3): p. 157-163.
66. M. Borecki, M. Szmidt, M. K. Pawłowski, M. Bebłowska, T. Niemiec, and P. Wrzosek, "*A method of testing the quality of milk using optical capillaries*," Photonics Letters of Poland, 2009. **1** (1): p. 37-39.
67. A. K. Yetisen *et al.*, "*Light-directed writing of chemically tunable narrow-band holographic sensors*," Advanced Optical Materials, 2014. **2** (3): p. 250-254.
68. A. J. Marshall, J. Blyth, C. A. Davidson, and C. R. Lowe, "*pH-sensitive holographic sensors*," Analytical chemistry, 2003. **75** (17): p. 4423-4431.
69. A. K. Yetisen *et al.*, "*Glucose-Sensitive Hydrogel Optical Fibers Functionalized with Phenylboronic Acid*," Advanced Materials, 2017. **29** (15): p. 1606380-1606391.

Chapter 7: Conclusion, contribution, and Future work

7.1 Conclusion

Two categories of smart contact lenses (SCLs) with point-of-care clinical applicability for diabetes screening were demonstrated. Smartphones were potentially employed to serve as readers for glucose concentration assays. The smartphone technology has the advantage of being used in resource-limited settings, where trained healthcare professionals are in shortage. Free android app recorded the optical signals exploiting the smartphone ambient light sensor. The smart contact lenses were based on two different optical glucose sensors. Both sensors were made of the same hydrogel matrix (polyacrylamide) and the phenyboronic acid derivative, 3-(acrylamido) phenylboronic acid. However, the transduction systems were different; i) photonic microstructure (PS), ii) light diffusing microstructures (LDMs). The optical glucose sensors were fabricated in a single step by the replica mould and the free radical polymerization methods. For the free-standing PS sensors, the glucose-boronate complexation induced a positive shift of the periodic constant. This shifts in the periodic constant allowed predicted measurements over the physiological glucose concentration up to 100 mM. A laser pointer and a paper screen were the only required equipment for the interrogation of these sensors. Attaching the PS sensor to the contact lens constrained the sensor's swelling in x- and y- directions. Hence, binding glucose with the sensor has no influence on the periodicity constant but altered the groove depth inducing a change in the diffracted power of the first order spots. Glucose quantification measurements by the smart lenses were carried out in reflection mode by a smartphone and a power meter, separately in the physiological conditions. The trends of the output signals recorded by the smartphone

and the power meter were similar confirming reliability of smartphones as potential readers. The contact lenses displayed high sensitivity, and impressive short response and saturation times to be 3 s and 4 min, respectively. The second category of the developed smart contact lenses relied on the LDMs sensors. The LDMs work as a light diffuser with an ability to diffuse the incident light in the forward and backward directions, whether the incident light is polychromatic or monochromatic. For the free-standing sensor based on LDMs, glucose-boronate complexation induced a change in the dimensions and the refractive index of the LDMs, subsequently the light diffusion efficiency decreased. Accordingly, the maximum optical power transmitted/reflected measured at the center of the diffused spot increased. This change in the optical power allowed detection of glucose concentration in the range of 0-100 mM. The sensor displayed robust performance and a high sensitivity ~ 2.3 % mM^{-1}. Kinetic of swelling, and reusability were investigated. The sensor showed limited hysteresis through the test for four cycles. Additionally, influence of pH on the sensor was evaluated. The contact lens based on LDMs sensor was interrogated by a white light beam for glucose detection under the physiological conditions in reflection configuration. A smartphone as a reader recoded the response of the contact lens for glucose concentrations up to 50 mM.

On the other hand, invasive and implantable glucose sensors have been developed. Novel fiber optic probes for blood glucose detection were demonstrated. Multimode silica fiber and inhouse-made biocompatible hydrogel fiber were functionalized for continuous glucose detection. The glucose-responsive hydrogels were imprinted with the LDMs using the replica mould method and chemically attached to the distal ends of the fibers. Constraining the LDMs on the fibers tips prohibits the hydrogel expansion (due to glucose-boronate

complexation) except in the z-direction. Thus, the thickness and the refractive index of the LDMs changed with glucose-boronate binding; however, the slight change in the refractive index was enough to influence the diffusion efficiency which led to the increasing of the maximum optical power (P_{max}). Primary investigations of the sensors constrained on glass substrates were carried out. The readout setup involved a light source (broad band white light or monochromatic light) and a photodetector (a smartphone or a power meter). Recording the P_{max} coming out of the sensor enabled monitoring of glucose concentrations up to 50 mM. Increasing P_{max} in the transmission and reflection configurations was on account of the scattering efficiency of the sensor in the forward and backward directions. The constrained LDMs sensor displayed a sensitivity of 0.8% mM^{-1}, which is three times less than that of the free-standing counterpart (2.3% mM^{-1}). The silica fiber probe displayed even lower sensitivity of ~0.37 % mM^{-1}. The smartphone was compatible with the fiber probe in transmission configuration; however, an optical power meter was used in reflection mode measurements. The biocompatible fiber displayed less sensitivity ~ 0.25 % mM^{-1} compared to the silica. The kinetic of swelling for the probe showed impressive results as the probe presented a rapid response of 30 s and short saturation time, 15 min at room temperature. Also, influence of temperature on the probe was evaluated. Additionally, performance of the probe was analyzed at various pH environments and it was found that the sensitivity improved in higher alkaline solutions. Furthermore, the potential interference of lactate was evaluated to be less than 0.1% in the physiological lactate range. The proof-of-concept study may be vital for diagnosing chronic diseases, especially for type 1 diabetics, where continuous glucose monitoring is a necessity for blood glucose management.

Based on integration of the fiber optic and the stimuli-response hydrogels engraved with the LDMs, various sensing probes were realized to cover a wide range of applications. Alcohol and pH sensing fiber optic probes were demonstrated. Initial investigations to the sensors constrained on glass substrates were carried out in transmission and reflection configurations. Similar response trends were detected for the fiber optic probes in both configurations. The alcohol sensitive fiber probe responded to ethanol, propna-2-ol, and dimethyl sulfoxide (DMSO) displaying a superior limit of detection (2% v/v). The response time was instantaneous and the saturation time was ~ 60±3 s, and the highest sensitivity was recorded for DMSO (2.5% vol^{-1}). Reusability of the probe was examined in ethanol solution showing a robust performance. The pH probe was tested in a pH range of 4.3-9 and displayed a high sensitivity in the acidic region, especially in the range of 5-7. Same pH range (5-7) influenced the probe's output signals the most in reflection configuration. Investigation of sensitivity, kinetics of swelling, and reusability showed that the probe has a suitable performance for real-time monitoring. To realize broader applications, the fiber probe can be functionalized with chelating agents and aptamers for continuously sensing a wide range of biomolecules such as proteins, DNA, and RNA in clinical samples.

7.2 Contribution

1. Smart contact lenses integrated with optical glucose sensors have been reported in the literature; however, their practical applications were hindered due to technical limitations including the low sensitivity, and the time-consuming and complicated fabrication process. The glucose sensors were based on 1D-holographic grating and 3D crystalline colloidal array (3D-CCA). In this dissertation we introduced novel optical transducers (1D-grating and

LDMs) to facilitate and expedite the fabrication process. Fabrication of the glucose sensor included preparing the hydrogel matrix, functionalizing the hydrogel with PBA, replication of the optical transducers, and integrating the sensor to the contact lens were executed in a single stage lasting for about 5 min. In contrast, 3D CCA glucose sensors require two to three weeks to obtain highly order nanoparticles by self-assembly method. Also, 1D-holographic grating sensors necessitate advanced techniques and multistage fabrication process. Facilitating the fabrication may open doors for mass production and cut down the sensor cost.

2. The readouts of the contact lenses were simple and compatible with smartphone technology.
3. The contact lens sensor displayed impressive rapid response (3s) and saturation time (4min) in continuous glucose quantification testing. To the best of our knowledge, the fastest response recorded was 90s for the optical glucose sensors based on PBA derivatives.
4. Fiber optic probes employed for remote and implantable sensing applications such as SPR, and interferometric fiber probes require expensive coherent light sources, signal processing, bulky instruments, advanced fabrication techniques. In this dissertation we have introduced a novel class of fiber optic probes by integrating fiber optic with light diffusers. The probe overcame many technical limitations including the complex fabrication, the bulky interrogation setup, the low sensitivity, the long response time, and the cost. Firstly, the fabrication of the developed probes was facile without need of any advanced techniques or vacuum systems. Secondly, the interrogation setup was compact, handy, and portable, without any coherent light sources, bulky instruments, costly devices like spectrometers, or data processing equipment. Finally, the probes were suitable for functioning in the reflection mode configuration, which is the more desirable mode for remote sensing applications.

7.3 Future work

The novel class of fiber optic probes that have been developed in this dissertation can be exploited for a wide range of applications. For example, the glucose probe can be further investigated in ex vivo blood plasma, and *in vivo* blood, to be implement in intensive care units (ICUs).

Normal cellular metabolism and function necessitates the blood pH to be maintained within the range of 7.35-7.45. In case, the blood pH moves out of this range, the body attempts to correct the imbalance by tapping its stores of neutralizing nutrients. Unluckily, these nutrients are often run out. In the acidosis condition, bones are the sacrifice as the bone tissues dissolves into its basic mineral constituents (alkaline salts) to be used as neutralizing elements. The pH-fiber optic probe can be functionalized with an alternative pH-sensitive hydrogel which is highly sensitive in the physiological pH range. Hence, the probe can be injected in veins to detect the blood pH.

Increasing lactate levels are related to organ dysfunction and lactate is a biomarker which has been used for a long time for the diagnosis of sepsis and sepsis shock. Recently, it has been found that monitoring lactate levels help in diagnosis of many other clinical conditions such as cardiac arrest, trauma, sever lung disease, respiratory failure or pulmonary edema, and cardiogenic. Fiber optic probe for lactate detection in arteries or veins can be developed by attaching the lactate-responsive hydrogel imprinted with LDMs to the fiber optic.

Fiber optic probes can be developed for real-time detection of heavy metals such as lead and mercury in drinking water. For example, acrylamide hydrogel matrix can be functionalized with urease enzyme to produce mercury-responsive hydrogel (MRH). When MRH is exposed to the urea solution, the immobilized urease enzyme hydrolyzes the urea and produce NH_4^+ and HCO_3^- ions within the hydrogel. Theses ions result in a charge-screening between the carboxylate groups of the ionic polyacrylamide backbone inducing shrinkage of the hydrogel. In case, MRH was exposed to a solution of urea and Hg^{+2}, Hg^{+2} inhibit the urea hydrolysis and suppress the production of NH_4^+ and HCO_3^-. Therefore, the volumetric shift of the MRH can be function of Hg^{+2} for a fixed urea concentration.